Université de Montréal

# The Correlation between the Structural properties and Giant Magnetoresistance in Co/Cu Multilayers

Par

Meng Cai

Département de physique
Faculté des arts et des sciences

Thèse présentée à la faculté des études supérieures
en vue de l'obtention du grade de
Philosphiæ Doctor (Ph.D.)
En physique

Avril 2000



*To my parents*

## Sommaire

Cette thèse a pour but d'établir une corrélation des propriétés magnétiques et de transport des multicouches Co/Cu avec la nature et la structure de leurs interfaces.

Nous avons déposé plusieurs séries d'échantillons par pulvérisation cathodique radio fréquence, sur substrats de verre et de silicium. Nous avons ensuite induit d'une manière systématique des modifications structurales en utilisant plusieurs techniques. Il s'agit notamment de la variation de la température du substrat, du recuit thermique, et de l'irradiation ionique. Ces différents traitements ont eu des effets spécifiques sur la rugosité et le mixage des interfaces ainsi que sur la taille des grains et la texture des films.

Les mesures de réflectivité spéculaire et diffuse des rayons X à faibles angles d'incidence ainsi que celles de diffraction à grands angles nous ont permis de mettre en évidence ces effets, tandis que les mesures de magnétorésistance et d'aimantation nous ont permis de suivre l'évolution des propriétés magnétiques et de transport de nos multicouches.

En variant la température du substrat entre –40 °C et 120 °C, nous avons pu mettre en évidence des changements significatifs dans la structure des interfaces, ainsi que dans l'homogénéité et la texture des multicouches. La magnétorésistance géante (GMR) maximale a été obtenue pour des multicouches déposées à 15 °C. Ces dernières présentent aussi la meilleure qualité des interfaces. D'autre part le recuit thermique des multicouches Co/Cu a eu comme effet une forte décroissance de la GMR avec la température de recuit. Nous avons montré aussi que cet effet dépend fortement de l'épaisseur de la couche de Co et peut être attribué à une diffusion atomique le long des joints de grains.

L'étude des multicouches irradiées avec des ions $Si^+$ d'énergie 1 MeV a montré qu'il se produit un faible intermixage aux interfaces, accompagné par une suppression systématique du couplage antiferromagnétique et de la GMR lorsque la dose d'irradiation est faible. Cependant, tant que ces doses restent inférieures à $5x\ 10^{14}$ ions/cm$^2$, le recuit thermique peut rétablir aussi bien les interfaces abruptes que l'effet GMR. En alternant l'irradiation ionique à faible dose et le recuit thermique, il devient alors possible de modifier la structure des interfaces d'une manière réversible. Ceci nous a permis de

d'établir une corrélation entre l'amplitude de la GMR et la fraction volumique des régions magnétiques ayant un couplage antiferromagnétique.

## Abstract

Co/Cu multilayers with periods of ~10-150 Å have been prepared on glass and silicon substrates by using a magnetron sputtering system. Low-angle x-ray reflectivity measurements have been carried out and confirmed well-defined compositional modulation along the growth direction of these mutlilayers. High-angle diffraction measurements have revealed that the films are highly textured in the fcc (111) direction and grow coherently across Co/Cu interfaces. Giant magnetoresistance (GMR) ratios over 20% at room temperature have been obtained and have been found to oscillate with Cu layer thickness. A corresponding oscillatory interlayer magnetic coupling has also been clearly evidenced.

Aiming at correlating the structural properties and GMR, the structures of the multilayers have been modified systematically by a variety of techniques and their effects have been compared. Varying deposition temperature between –40 °C and 120 °C generates significant changes in the interface structure, uniformity and film texture of Co/Cu multilayers. Large GMR can be obtained only if the deposition temperature is maintained in the range of 0 °C – 60 °C. The optimized GMR effect is observed in the multilayer grown at 15 °C, which also exhibits the highest interface quality. Thermal annealing effects on the GMR of Co/Cu multilayers have been studied as well. It is found that the annealing effects strongly depend on the Co layer thickness, and the decrease of GMR upon annealing can be ascribed to atomic diffusion along columnar grain boundaries.

The effects of 1 Mev $Si^+$ ion beam irradiation on the structure, magnetism and magnetotransport properties of Co/Cu multilayers have been examined. At high doses, ion beam irradiation produces non-equilibrium Co-Cu alloys. At low doses, it generates short-range interfacial mixing which is accompanied by a systematic suppression of the antiferromagnetic (AF) coupling and the GMR. For ion doses not exceeding $5\times10^{14}$ ions/cm$^2$, subsequent thermal annealing restores the abrupt interlayer structure as well as the GMR. The combination of low-dose ion bombardment and thermal annealing provides an *ex-situ* technique to modify interface structure *reversibly* over a significant range. Based on this technique, the role of interface scattering in the GMR of Co/Cu, as

well as the relationship between the GMR and the volume fraction of AF regions of Co/Cu multilayers are discussed.

**Keywords:** magnetic multilayer, giant magnetoresistance, antiferromagnetic interlayer coupling, interface structure, ion-beam irradiation

# Contents

## Acknowledgements

I would like to express my most profound and sincere gratitude to my supervisor, Professor R. W. Cochrane, for his guidance, support, patience, constant encouragement and inspiration during the entire course of my Ph.D. program.

I would like to thank Teodor Veres for numerous fruitful discussions, his constant help during my experiments, and his friendship. I wish to thank Professor S. Roorda for introducing me into the field of ion-beam irradiation, for many enlightening discussions and helps during ion-beam experiments. Thanks also go to Dr. M. Rouabhi for a lot of useful discussions, Dr. F. Schiettekatte for his assistance with the ion-beam experiments, G. Rinfret, R. Rinfret, P. Bérichon, and R. Gosselin for their excellent technical support.

I would like to thank Professor M. Sutton at McGill University for his help in multilayer structure analysis. I am also indebted to Li Cheng, Randa Abdouche, Dok Won Lee, and James Freitag at McGill University for their assistance with x-ray measurements.

Last but not least, thank all the professors and all the graduate students in the solid state physics group at the Université de Montréal..

## List of Tables

# List of Figures

## Chapter 2:



## Chapter 3:

**Chapter 5:**

## List of Abbreviations

| | |
|---|---|
| **AF** | antiferromagnetic |
| **AMR** | anisotropic magnetoresistance |
| **CPP** | current perpendicular to the film plane |
| **DWBA** | distorted-wave Born approximation |
| **FC** | field-cooled |
| **FWHM** | full width at half maximum |
| **FM** | ferromagnetic |
| **GMR** | giant magnetoresistance |
| **LMR** | longitudinal magnetoresistance. magnetoresisance measured with both magnetic field and electrical current in the film plane and the magnetic field parallel to the current. |
| **MR** | magnetoresistance |
| **NM** | nonmagnetic |
| **NMR** | nuclear magnetic resonance |
| **PMR** | perpendicular magnetoresistance. magnetoresistance measured with the electrical current in the film plane and the magnetic field perpendicular to the film plane. |
| **RED** | radiation-enhanced diffusion |
| **RKKY** | Ruderman-Kittel-Kasuya-Yosida model |
| **TEM** | transmission electronic microscopy |
| **TMR** | transverse magnetoresistance. magnetoresisance measured with both magnetic field and electrical current in the film plane and the magnetic field perpendicular to the current. |
| **TRIM** | a computer program to simulate transport of ions in matter |
| **ZFC** | zero-field-cooled |

# Chapter 1: Introduction

A novel MR phenomenon known as giant magnetoresistance (GMR) has been discovered in recent years in a variety of heterogeneous magnetic systems [1]. The most interesting example of such systems is a magnetic multilayer which consists of very thin (typically 5 to 100 Å) alternating layers of a ferromagnetic metal and a non-magnetic metal (e.g., Cu, Ag). The study of these multilayer systems has been motivated by the idea that their properties can be significantly different from those of any of the components. The first GMR was observed by Baibich *et al.* in Fe/Cr multilayers[2]. Since then, GMR effects have been found in many other multilayer systems, such as Co/Cu, Co/Ag, Ni-Fe/Cu, Ni-Fe/Ag, Ni-Co/Cu, Co-Fe/Ag, Fe/Cu, etc. GMR has stimulated great interest for its applications in the new generation of high density magnetic recording devices, as well as its importance in understanding the fundamental issues of magnetic ordering and electron scattering in heterogeneous magnetic structures.

Among many GMR systems, Co/Cu multilayers are of particular interest since they exhibit small temperature dependence and the largest GMR ratio at room temperature. In these multilayers, it has been reported that the GMR is extremely sensitive to their structures. However, so far no clear picture has emerged regarding the correlation between the structural properties and the GMR in Co/Cu multilayers. The reported data are apparantly contradictory. Obviously, a detailed and systematic study of such a correlation is crucial both in clarifying the mechanism of GMR in Co/Cu multilayers and optimizing GMR for industrial applications.

In this work, various techniques, including varying growth temperature, thermal annealing and ion beam irradiation, are applied to modify the structures (particularly, interface structures) of Co/Cu multilayers. The structure modification induced by these methods are carefully analyzed by using x-ray scattering techniques and its effects on the GMR and other magnetic and magnetotransport properties of Co/Cu multilayers are investigated. The results are discussed in the context of the relationships among the structural properties, the interlayer magnetic exchange coupling, and the spin-dependent electron scattering in Co/Cu multilayers.

## 1.1. Basic Concepts

### 1.1.1. Magnetoresistance

Magnetoresistance (MR) defines the variation of the electrical resistivity of a material under magnetic field. The best-known MR effect is the ordinary magnetoresistance[3], which originates from the Lorentz force acting on conduction electrons. This effect is common for non-magnetic metals and semiconductors, and is typically of the order of $\Delta\rho/\rho = 10^{-7}$ where $\rho$ is the resistivity.

In homogeneous magnetic materials (Co, Fe, Ni and their alloys), on the other hand, it is well known that the MR is dominated by scattering from the magnetic moments, and its magnitude depends on the relative orientation of the electrical current and the magnetization. This MR is known as anisotropic magntoresistance (AMR); it has attracted attention for more than 30 years, and has been widely applied as the basis of magnetoresistive read-back heads. The magnitude of AMR varies from material to material, ranging from 0.1% (for Fe) to 2-3% (for Co-Ni, and Ni-Fe alloys), and has been suggested to be correlated with such factors as the number of electrons associated with the 3d band, the spin-orbit coupling strength, the d-band splitting parameter, and the magnetostriction. [4]

The magnitude of GMR of a magnetic multilayer is typically at least one order greater than the AMR. By defining the MR ratio as $\Delta\rho/\rho_{sat}$ where $\rho_{sat}$ is the saturation resistivity at high field, the MR ratio of a [Fe(14 Å)/Cr(8 Å)]×50 multilayer was reported to be about 30%. An important fact of GMR is that, in magnetic multilayers, its value oscillates with the thickness of the non-magnetic layer. For example, in Co/Cu multilayers, as reported by Mosca *et al.* [5], GMR exhibits three maxima at Cu layer thickness of 9 Å, 20 Å and 33 Å respectively. This oscillation of GMR is directly correlated with the oscillatory interlayer magnetic coupling, which refers to the phenomenon that for coupling of two ferromagnetic layers through a nonmagnetic spacer layer [6], the interlayer coupling strength $J_{12}$ oscillates back and forth from positive to negative with a period of ~ 10 Å. With positive $J_{12}$, the magnetic moments in adjacent magnetic layers tend to align parallel (ferromagnetic coupling), while with negative $J_{12}$,

the magnetization in the two neighboring magnetic layers tend to align in anti-parallel directions (antiferromagnetic coupling).

### 1.1.2. Models of Interlayer Magnetic Coupling

The oscillatory interlayer coupling behavior can be explained by either the extended Ruderman-Kittel-Kasuya-Yosida (RKKY) model[7], or a quantum well model[8]. In the extended RKKY model, the first ferromagnetic (FM) layer interacts with the conduction electrons of the spacer and induces a spin-polarization in the latter; this spin-polarization extends throughout the spacer and eventually interacts with the neighboring FM layer, and thus gives rise to an effective exchange interaction between the two FM layers. Based on this picture, and under free-electron approximation, the RKKY model gives the interlayer coupling between the two FM layers as,

$$I_{1,2} \approx -I_0 \frac{d^2}{z^2} \sin(2k_F z) \qquad (1.1)$$

where z is the distance between the two magnetic layers, d is the atomic spacing, $I_0$ is a coupling strength parameter, and $k_F$ is the Fermi vector of the spacer. As suggested by Eq. 1.1, the interlayer coupling oscillates with a period $\pi/k_F$ and decays as $z^{-2}$. More general calculations within the RKKY theory taking into consideration the nonspherical Fermi surface have been performed by Bruno and Chappert[7]. Their results showed that the coupling strength and period not only depend on the material but also the crystallographic orientation of the spacer, and furthermore, the occurrence of the multiperiodic (short period) oscillations was predicted. Fitting the extended RKKY model to the experimental data has confirmed that the RKKY model provides a good description of the oscillatory interlayer coupling observed in magnetic multilayers [6].

However, the RKKY model is not the only model that can explain the oscillatory behavior. The same spacer thickness dependence of magnetic interaction is also predicted by the quantum-well model, in which quantum-well states are formed for a ferromagnetic alignment of the magnetic layers where, for example, all majority-spin bands lie below

the Fermi energy and thus electrons of this spin at the Fermi energy are confined to the nonmagnetic layer[8]. The confinement causes a discretization of states, which become more closely spaced with increasing spacer thickness. When they cross the Fermi level, the energy gained or lost from filling them changes the relative energies of the configurations with parallel and antiparallel magnetizations. Remarkably enough, the quantum-well model and the RKKY theory predict the same period of oscillation, and thus it cannot be decided on the basis of the periods alone which of the models more appropriately describes the coupling. However, Schilfgaarde and Harrison[8] have pointed out that the effects of the two mechanisms can be distinguished by noting the dependence upon moment. Specifically, with RKKY theory, the interlayer coupling is proportional to the square of the magnetic moments, while with the quantum-well model, the coupling tends to saturate. Their experimental results revealed a picture of a transition to a quantum-well character from an RKKY description at small moments. Nevertheless, it has also been found that the transition is *partial* only, probably due to the incomplete confinement of states in nonmagnetic layers. As a result, the two mechanisms may coexist in an actual multilayer.

### 1.1.3. Models of GMR

No matter which mechanism is responsible for the oscillatory interlayer exchange coupling, GMR is observed in the antiferromagnetically coupled multilayers. This can be explained by the so-called *spin-dependent* electron scattering in ferromagnetic materials. By the term *spin-dependent* scattering, we refer to the fact that in ferromagnets, the scattering rate of an electron depends on its spin polarization (spin-up or spin-down). The possible microscopic mechanisms of this effect will be discussed shortly.

The two current network model is a phenomenological model that intuitively demonstrates how the magnetoresistance results from the interplay of the anti-ferromagnetic interlayer coupling and spin-dependent electron scattering. In the two current model, the total resistivity of a magnetic thin film (neglecting spin-flip effect) is written as,

$$\rho = \frac{\rho^{\uparrow}\rho^{\downarrow}}{\rho^{\uparrow} + \rho^{\downarrow}} \tag{1.2}$$

where $\rho^{\uparrow}$ and $\rho^{\downarrow}$ are the resistivities for the spin-up and spin-down electrical current channels respectively. If the electron scattering is *spin-dependent*, we have $\rho^{\uparrow} \neq \rho^{\downarrow}$. With magnetic layers that are antiferromagnetically coupled, at zero external field, electrons of each spin direction experience the same resistance, since they sample both the higher and the lower resistances equally as they transverse a double bilayer. The total resistivity is,

$$\rho^{AF} = (\rho^{\uparrow} + \rho^{\downarrow})/4 \tag{1.3}$$

By applying an external magnetic field, the relative orientation of the magnetizations in neighboring layers is switched, and as the field becomes sufficiently large ( $\geq H_{sat}$, where $H_{sat}$ denotes the saturation field), the magnetizations of all the magnetic layers are aligned parallel to the direction of the external field. When this occurs, there is a short-circuit effect, i.e., electrons of one spin have a lower resistance and carry more of the current. The total resistivity becomes,

$$\rho^{F} = \frac{\rho^{\uparrow}\rho^{\downarrow}}{\rho^{\uparrow} + \rho^{\downarrow}} \tag{1.4}$$

Noticeably, as long as $\rho^{\uparrow} \neq \rho^{\downarrow}$, $\rho^{F}$ is always lower than $\rho^{AF}$. The magnetoresistance (MR) ratio is defined as,

$$MR = \frac{\rho(H=0) - \rho(H=H_{sat})}{\rho(H=H_{sat})} = \frac{\rho^{AF} - \rho^{F}}{\rho^{F}} = \frac{(\alpha-1)^2}{4\alpha} \tag{1.5}$$

where $\alpha = \rho^{\uparrow} / \rho^{\downarrow}$, and is known as the coefficient of scattering asymmetry. As suggested by Eq. 1.5, the MR ratio may exceed 100% for $\alpha \cong 8$ to 10.

Quantitative interpretation of GMR requires more sophisticated models such as the semi-classical model initiated by Camley and Barnas [9] or the quantum theory proposed by Levy, Zhang and Fert [10]. In the semi-classical model, the currents carried by the two spin-channels are calculated separately by solving the Boltzmann transport equation with proper boundary conditions at interfaces. In the original model, spin-dependent electron scattering was included only through spin-dependent transmission coefficients at interfaces. Further refinement of the model has also taken into account the contributions to the spin-dependent scattering originating from the bulk of the ferromagnetic layers and spin-dependent potential barriers between the adjacent layers. On the other hand, the quantum theory calculates the point-dependent conductivity in a magnetic superlattice by using the Kubo formalism. Compared with the semi-classical model, the biggest advantage of the quantum theory lies in the fact that it treats the bulk and interface scattering on an equal footing. The semi-classical model, however, is simpler and the parameters it introduces, such as mean free paths and transmission coefficients at interfaces, are easily understood and related to experimental results.

### 1.1.4. Origins of Spin-dependent Electron Scattering

After all, what are the origins of the *spin-dependent* electron scattering in these magnetic multilayers? This is still a subject of controversy. Several pictures have been suggested. In the simplest model, in 3d-ferromagnetic metals, it is assumed that the conductivity is primarily carried by electrons from the s-bands that are broad, and as a consequence, have low effective masses. In contrast, the d-bands are narrow and have high effective masses. Dating back to Mott[11], it is commonly assumed that there are two largely independent conduction channels, corresponding to up-spin and down-spin electrons. The d-bands play an important role in providing final states into which the s-electrons can be scattered. As a result of the d-band splitting due to exchange interactions, which is characteristic of the magnetism of transition metals, the densities of states at the Fermi level for the spin-up and spin-down d-electron bands are very different. This difference means that the scattering rates into these states will be

significantly different for the two conduction channels, leading to substantially different mean free paths $\lambda^{\uparrow(\downarrow)}$ and conductivities $\sigma^{\uparrow(\downarrow)}$ in the two channels.

The second picture of *spin-dependent* scattering assumes that the electron scattering in a magnetic multilayer is dominated by scattering processes from the non-magnetic impurities dissolved in the magnetic matrix near interfaces due to interdiffusion. In this scenario, the strong *spin-dependence* arises from the resonant scattering of the virtual bound state of an impurity atom in (or near) the d-band of the ferromagnetic material. For example, in the case of Ni (or Fe) containing Cr impurities[12], a d $\uparrow$ virtual bound state from a Cr impurity is close to the Fermi level ($E_M$), which leads to a strong repulsive potential for the spin-up electrons at the Cr impurity sites, and consequently, a strong scattering in the spin-up channel. For dilute Cr impurities in Fe host [13], the value of $\alpha$ obtained is about 0.17 (or $1/\alpha \cong 6$). For another important system, Co/Cu, unfortunately, direct experimental data is not yet available, due to the fact that these elements are immiscible and do not form homogeneous alloys. However, the possibility of scattering asymmetry based on the same picture of virtual bound states has also been suggested for Cu-based multilayer systems (including Co/Cu) [14].

The third origin of electron scattering asymmetry is related to spin-dependent interface potential barriers. These potential barriers result from the difference in energy between the Fermi energy and the bottom of the conduction bands in the adjacent materials. This potential modulation is expected to play a small role if s-electrons dominate the conduction of the current but can play an important role in MR if d or hybridized sd electrons contribute significantly to the electric conduction. In Fe/Cr multilayers[15], and using the free electron approximation, the potentials for majority electrons ($V_M$) and minority electrons ($V_m$) are $-8.23$ eV and $-5.73$ eV respectively in Fe, and the potential ($V_{Cr}$) in Cr is $-5.77$eV. It turns out that $V_{Cr}$ is very close to $V_m$, and therefore, the minority electrons are more likely to be transmitted across interfaces, while the majority electrons are more likely to be scattered. For Co/Cu multilayers, first-principles calculations by Stiles[16] show that the potentials in Cu are very similar to the potentials for the majority electrons in Co, but significantly different from those for the minority. Of particular interest, the majority Fermi surface in Co is similar to the Fermi surface in Cu, but is smaller. The similarities lead to almost complete transmission from

the majority states in Co into Cu, but the smaller size leads to complete reflection for the states in Cu with group velocities parallel to the interface. On the other hand, due to the very complicated nature of the minority Fermi surface of Co, minority electrons with the largest velocities parallel to the interfaces may still be transmitted into Co from Cu. Stiles has suggested that, even if there is no spin-dependent defect scattering, the channeling effect by these electrons is strong enough to give a large magnetoresistance.

A typical magnetic multilayer contains a lot of intrinsic structural defects, such as vacancies, stacking faults, lattice distortions and grain boundaries, that are produced during the process of deposition. Each of these defects makes its own contribution to the scattering potentials and, consequently, to the resistivity. In general, however, there is no reason for the potentials related to most of these defects to be spin-dependent. Therefore, GMR is the result of the competition between the *spin-independent* and *spin-dependent* electron scattering processes. In an anti-ferromagnetically coupled multilayer, enhanced *spin-dependent* scattering increases GMR, while enhanced *spin-independent* scattering suppresses GMR. As for the three possible origins of *spin-dependent* scattering mentioned above, it is also an important question whether one of them prevails, and if so, which one is dominant? It is noted that the scattering processes corresponding to these mechanisms occur at different locations within the multilayer. The first is a pure bulk effect, the third is a pure interface effect, while the second one is related to the characteristics of the regions near interfaces and can be considered as a quasi-interface effect. Thus, a study of the correlation between the structure and GMR provides valuable information about the relative importance of the above origins. For example, if *spin-dependent* processes associated with impurity scattering dominate the GMR of a multilayer, then enhanced interfacial mixing is expected to increase GMR. Such ideas have generated enormous interest among experimentalists, and a lot of work has been published with controversial results. In section 1.2, a review will be given about these results. The same is also one of the primary motivations of this work. Needless to say, the answers to the above questions are extremely important in understanding the GMR phenomenon.

### 1.1.5. GMR without Antiferromagnetic Coupling

Finally, it is also worth mentioning that the GMR effect is not only restricted to antiferromagnetically coupled multilayers, but is also observed in a variety of inhomogeneous magnetic media. Examples include granular alloys, spin-valve sandwiches, and multilayers comprising ferromagnetic layers of different coercivities. A granular alloy is made up of small ferromagnetic particles (e.g., Co) embedded in non-magnetic matrix (e.g., Cu, Ag). At zero external field, the magnetic particles are de-coupled and their moments are randomly orientated with respect to each other. Large external field aligns the magnetic axis of these entities, and similar to the case of a multilayer, the resistivity drops due to the existence of *spin-dependent* electron scattering processes. Very large MR values have been reported for CoCu[17] ( ~30% at 5 K) and CoAg[18] ( ~40% at 5 K, ~20% at 300 K ) alloys. However, two factors make such alloys impractical for applications. First, very large external fields (typically > 1 Tesla) are required to saturate a MR curve. Second, the MR is very sensitive to the shapes and sizes of the magnetic particles (normally, it is optimized at the sizes of the order of the electron mean free path) that are difficult to control.

A spin-valve sandwich[19] comprises two ferromagnetic layers (F1 and F2) separated by a non-magnetic metal (NM). The NM layer is usually chosen to be thick enough so that no intrinsic antiferromagnetic coupling exists between F1 and F2. However, the magnetization of F2 is constrained by coupling to an antiferromagnetic layer (e.g., FeMn) (by exchange coupling). Therefore, when the external field is swept, the reversals of the magnetizations of F1 and F2 occur at different fields, and a switch from fully antiparallel configuration to fully parallel configuration between the two layers happens at a field that depends on the pinning strength. The highest GMR reported for a spin-value sandwich is around 10% at room temperature. The most impressive feature of a spin-valve sandwich is its very high field sensitivity (> 2% per Oe ), due to the abrupt response to the external field. However, its structure is relatively more complicated, and from the basic research point of view, it is more difficult to isolate a single effect. A multilayer comprising ferromagnetic layers of different coercivities follows the same idea. However, instead of using an antiferromagnetic layer to pin F2, the neighboring

magnetic layers in such a multilayer intrinsically have different coercivities. The highest MR reported for such multilayers is 16% at room temperature in a (NiFeCo/Cu/Co/Cu) structure. Nevertheless, the coercivity of a magenetic layer depends sensitively on many structural parameters (grain size, defects, etc.) that are difficult to control. As a result, the properties of such multilayers are difficult to reproduce.

In spite of the fact that GMR has been observed in many inhomogeneous magnetic structures, conventional multilayers with antiferromagnetic coupling have attracted most of the attention due to their simple structure, large GMR ratios, and reasonable field responses. In this work, we focus on such multilayers.

## 1.2. Correlation between Structural Properties and GMR

The GMR effect in a magnetic layer is highly correlated with its structural properties. This section summarizes some of the recent experimental and theoretical results concerning this problem.

### 1.2.1. The Effects of Layer Discontinuity

First, since the individual layers of a GMR superlattice are typically extremely thin, the layer discontinuity plays an important role in GMR. For example, in permalloy/Ag multilayers, Hylton *et al.*[20] has reported that precise annealing procedure created discontinuities of the permalloy layers which were filled with Ag. The resulted Ag gaps tend to align their positions in neighboring magnetic layers and thus, through magnetostatic interlayer coupling, favors antiparallel alignments of the magnetization needed for GMR. This effect enhances GMR, and in particular, due to the weakness of the magnetostatic coupling, very high field-sensitivity is obtained. Alternatively, if the gaps in the magnetic layers are sufficiently large, the layers are broken up into a great number of magnetic islands. Such multilayers are intermediate between multilayers and granular films. In Co/Ag multilayers with thin Co, Loloee *et al.* [21] have reported that the granular contribution greatly enhances the GMR. The importance of the granular-like GMR component in Co/Ag multilayers has also been confirmed by Honda *et al* [22]. A

detailed theoretical treatment of the effects of these two cases of magnetic layer discontinuity has been addressed by Slonczewski [23]. On the other hand, if the non-magnetic spacer layers become discontinous, direct magnetic bridging between the neighboring magnetic layers may result. This effect tends to reduce the volume fraction of the AF-coupled regions, and hence reduces GMR [24].

### 1.2.2. The Effects of Film Texture

The second structural factor that may affect the GMR is the crystallographic orientation of the multilayer film. The orientation of the spacer layer has profound effects on its electronic structure and thus influences the period, the sign and the strength of the interlayer coupling. This effect has been observed in many multilayer systems. For example, in Co/Cu multilayers, the interlayer coupling has been found to be extremely sensitive to the crystalline orientation. While strong oscillatory antiferromagntic coupling has been observed across a Cu(100) spacer, several groups have reported the absence of evidence for antiferromagnetic coupling in single crystalline Co/Cu multilayers grown orientated along (111). Theoretical models have also shown that in Co/Cu, the coupling is stronger along (100) and (110) than along (111)[25]. However, for polycrystalline Co/Cu multilayers textured in the (111) direction, antiferromagnetic coupling has been widely observed. Egelhoff and Kief [26] have suggested that the interlayer coupling exhibited by these multilayers is a result of a minority constituent of crystalline grains oriented at or near (100), while Parkin *et al.* [27] has argued that the antiferromagnetic coupling at (111) orientation is present but obscured by structural defects. In spite of years of investigation, this question remains contentious.

### 1.2.3. The effects of Interface Imperfections

The third, and perhaps the most interesting property is the interface structure of a multilayer. As mentioned earlier, the effects of interface structure are directly connected to the mechanism of GMR. The interfaces in a multilayer may consist of a great number of structural defects formed either during deposition or by post-growth treatments. These

structural imperfections can be classified into two types: interface roughness and interfacial mixing. Interface roughness (e.g., atomic steps or terraces) can be described in terms of a random variable defined as the deviation of the interface from its mean position. Interfacial mixing (or interdiffusion) means that in regions adjacent to the interface between layers *A* and *B*, atoms *A* and *B* are mixed randomly. An important distinction between interfacial mixing and interface roughness lies in that interfacial mixing has a much smaller lateral correlation length. In other words, interfacial mixing can be regarded as interface roughness on a very local scale.

**Fe/Cr Multilayers**

The effects of these interfacial imperfections on GMR have received a lot of attention. In Fe/Cr multilayers, Fullerton *et al.* [28] modified the interface roughness by three independent methods: varying sputtering gas pressure, changing sputtering power, and increasing the total thickness of the superlattice. Their results showed that, in all cases, increasing roughness and/or intermixing always resulted in enhancements of the GMR. Petroff *et al.* [29] found that roughnening the interfaces of Fe(001)/Cr(001) MBE-grown superlattices by an annealing treatment enhances the MR for annealing up to 300 $^{o}$C and reduces it at higher temperatures. This suggests the existence of an optimum roughness. Very similar results have been reported by Belien *et al.* [30] and Kelly *et al.* [31], in whose work the interfaces of Fe/Cr multilayers were modified by varying substrates, deposition temperatures or ion irradiation. These experiments suggest that interface roughness or intermixing play an important role in the GMR of Fe/Cr. This can be best explained by the picture that spin-dependent scattering from the Cr impurities dissolved in Fe near interfaces dominates the GMR effect. As discussed in section 1.1, bulk spin-dependent scattering comes from the difference in the spin-split density of states at the Fermi surface. However, compared to Ni and Co, the asymmetry in bulk Fe is much smaller. On the experimental side, the scattering asymmetry ratio $\alpha$ for bulk Fe has been measured by several groups: Dorleijn and Miedema [32] give $\alpha = 2.7$; Gurney *et al.* [33] give $\lambda\uparrow = 15 \pm 2$Å and $\lambda\downarrow = 21 \pm 2$Å, corresponding to $\alpha \approx 1.4$. These results confirm that the bulk spin-dependent scattering in Fe is rather weak. On the contrary, Fert and Campbell[13]

reported that the scattering asymmetry of dilute Cr impurities in Fe host is about $\lambda\uparrow/\lambda\downarrow$ = 6, which is much larger than the bulk scattering asymmetry. Gijs and Okada[34] concluded that an assumption of strong spin dependent interface scattering is essential to account for the steep decrease of the MR with Cr thickness. They obtained $\alpha = \lambda\uparrow/\lambda\downarrow \approx 12$ between the spin-up and spin-down scattering rates at the interfaces. Consequently, it seems to be reasonable to assume that the spin-dependent impurity scattering at Fe/Cr interfaces is of overwhelming importance in the MR.

This assumption has been further confirmed by the so-called "doping" experiments. Baumgart *et al.* [35] inserted selected elements at Fe/Cr interfaces. These additional impurities have known asymmetry in Fe for scattering of spin-up and spin-down electrons. It was found that the impurities (V and Mn) that have values of $\alpha$ close to that of Cr in Fe (i.e., $\lambda\uparrow >> \lambda\downarrow$) did not degrade the GMR significantly, while the impurities (Al and Ir) with $\alpha$ opposite to Cr in Fe (i.e., $\lambda\uparrow << \lambda\downarrow$) result in substantial reductions of the MR. Petroff *et al.* [29] intentionally mixed Cr with Fe by opening the shutter of Cr (Fe) cell a few seconds before closing the shutter of the Fe(Cr) cell during sputtering. In this way a mixed layer of approximately 1 Å was intercalated between Fe and Cr layers. It turned out that this artificial mixing increases both the resistivity and the GMR significantly. Chen *et al.* [36] and Daniels *et al.* [37] both introduced Cr impurities into the bulk layers of FE. By Cr alloying of the Fe layers, GMR effect was improved.

However, the conclusion drawn from the Fr/Cr multilayers cannot be easily generalized to other systems. For example, it has been reported that, while it increases the GMR in Fe-Co/Cu multilayers [38], thermal annealing leads to progressive loss of GMR in Ni-Fe/Cu multilayers [39] and related spin-valve structures [40], Ni-Fe/Au multilayers [41], and Co/Cu multilayers[42]. Therefore, the role of interface scattering in GMR may vary from system to system, and has to be evaluated individually.

## Co/Cu multilayers

Among the many GMR systems, Co/Cu multilayers are of particular interest due to the largest GMR. Ironically, the mechanism of GMR in this system is very controversial. Thomson *et al.* [43] and LeDang *et al.* [44] both studied the issue using the

nuclear magnetic resonance (NMR) techniques. In NMR measurements, the hyperfine interaction $B_{hf}$ has a substantial contribution from the magnetic moment of the nearest neighbors and replacement of nearest neighbor Co atoms by non-magnetic Cu atoms at an interface yields a discrete shift of $B_{hf}$ due to the reduction of electron polarization. As a result, intermixing leads to satellite peaks in NMR spectra. Their results show that for the Co/Cu multilayers revealing large magnetoresistance, the satellite peaks are largely suppressed, indicating that the increase in GMR is correlated with improvements in the interface qualities. Meanwhile, intentionally introduced interface roughness by either high argon pressure during sputtering[45] or post-annealing [46] was found to suppress GMR severely. Suzuki and Taga [47] studied the effects of the interfacial mixing using artificial co-deposition and found GMR decreases monotonically with intermixing width. Parkin [24] showed that Co/Cu multilayers grown on Fe buffer layers, which have much flatter interfaces, also exhibits much larger GMR than those grown on Cu buffer layers. These results lead to the conclusion that the spin-dependent scattering in Co/Cu multilayers occurs mainly within the bulk of the Co layers [48].

Nevertheless, the opposite conclusion can be drawn from other experimental results. For example, Saito *et al.* [49] modified the interfacial mixing by varying the *in-situ* argon sputtering voltage and concluded that GMR in Co/Cu requires atomically mixed interfaces. Strong evidence of spin-dependent scattering at Co/Cu interfaces has also been found by "planar doping" methods. "Planar doping" refers to inserting thin layers of a third material at interfaces. For instance, George[50] found that the GMR of a Co/Cu multilayer decreases steeply when a few atomic layers of Fe are inserted at interfaces, indicating much stronger spin-dependent effects at Co/Cu interfaces than at Fe/Cu interfaces. They also demonstrated that before Fe layers are inserted, the GMR of Co/Cu multilayer decreases with increasing thickness of Co. After 3 Å Fe layers were inserted at each interface, however, the variation of the GMR with the Co thickness exhibited the typical behavior expected for bulk spin-dependent scattering. This shows that the spin-dependence scattering at Co/Cu interfaces dominate the GMR, while the bulk spin-dependent scattering also exists but determines the behavior of the MR only when the much stronger interface contribution has been removed. Parkin [51] followed the same idea by inserting thin layers of Co at each Ni-Fe/Cu interface. Since the GMR of Ni-Fe/Cu

multilayers is less than half that of Co/Cu multilayers with layers of comparable thickness, a significant increase in the GMR of Ni-Fe/Cu is expected if the GMR in Co/Cu multilayers is primarily due to interface spin-dependent scattering. This behavior was indeed observed. It was shown that the properties of Ni-Fe/Cu multilayers were dramatically modified by inserting thin Co layers at the interfaces and the addition of Co layers just 3-4 Å thick dramatically increases the GMR (almost quadrupling it.) Quantitatively, the dependence of GMR on the thickness of the inserted Co interface layer ($t_{Co}$) was well described [52] by a function of the form: $\Delta R/R = a + b[1 - \exp(-t_{Co}/\xi)]$, where $\xi \approx 2.2$ Å. This characteristic length scale describes the thickness of the interfacial layer required to establish the character of the interface and thus the magnitude of GMR.

Band calculations for bulk Co give the value of scattering asymmetry as $\alpha = 8$ [48], which is much greater than that of bulk Fe. From the simple resistor network model described in section 1.1, this value can easily explain the large magnetoresistance observed in Co/Cu multilayers. In addition, significant bulk spin-dependent scattering in sputtered Co layers has also been confirmed by experiment. As for the scattering asymmetry at Co/Cu interfaces, however, very inconsistent data have been reported. Hall *et al.* [42] extended the resistor model, and used $\alpha = 1$ (assuming spin-independent interface scattering) to fit the zero-field resistivity dependence of GMR for Co/Cu multilayers annealed at various temperatures. The fitting curve was shown to be in good agreement with experiments. On the contrary, Lenczowski *et al.* [53] extracted an $\alpha$ of $21 \pm 3$ for Co/Cu interface scattering by fitting the dependence of the MR on the Cu spacer layer thickness using the quantum GMR model. Pratt [54] obtained an $\alpha$ value that lies somewhat between the two extremes. From measurements with the current perpendicular to the multilayer planes, they showed that the interface scattering asymmetry for sputtered Co/Cu (111) multilayer is $6.1 \pm 1.5$. It is also noted that the bulk scattering asymmetry for Co layers obtained by Pratt and Lenczowski *et al.* are consistent with each other ($\alpha \approx 2$ to 3), but much smaller than the value from the band calculations. The obvious discrepancies mentioned above stress the necessity to clarify the role of interface scattering in the GMR of Co/Cu in a more direct way.

In order to clarify the role of interface for Co/Cu multilayers, the following four aspects are critical. First, a careful characterization of interfacial structure, especially with

respect to various interfacial modification techniques, is necessary. In the current literature, a lot of ambiguities and inconsistencies still exist. For example, while Hall *et al.* [42] ascribed the decrease of GMR upon annealing to intermixing, Laidler and Hickey [55] showed that, at similar temperatures, annealing does not change at all the structure of Co/Cu interfaces. Second, the modifications on various aspects of structural properties need to be isolated. For example, Suzuki *et al.* [47] showed a drastic change in crystallographic texture as the Co/Cu interfaces are artificially mixed through co-deposition. It is therefore difficult to conclude unambiguously whether the decrease of GMR resulted from the intermixing or from the changes in film texture. Similar problems may also arise when additional layers are inserted at interfaces, since these layers will inevitably affect the growth of the subsequent layers. Third, it is important to separate the effects of interfacial modification on the GMR directly through the changes in spin-dependent scattering or indirectly through the changes in interlayer antiferromagnetic coupling. The interlayer magnetic coupling in Co/Cu multilayers is relatively weak and thus this aspect is particularly important. Any subtle change in the interface might affect the magnetic exchange coupling, which also drastically influences the GMR. Fourth, the initial states of the samples should be considered. A lot of discrepancies may stem from the different sample qualities. It is therefore interesting to compare the effects of interface modifications by *various* techniques in similar samples. In particular, it is desirable to modify systematically the interface structure in a *single* multilayer and verify its effect on GMR. The remaining chapters in this thesis represent our efforts in this regard.

The remainder of this thesis is organized as follows. In chapter 2, the experimental methods, including multilayer fabrication, structure characterization, electrical, magnetic, and magnetotransport measurement techniques, are outlined briefly. In chapter 3, details of the structural, magnetic and transport properties of our Co/Cu multilayers are described, as a base for further discussion of the correlation between the structure and GMR in these multilayers. Focus is placed on the analysis of interfacial structure, as well as the layer thickness dependence of GMR. In chapter 4, the effects of deposition temperature on the interfacial structures, interlayer magnetic coupling and GMR of Co/Cu are discussed. Chapter 5 presents the ion-beam irradiation effects in the

Co/Cu multilayers. Ion-beam mixing of the immiscible Co/Cu system is investigated in detail using a variety of techniques, and its influence on GMR is addressed. Chapter 6 describes the thermal annealing effects on the GMR in Co/Cu multilayers. In particular, very interesting results obtained in ion-beam irradiated Co/Cu multilayers are presented. Chapter 7 concludes the thesis.

# Chapter 2: Experimental Methods

## 2.1. Sample Preparation

In this work, the sputtering technique is applied to prepare high-quality Co/Cu multilayers. Sputter deposition is one of the mostly widely used methods to prepare metallic thin films. Fig. 2.1 shows schematically the triode RF sputtering system in our laboratory. During the deposition, energetic $Ar^+$ ions are accelerated into the Co and Cu targets, and knock off the target atoms. The ejected atoms are then deposited onto substrates placed above the targets. In order to prepare multilayers, the substrates are mounted on the substrate platform which can be rotated by a computer-controlled stepping motor. Two shutters driven by electromagnets are inserted between targets and substrates to regulate the deposition periods (and thus thicknesses) of the individual layers. Since the two shutters are opened and closed alternatively during deposition, they are also effective in avoiding the mixture of the two atomic fluxes. A cooling tank is installed for two purposes. First, for normal depositions, cooling water is circulated through the tank, which prevents the shutter-driving electromagnets from overheating. Second, for low temperature deposition, the substrate temperature can be stablized in the range between 0 $^{o}$C and -60 $^{o}$C by flowing liquid nitrogen through the tank. In addition, an electrical heater is embedded into the substrate holder, for heating the substrate up to 300 $^{o}$C. The substrate temperature is read by the computer via a thermocouple detector attached to the substrate holder.

Deposition rates are measured by a quartz-crystal monitor placed at the positions of the substrates. The rates were calibrated by comparison to thickness measurements on the deposited films using a DEKTAK thickness profiler and low-angle x-ray reflectivity measurements. It has been found that the deposition rates strongly depend on the growth parameters, such as sputtering gas pressure, RF power, and target-substrate distance. Reduced target-substrate distance increases the deposition rate, at the price of poorer uniformity over the area of substrate. As a compromise between these two factors, the target-substrate distance is fixed at 9.2 cm in this work. Fig. 2.2 shows the deposition rates for Co and Cu at this target-substrate distance with various sputtering pressures and

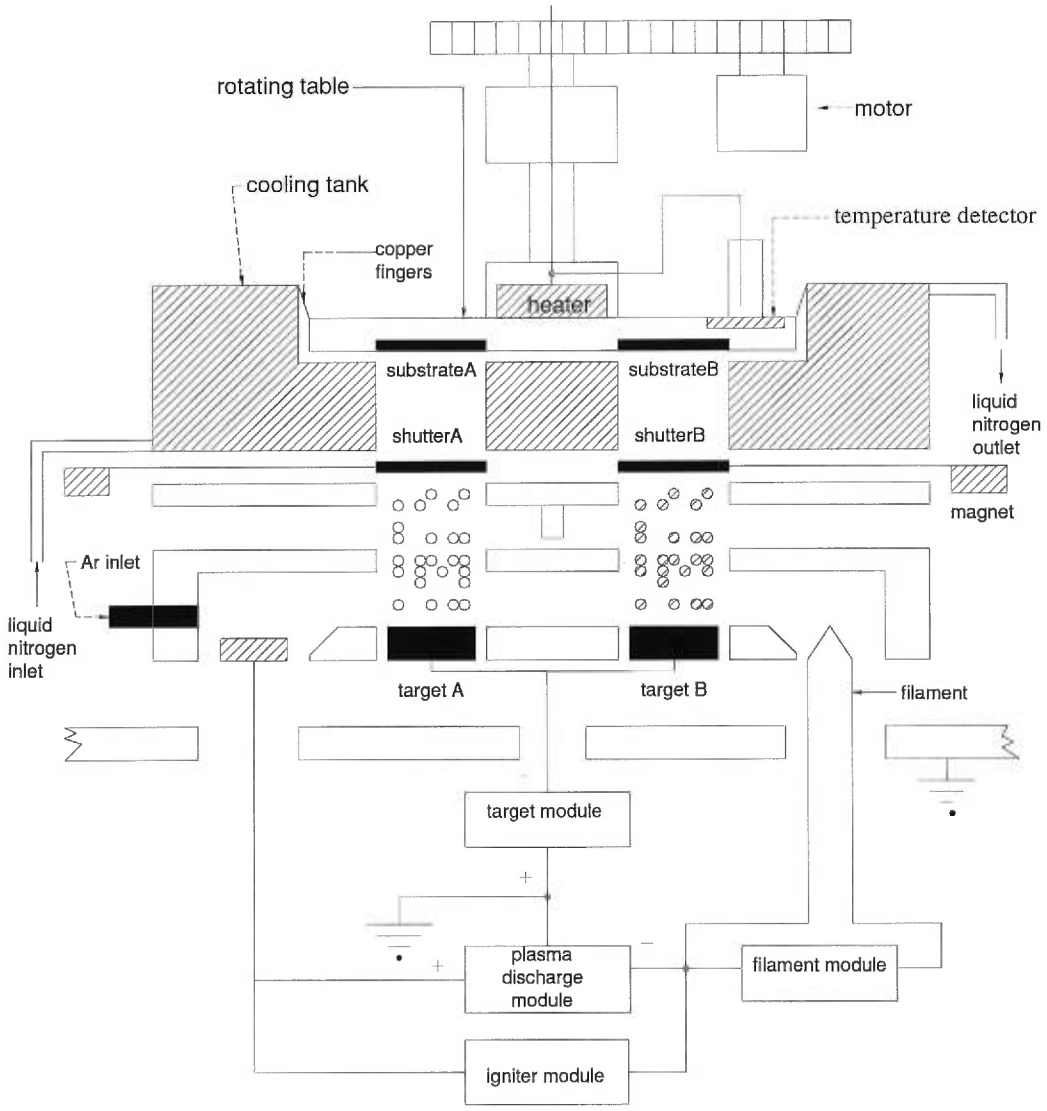


Figure 2.1: Schematic diagram of the sputtering system

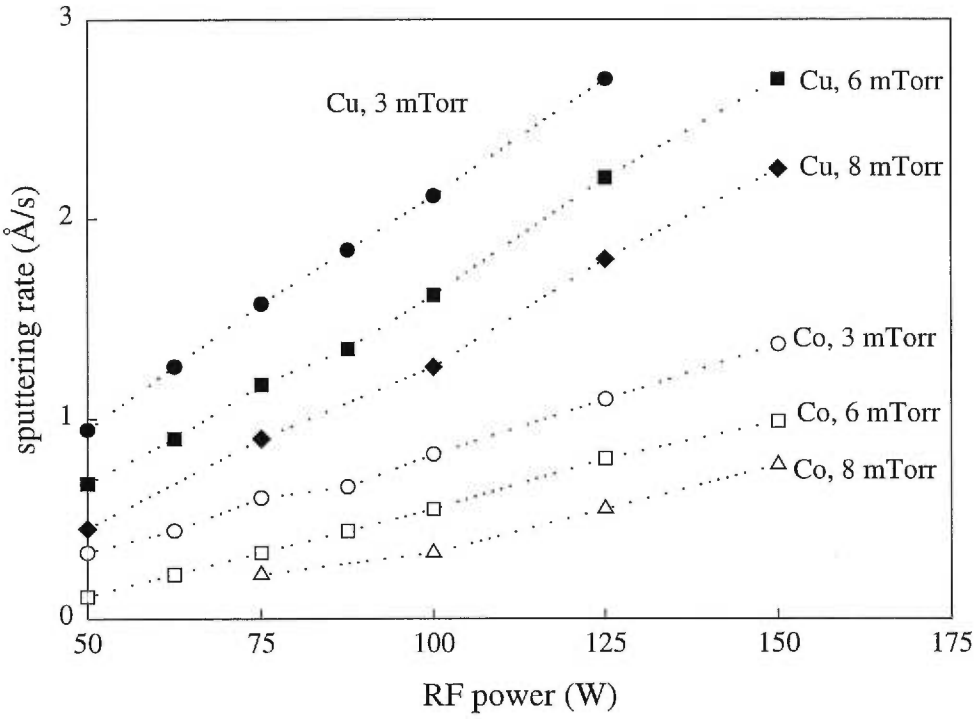


Figure. 2.2. Sputtering rates for Co and Cu as functions of RF power at various argon pressures.

RF powers. Since the sputtered atoms collide with gas molecules when travelling from target to substrate, increased gas pressure reduces the energies of the atoms and their chances of arriving at the substrates. As a result, the deposition rate decreases with increasing sputtering gas pressure. For a similar reason, the deposition rate also decreases with decreasing RF power. Furthermore, these factors also affect the structural quality of a multilayer. For example, increase of the sputtering pressure results in rough surfaces due to the enhancement of the self-shadowing effects, while decrease of the sputtering pressure might promote interfacial mixing and produce other structural defects. Taking these aspects into consideration, we have selected the moderate argon pressure of 6 mTorr and RF power of 125 W. With such a combination, the deposition rates are reasonably large (0.8 Å/sec for Co and 2.2 Å/sec for Cu), and the ratio between the deposition rates of the two elements is relatively small. According to our experience, such a choice leads to Co/Cu multilayers with good interfacial and crystallographic properties and the largest giant magnetoresistance values.

Prior to deposition, glass (Corning 7059) and silicon substrates are carefully cleaned by acetone and proponal solvents and dried by high purity air flux before being mounted on the substrate holder. The system is then pumped by a cryopump until the base pressure in the vacuum chamber reaches $1 \times 10^{-7}$ Torr. The targets are pre-sputtered (with the shutters closed) for 15 minutes to stabilize the system and substrate temperature before the desired film is sputtered onto the substrate. Unless otherwise stated, a Co/Cu multilayer starts with a Cu buffer layer of 50 Å which is followed by a number of repeated Co/Cu bilayers, and ends up with a 50 Å (including the thickness of the top Cu layer in the repeated pattern) Cu cap layer. The buffer layer is deposited to improve the interfacial qualities of the subsequent layers, while the cap layer serves to protect the rest of the film from oxidization. For simplicity, however, the buffer and cap layers are ignored in the notation of a multilayer configuration hereafter. Fig. 2.3 presents the in-plane dimensions of a multilayer sample, as defined by sputtering through a mask placed in front of the substrate.

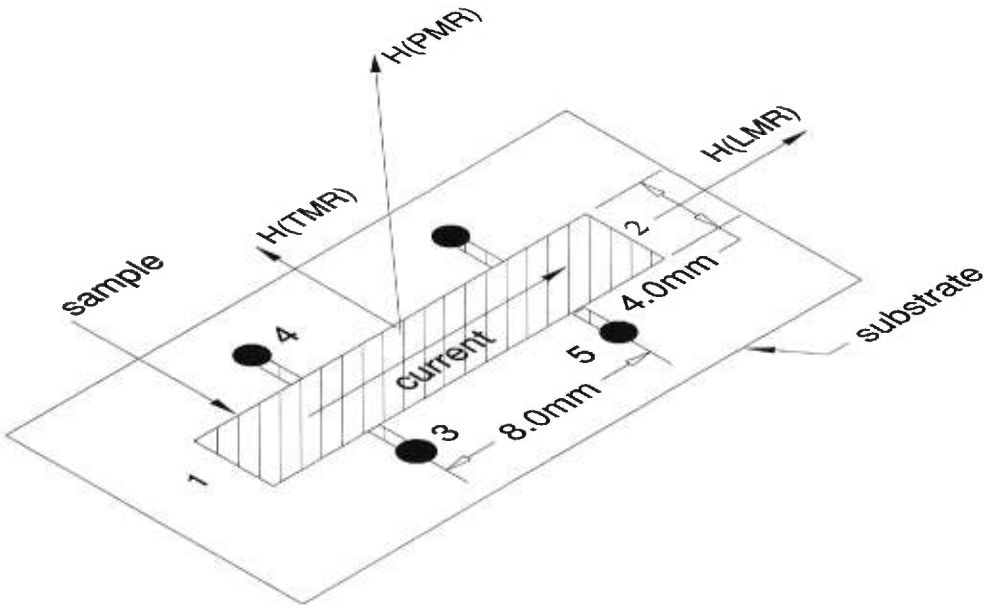


Figure 2.3. Sample dimensions and geometries for transport measurements

## 2.2. Structural Modification Techniques

In order to study the correlation between structure and physical properties of Co/Cu multilayers, various *ex-situ* techniques for structural modification have been used. This section describes two of these methods: thermal annealing and ion irradiation.

### 2.2.1. Thermal Annealing

Thermal annealing is one of the simplest techniques to modify the structure of a metallic thin film. Post-growth heat treatment drives a sample towards its equilibrium state, promotes grain growth and induces atomic diffusion. In our experiments, the sample is mounted onto a copper holder which can be electrically heated up to 400 °C. The annealing times range from 1 hour to 4 hours. During annealing, the sample and the sample holder are placed inside a metallic chamber, whose vacuum is maintained below 1 $\times 10^{-6}$ Torr.

### 2.2.2. Ion Irradiation

Ion-beam irradiation experiments were performed using the Université de Montréal Tandetron accelerator [56], manufactured by High Voltage Engineering Europe BV. The accelerating voltage can be varied from 50 kV to 1.7 MV. In this work, 1 MeV $Si^+$ ions from the accelerator were used to bombard the Co/Cu multilayers at normal incidence in a vacuum of $10^{-7}$ Torr. This ion energy was selected such that its projected range was much greater than the total film thickness (about 1000 Å) so that a uniform damage profile throuhout the multilayer is expected. According to TRIM simulations [57], the energy deposited per unit length due to nuclear collisions is about 35 eV/Å . The energy loss of the 1 MeV $Si^+$ ions in the samples of such thicknesses amounts to roughly 200-300 keV; only a very small fraction (<0.1%) of the implanted ions come to rest in the multilayer, the rest being transmitted or backscattered.

To ensure the irradiation on a sample is well defined and laterally homogeneous, a raster scanner employs horizontal and vertical scanning over a region that is at least as

wide and as high as the size of the aperture placed in front of the sample, plus twice the width of the ion beam. This minimizes edge effects. In addition, an electrostatic deflector is used to reject neutral atoms to prevent these atoms from hitting the sample in the middle of the scanned area.

To avoid heating effects during irradiation, the beam current was maintained below 50 nA/cm$^2$. Furthermore, the samples were placed in thermal contact with the copper sample holder, which is hollow and filled with liquid nitrogen (77 K) during irradiation. The temperature of the sample holder was checked before and after irradiation.

The ion dose was measured by monitoring the ion current on the sample holder that is electrically isolated from the flange used to mount it on the vacuum chamber. A screen biased at –500 V is wrapped around the sample holder to repel secondary electrons emitted from the sample. In this study, the applied ion doses ranged from $10^{12}$ ions/cm$^2$ to $10^{17}$ ioms/cm$^2$. These ion doses resulted in about 0.001 to 100 displacements per atom as estimated by TRIM simulations. The structural effects induced by ion irradiation at such doses will be described in detail in chapter 5.

## 2.3. Structural Analysis Techniques

Low-angle x-ray reflectivity measurements and high-angle x-ray diffraction measurements were performed to characterize the interface morphology and crystallographic structure of the multilayers respectively. In this section, we describe the experimental setups of these techniques. Data analysis methods will be discussed in the next chapter.

### 2.3.1. Low-angle X-ray Reflectivity Measurements

Low-angle x-ray reflectivity experiments were carried out using a high-resolution triple-axis four-circle diffractometer with a 2.2 kW Cu-K$\alpha$ ($\lambda \cong 1.54$ Å) tube source, as schematically shown in Fig. 2.4. By positioning two identical Ge (111) single crystals in front and behind the sample as monochromator and analyzer respectively, a resolution of

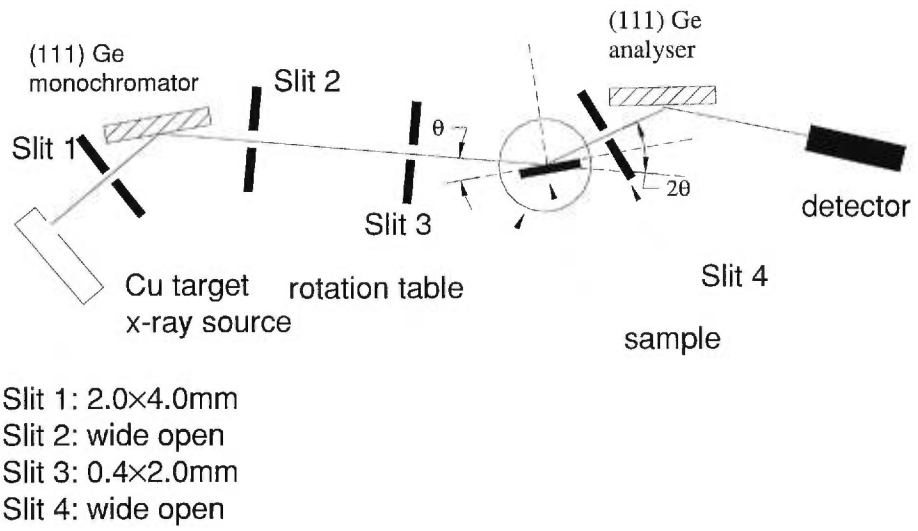


Figure 2.4. The setup of low-angle x-ray reflectivity measurements

0.01 degrees, full width at half maximum (FWHM), was achieved. The slit sizes varied slightly throughout this work, and the typical settings are shown in the figure. The total distance between the source and the sample was 1055 mm. For a conventional (θ, 2θ) scan, the intensity of total reflection (below critical angle) was between $10^4$ and $10^5$ counts per second (cps), and the noise level was around 0.2 cps. Most mesurements were performed in a 2θ range between 0.3° and 8° with a step of 0.01°.

To have a full characterization of the interface structure of a multilayer, three geometries[58] have been used, as shown in Fig. 2.5. The first geometry is the conventional (θ, 2θ) scan (Fig. 2.5a). In this setup, the angle between the incident beam and the detector remains twice as large as the incident angle (θ) between the beam and the sample surface, and the specular reflectivity intensity is collected as a function of θ. In the second setup, offset (θ, 2θ), the sample is tilted by a small fixed amount (Δω typically between 0.2° and 0.5°), and then a conventional (θ, 2θ) scan is taken. This is illustrated in Fig. 2.5(b). With the offset (θ, 2θ), diffuse scattering intensity is measured as a function of θ. In the third setup, rocking scan, the x-ray scattering intensity is measured by rocking the sample through the specular reflection with fixed 2θ, as shown in Fig. 2.4(c). Fig.

2.5(d) further presents the trajectories through reciprocal space of the three kinds of scans[59]. By combining these methods, not only the average magnitude but also the vertical or lateral correlation length of the interfacial roughness of a multilayer can be determined. Details about the information conveyed by the spectra of each kind of scan will be addressed in chapter 3.

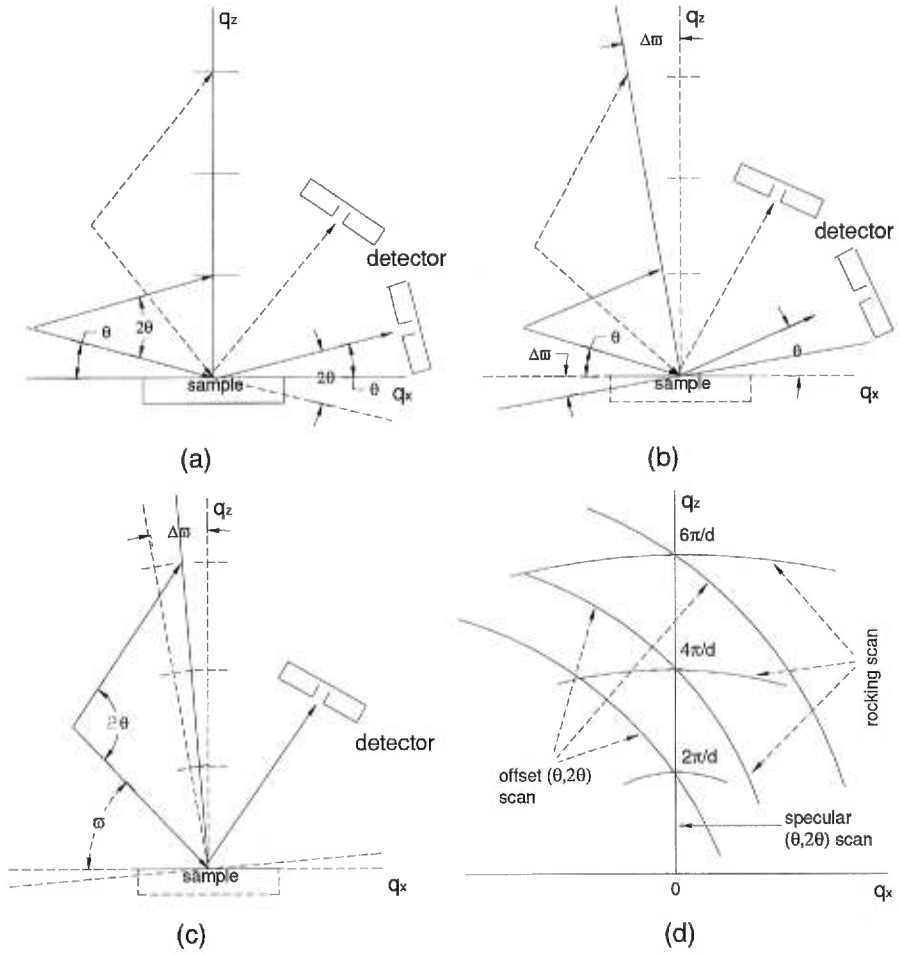


Figure 2.5. Three different low-angle x-ray measurement geometries: (a) specular (θ, 2θ) scan; (b) offset (θ, 2θ) scan; (c) rocking scan. (d) shows the trajactories through reciprocal space of the three types of scans described in (a)-(c). In the figures, $q_x$ and $q_z$ are the vertical and lateral compoments of the scattering vector, respectively. d is the bilayer period of a multilayer.

### 2.3.2. High-angle X-ray Diffraction Measurements

High-angle x-ray diffraction measurements were performed using an automated Nicolet-Stöe L11 powder diffractometer with Cu-Kα radiation. The system consists of a 2.2 kW Cu-target tube source and the detector-analyzer assembly. Further details of the system can be found in reference [60]. The instrumental broadening for the diffractometer estimated from Al powder diffraction was 0.15 degrees, FWHM. Conventional (θ, 2θ) scans were carried out in 2θ range between 40° and 55° (for most samples), or between 40° and 100° (for selected samples), with a step of 0.1 °.

## 2.4. Measurements of Transport and Magnetic Properties

### 2.4.1 Transport Measurements

Electrical resistivity, magnetoresistnace and Hall effects were measured at room temperature using a computer-controlled high-resolution ac bridge with 4-point method. During the measurements, separate but identical alternating currents are driven through a sample and a standard resistor. The standard voltage is divided using an inductive voltage divider and compared with the signal across the sample using a lock-in amplifier. Details of the system has been described elsewhere [61]. The value of sample resistance is read directly in ohms and small changes in this value are obtained as a voltage which is linearly related to the change in resistance. One of the primary features of the system is its high sensitivity. It can easily detect changes in resistance of $10^{-5}$ Ω in a 1 Ω resistor, which permits measurement of very small variations in resistance under magnetic field.

The magnetic field was generated by an electromagnet with maximum field capacity of 1.5 Tesla. The magnet can be rotated so that the magnetic field can be imposed at any direction either in the sample or normal to it. On the contrary, the electrical current is always applied within the sample plane. Fig. 2.3 also shows the relationship between the directions of the magnetic field and the electrical current for the various MR configurations. The current flows between point contacts 1 and 2 in all the configurations. The resistance and magnetoresistance were measured between contacts 3

and 5, and the Hall effect was measured between contacts 3 and 4. To measure the longitudinal magnetoresistance (LMR), the magnetic field is in the film plane and parallel to the current direction. To measure the transverse magnetoresistance (TMR), the magnetic field is also in the film plane but perpendicular to the current direction. Finally, to measure the perpendicular magnetoresistance (PMR) and Hall resistance, the magnetic field is perpendicular to the film plane. Electrical contact between sample and leads is made using silver paste. The field sweep or data acquisition was carried out automatically under computer control.

### 2.4.2. Magnetic Measurements

The magnetization curves of the multilayer samples were measured with a vibrating sample magnetometer (VSM), as schematically shown in Fig. 2.6. VSM is a simple but effective apparatus to measure sample magnetization. As illustrated, the thin film sample is fixed at the bottom of a plastic rod with silicone vacuum grease, and is carefully positioned at the center of the detector coil system. As the rod vibrates vertically with a frequency of 84 Hz, the magnetic flux through the coils also varies at this frequency. The resulting signal, which is proportional to the sample magnetization, is analyzed by a lock-in amplifier. The calibration of the system was made by measuring a cobalt standard sample. The sensitivity of the system is better than $10^{-5}$ emu. Magnetic field up to 8 kOe can be generated and can be oriented in any direction within the film plane. In order to remove the substrate signal, blank Si or glass substrates were also measured.

A number of zero-field-cooled (ZFC) and field-cooled (FC) magnetization runs were made using a modified Quantum Design 6000 Physical Property Measurement system (PPMS) at McGill University between 4.2 K and 300 K. During the measurements, the external field was fixed at a value typically between 10 Oe and 40 Oe, while the temperature was varied. In addition, the same system was used to measure magnetization curves at low temperature. In all cases, the samples were aligned so that the magnetic field was parallel to the film plane.

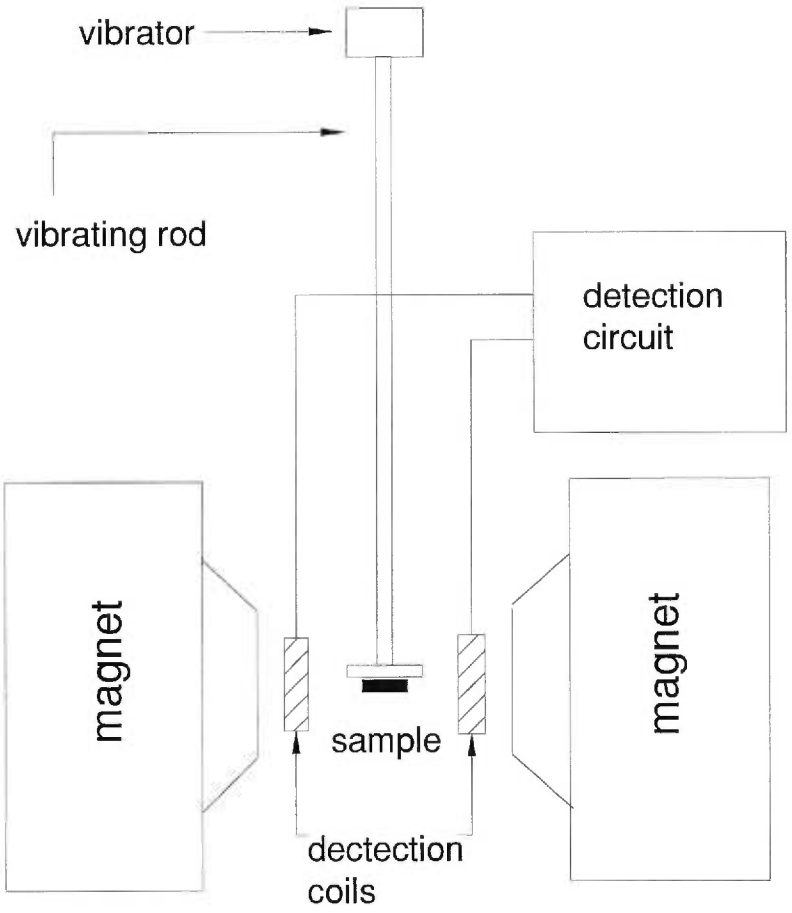


Figure 2.6. The schematic diagram of VSM

# Chapter 3: Structural, Magnetic and Magnetotransport Properties of Co/Cu Multilayers

## 3.1. Structural Analysis of Co/Cu Multilayers

The structural parameters of Co/Cu multilayers play crucial roles in determining their physical properties. Hence, a thorough structural analysis is an essential step in understanding the magnetic and magnetotransport behaviours of a Co/Cu multilayer. As mentioned earlier, Co/Cu multilayers exhibiting GMR and other interesting magnetic properties typically have compositional modulation wavelengths of 1-10 nm. At such small scales, x-ray scattering has been widely used as a non-destructive technique to characterize thin-film structures[62]. X-ray scattering from superlattices can be divided into two regimes, which are commonly referred to as "low angle" and "high angle" respectively. The low-angle regime is defined by $|q| \sim 2\pi/\Lambda$, while the high-angle regime is given by $|q| \sim 2\pi/d$, where q is the scattering transfer vector (the difference between the incident and reflected wave vectors), $\Lambda$ is the artifically induced bilayer period, and d is the average interatomic spacing parallel to the scattering vector. At high angles, x-ray diffraction yields information about a system on a crystallographic scale: lattice constants, texture, strains, grain sizes etc., while at low angles, it yields information related to the mesoscopic structure of the material. Low-angle x-ray scattering techniques can be further grouped into two categories in terms of the momentum transfer parallel to ($q_{\parallel}$) and perpendicular to ($q_{\perp}$) to the film surface: specular reflectivity measurements (with $q_{\parallel}=0$) and non-specular scans (with $q_{\parallel}\neq 0$). Specular scans provide information on vertical composition modulation of a superlattice structure, such as bilayer period, composition profile, interfacial roughness etc. On the other hand, non-specular data provide information on the lateral roughness correlation which is particularly valuable in distinguishing various possible origins of interfacial roughness. By combining these x-ray scattering techniques, and moreover, by comparing the results obtained from these techniques with the theoretical calculations, precise structural parameters can be obtained for Co/Cu multilayers in order to provide a basis upon which

the correlations between the structural, magnetic and magnetotransport properties of Co/Cu multilayers can be investigated systematically.

### 3.1.1. Low-Angle Specular X-ray Reflectivity Analysis

Low angle specular x-ray measurement is performed with equal incident and reflected angles (thus $q_{\parallel}=0$), and records reflected x-ray intensities as a function of $q_{\perp}$. The data analysis is based on a standard optical model. For an incoming x-ray beam illuminating a film surface, the refractive index n of most materials in the x-ray wavelength range is slightly less than 1, and can be expressed as $n=1-\delta-i\beta$, where $\delta$ and $\beta$ can be written as

$$\delta = \frac{N_o r_e \lambda^2}{2\pi}(f_o + \Delta f') = \frac{r_e \lambda^2}{2\pi}\rho_e \tag{3.1}$$

$$\beta = \frac{N_o r_e \lambda^2}{2\pi}(\Delta f'') = \frac{\lambda}{4\pi}\mu \tag{3.2}$$

where $r_e$ is the classical electron radius $e^2/mc^2 = 2.818\times10^{-13}$ cm, $N_0$, the number density of atoms, $\lambda$, the x-ray wavelength, $f_0$, the atomic scattering factor at zero momentum transfer (equal to Z, the atomic number of the considered element); $\Delta f'$ and $\Delta f''$ are the real and imaginary parts of the dispersion corrections to $f_0$, $\rho_e$, the electron density and $\mu$, the linear absorption coefficient. The critical angle for total external reflection $\theta_c \approx \sqrt{2\delta}$ has values typically in the range of $0.2^\circ - 0.6^\circ$ for an x-ray wavelength around 1.5 Å. For incident angles greater than the critical angle, most of the x-ray beam is refracted into the material, allowing interference between reflections from various interfaces.

Fig. 3.1 shows the x-ray reflectivity spectra of a nominal 800 Å pure Co film and a 800 Å pure Cu film deposited on Si substrates. In the figure, the data are plotted on a logarithmic scale as functions of the vertical scattering vector $q_{\perp}=4\pi\sin\theta/\lambda$, where $\theta$ is the incident angle. As shown, Co and Cu give very close critical angles around $0.3^\circ$ or $q_c$

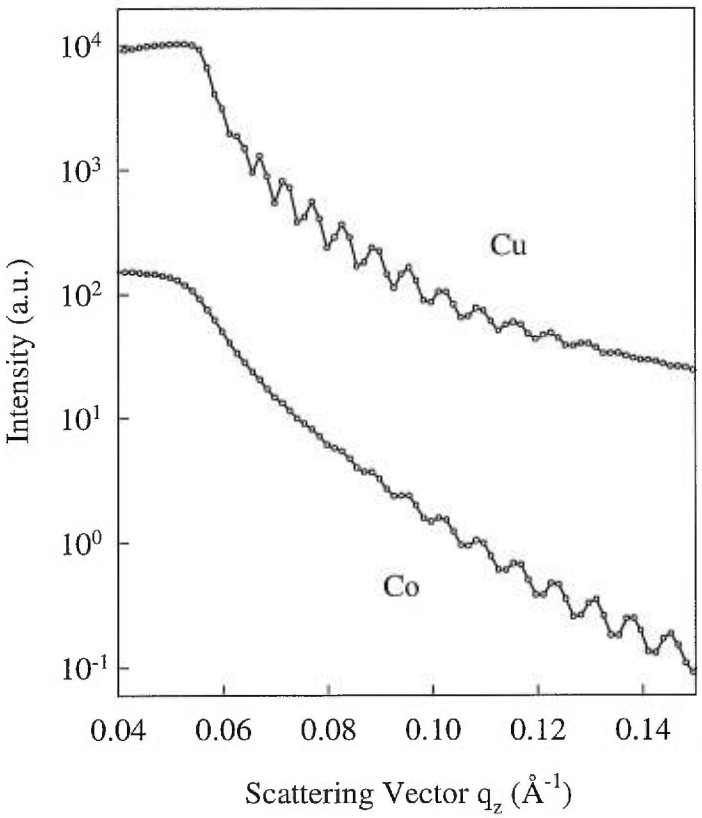


Figure 3.1. Low-angle x-ray reflectivity spectra for a pure Co film and a pure Cu film. Curves have been displaced for clarity.

$\approx 0.051$ Å$^{-1}$. Above the critical angles, rapid oscillations are clearly visible for both Co and Cu films. Such oscillations, usually called Kiessig fringes or finite-size oscillations, arise from multiple interference between beams reflected at the top surface of the film and at the film-substrate interface. The thickness of a film can be determined by the positions of these oscillations using the modified Bragg law

$$\sin^2\theta = \sin^2\theta_B + 2\delta \tag{3.3}$$

where $\theta$ is the position of the oscillation peak and $\sin\theta_B$ satisfies the relation

$$\sin\theta_B = \frac{n\lambda}{2t} \tag{3.4}$$

where t is the thickness of the film. Using Eq. 3.3 and Eq. 3.4, the thickness of Co and Cu films are found to be 776 Å and 815 Å respectively, in agreement with the nominal values to within 10%. Fig. 3.1 also shows that for the Cu film the Kiessig oscillations disappear at high $q_\perp$, suggesting the Cu film is relatively rougher than the Co film.

Fig. 3.2 presents the x-ray reflectivity spectrum of a [Co(17 Å)/Cu(34 Å)]×30 multilayer. For a Cu/Co multilayer structure that is highly periodic along the film growth direction, constructive interference occurs among the beams reflected at the Co-Cu and Cu-Co interfaces, which leads to strong superlattice Bragg peaks superimposed on the Kiessig fringes. The bilayer period (Λ) of a multilayer can be determined from the superlattice peak positions by using modified versions of Eq. 3.3 and Eq. 3.4, in which the total thickness (t) is replaced by Λ. In the case of Fig. 3.2, the bilayer period of the multilayer is found to be 50.7 Å, a value which agrees well with the nominal value (51 Å). Furthermore, the disappearance of the third-order superlattice peak confirms that the ratio between the Cu-layer thickness and Co-layer thickness is close to 2:1.

The intensities of the superlattice peaks are very sensitive to the interface quality of a multilayer. Increasing interface roughness strongly suppresses the intensities of the superlattice peaks (especially the high-order peaks). In Fig. 3.2, first and second order superlattice peaks are clearly visible, indicating a well-defined compositional modulation along the film growth direction. Nevertheless, in order to acquire quantitative information about the interface roughness, the multilayer structure has to be carefully modeled, and the experimental data has to be compared with the calculated x-ray spectra.

In this work, the x-ray reflectivity is calculated based on a matrix method[63]. Briefly, any single layer in a multilayer structure can be characterized by a matrix (2×2) as a function of the layer thickness, the complex refractive index, and the wave vector of the incident beam. The multilayer matrix is obtained from the product of the matrices of individual layers. The reflection coefficient of the multilayered film is then calculated using this matrix. Details of the method can be found elsewhere[64].

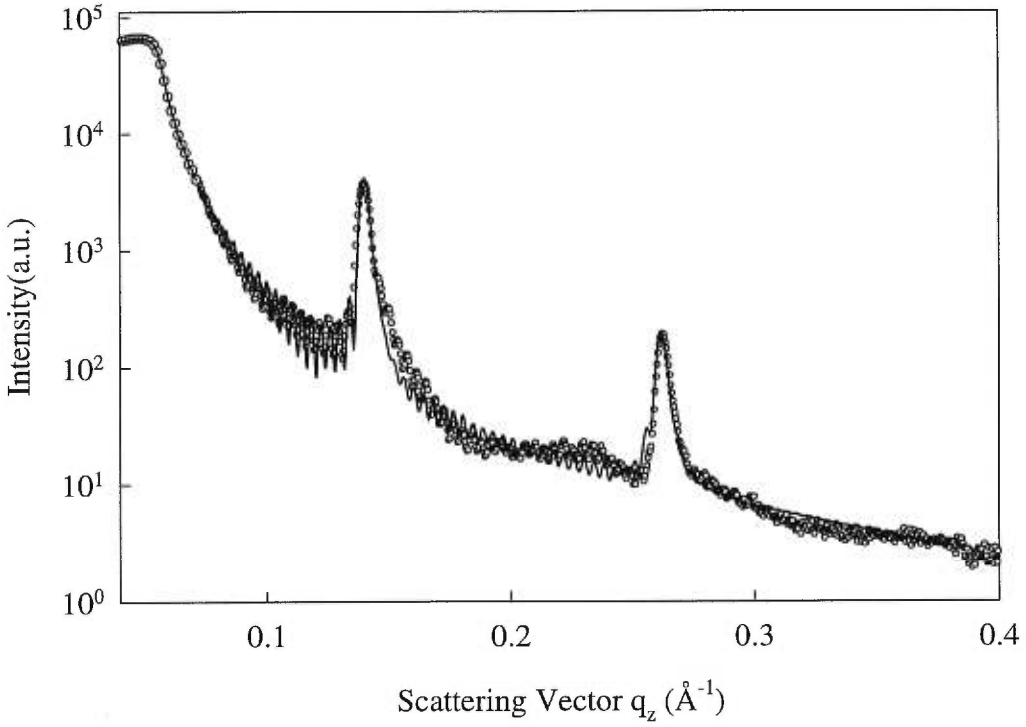


Figure 3.2. Low-angle x-ray reflectivity spectra for a [Co(17 Å)/Cu(34 Å)]×30 multilayer. The solid line is the fitted curve.

In the calculation of the x-ray reflectivity for a multilayer structure, a large number of factors have to be taken into account in order to simulate the real situation. Therefore, fitting calculation to experimental data involves optimizing a great number of parameters that may be correlated to each other. Fortunately, in practice, it is observed that these parameters can be separated into several groups. The parameters in each group mainly affect some features of a spectrum, and the correlation among the parameters belonging to different groups is relatively insignificant. These parameters are summarized as follows:

1. Cu-layer thickness ($t_{cu}$) and Co-layer thickness ($t_{co}$): $t_{cu}$ + $t_{co}$ determine the positions of the superlattice peaks. The ratio of $t_{cu}$/ $t_{co}$, on the other hand, affects the *relative* intensities of the superlattice peaks of various orders.

2. Interface roughness ($\sigma_i$), interfacial mixing width ($t_i$), and thickness gradient ($\Delta t$). Increase in any of these parmeters reduces the intensities of the superlattice peaks.

$\Delta t$ represents a macroscopic thickness variation that can be caused by a continuous change of growth conditions (e.g., drift in the sputtering rate), and can be distinguished from $\sigma_i$ and $t_i$ in that it not only suppresses superlattice peaks but also leads to peak broadening. On the contrary, neither $\sigma_i$ nor $t_i$ affects the long-range order of the composition profile and only reduce the peak intensities. $\sigma_i$ represents a locally sharp compositional boundary whose depth varies irregularly in the plane of the structure. In this work, interface roughness is incorporated into the calculation by assuming a Gaussian form (with a Debye-Waller factor multiplied into the multilayer reflectivity). Finally, $t_i$ refers to the width of the interfacial region where Co and Cu atoms are mixed and are randomly distributed. The Co/Cu system has a large positive heat of mixing and, in equilibrium, the two elements are virtually immiscible. Hence, $t_i$ is not incorporated into the x-ray reflectivity calculations for as-deposited Co/Cu multilayers. However, for multilayers modified by highly non-equilibrium techniques (for example, ion irradiation), such an effect should be considered.

3. Surface roughness ($\sigma_o$) and substrate roughness($\sigma_s$). $\sigma_o$ refers to the roughness of the outer surface of a film. $\sigma_s$ refers to the roughness of the interface between the film and the substate. With increasing $\sigma_s$ or $\sigma_o$, the intensities of the total-thickness oscillations (Kiessig fringes) decrease. These two parameters also strongly affect the overall profile of a spectrum. With greater $\sigma_o$ or $\sigma_s$, the reflected intensity drops more rapidly with scattering vector ($q_\perp$). In general, $\sigma_o$ has larger impact on the profile at small $q_\perp$ (incident angles), while $\sigma_s$ primarily affects the profile in the region with large $q_\perp$.

4. Oxide overlayer thickness ($t_o$), electron density of the overlayer ($n_o$), and linear absorption coefficient of the overlayer ($\alpha_o$). It is found that the quality of the fits to the experimental data can be dramatically improved by introducing an oxide layer on the top of a film. The existence of such oxide overlayers is responsible for some long wavelength oscillations observed in many multilayer samples. The oxide overlayer thickness can be determined by the wavelength of the oscillation whereas the electron density and absorption coefficient are determined by its strength. Typically, $t_o$ is around 20 Å, and $n_o$ and $\alpha_o$ are about 50% of the values of the cap layer (usually Cu) of the film.

In the calculation of the reflectivity, bulk values of electron density and absorption coefficient are used for Co and Cu. At the energy of Cu $K_\alpha$ radiation, E=8052 eV, the electron densities for Co and Cu are 2.25 $Å^{-3}$ and 2.28 $Å^{-3}$ respectively, and the contrast between them is almost zero. However, for Cu $K_\alpha$, the difference between the linear absorption coefficients of Co and Cu (3079 $cm^{-1}$ and 375 $cm^{-1}$ ) is sufficiently large to produce strong superlattice Bragg peaks and allows one to extract quantitative information about the roughness of Co-Cu interfaces.

The fitting process is outlined as follows. First, surface roughness ($\sigma_o$) and substrate roughness ($\sigma_s$) are adjusted to match the overall profile of the spectrum as well as the intensities of the Kiessig fringes. Next, if any long wavelength modulation is observed, an oxide overlayer thickness is added. Then, the Cu- and Co-layer thickness are adjusted to match the positions of the superlattice peaks. Next, the thickness gradient ($\Delta t$) is introduced to match the widths of the superlattice peaks and finally the interface roughness ($\sigma_i$) is adjusted to match the intensities of the superlattice peaks. Notice, however, that the above phases are not always distinct from each other, and the manual process usually has to be iterated until a fairly good agreement between the calculation and experimental data is achieved. At this stage, all the parameters are refined in a non-linear least square fitting procedure that minimizes

$$\chi^2 = \sum_{i=1}^{M} \left(R_i^m - R_i^c\right)^2 / w_i^2, \tag{3.5}$$

where $R_i^m$ and $R_i^c$ are the experimental and calculated x-ray intensities, respectively, M, the total number of data points, and $w_i^2$, the weighting function of the form,

$$w_i^2 = (\Delta R_i^m)^2 + 0.05\times(R_i^m)^2, \tag{3.6}$$

where $\Delta R_i^m$ is the uncertainty of the measurement (error bar).

The solid line in Fig. 3.2 plots the fitted curve to the x-ray reflectivity data for the [Co(17Å)/Cu(34Å)]×30 multilayer. As shown, the primary features, such as critical

angle, overall profile, Kiessig fringes, superlattice peak positions, intensities, widths, are all in excellent agreement with the experimental data. The relevant structural parameters obtained from the fitting are listed in Table 3.1. The rms interface roughness of the multilayer is found to be 5.2 Å (~3 monolayers). The top surface roughness and substrate roughness are 18.5 Å and 8 Å respectively. The thickness gradient is 0.14% (or 0.07 Å / period). Finally, it is necessary to include in the calculation an oxide overlayer with a thickness of 9.5 Å and 60% of the Cu-electron density in order to fit the data adequately.

Fig. 3.3. shows the reflectivity spectra of a series Co/Cu multilayers with various thickness combinations and period numbers. These configurations are selected due to their very interesting magnetic and magneto-transport properties that will be discussed later. For the samples with very thin layers, i.e, [Co(10 Å)/Cu(10 Å)]×50 and [Co(5Å)/Cu(20Å)]×50, only the first-order peaks are visible, indicating that structural imperfections at the interfaces are significant. For samples with thicker individual layers, higher-order peaks are visible. For the [Co(50 Å)/Cu(75 Å)]×14 multilayer, the superlattice Bragg peaks are clearly visible up to the 6th order. As well, with increasing bilayer period, the superlattice peaks shift systematically toward lower angles (scattering vectors). Noticeably, the ratio between the Co-layer thickness ($t_{co}$) and the Cu-layer thickness ($t_{cu}$) strongly affects the *relative* intensities of the superlattice peaks of different orders. For instance, due to the 2:3 ratio between $t_{co}$ and $t_{cu}$, the 5th superlattice peak for the [Co(50 Å)/Cu(75 Å)]×14 multilayer is completely suppressed while the 6th peak can still be seen. The disappearance of the 3rd superlattice peak for [Co(17 Å)/Cu(34 Å)]×30 multilayer can similarly be attributed to the 1:2 ratio between $t_{co}$ and $t_{cu}$. Combining such information and the bilayer period ($t_{co} + t_{cu}$) determined from superlattice peak positions, the individual layer thickness ($t_{co}$ and $t_{cu}$) can be verified definitively by x-ray reflectivity analysis.

The solid lines in Fig. 3.3 present the fitted curves to the spectra. The structural parameters extracted from the fitting are also listed in Table 3.1. One interesting conclusion drawn from the fitting lies in the fact that, for all the five samples with very different layer-thickness combinations, the interface roughness values are similar (4-6 Å), suggesting that the interface configuration of a Co/Cu multilayer does not dramatically

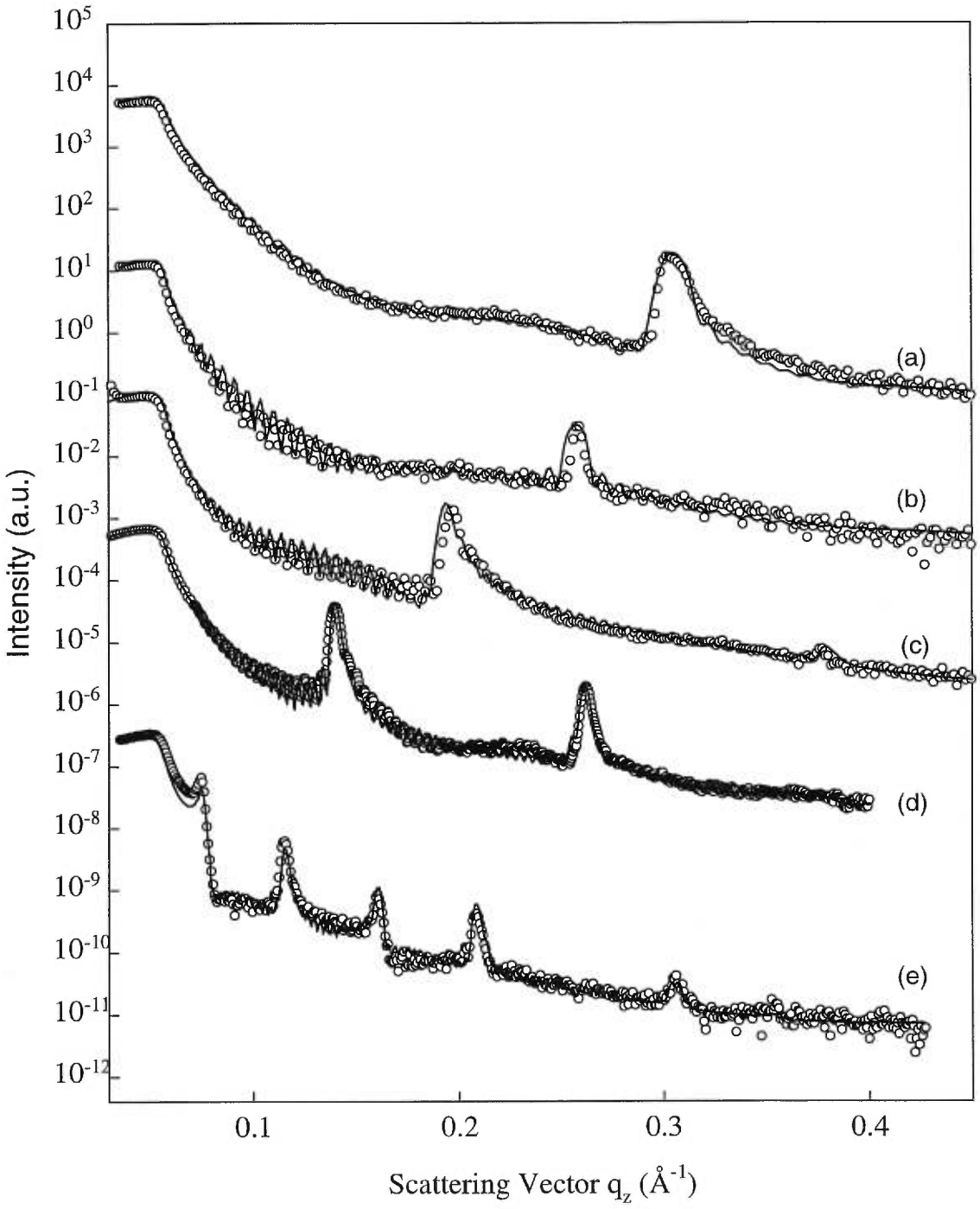


Figure 3.3. X-ray reflectivity data (circles), along with the fitted results (solid lines) for a series of Co/Cu multilayers with various layer thicknesses:
(a) [Co(10 Å)/Cu(10 Å)]×50, (b) [Co(5 Å)/Cu(20 Å)]×50, (c) [Co(15 Å)/Cu(22 Å)]×30, (d) [Co(17 Å)/Cu(34 Å)]×30, and (e) [Co(50 Å)/Cu(75 Å)]×14.

depend on the thickness of the individual layers. For [Co(10 Å)/Cu(10 Å)]×50 and [Co(5 Å)/Cu(20 Å)]×50 multilayers, however, interface roughness of 4-6 Å is comparable to the layer thickness, and is expected to disrupt the multilayer structures significantly. For multilayers with thicker layers, such interface roughness may have little effect on the integrity of a multilayer. In contrast to interface roughness, the parameters describing the oxide overlayer or outer surface roughness vary largely from sample to sample.

To study how the interface roughness is cumulated from one interface to another, the x-ray reflectivity was measured for a series of Co/Cu multilayers with the same layer-thickness combination, Co(17 Å)/Cu(34 Å), but different numbers of periods. Fig. 3.4 illustrates the measured spectra (dots) and fitted curves (solid lines) for the multilayers with 10, 20 and 30 periods. The parameters obtained from the fitting, again, are listed in Table 3.1. From the figure, the frequency of the Kiessig fringes increases but the intensities decrease with increasing number of bilayers (or total thickness of a film). In theory, if the number of bilayers in a multilayer structure is N, the number of Kiessig fringes between each pair of superlattice peaks is N-1. An inspection of these fringes permits us to verify the number of bilayers in a multilayer. For all three multilayers, the first and second order superlattice peaks are visible, and their intensities increase with increasing number of bilayers. However, such an increase in peak intensities with number of bilayers can be understood in terms that, with more bilayers, more interfaces contribute to the superlattice peaks, and does not necessarily mean interface structures are improved with increasing number of bilayers. On the contrary, as listed in Table 3.1, fitting to these spectra indicates that the interface roughness is actually increased from 4.2 Å for 10-period multilayer, to 4.8 Å for 20-period multilayer and 5.2 Å for 30-period multilayer. This evaluation suggests that the accumulation of interface roughness is possible for Co/Cu multilayers, but the effect may not increase interface roughness dramatically, at least for multilayers with 30 periods or less. It also suggests that all the Co/Cu interfaces can be considered identical for such multilayers.

In summary, structural parameters of our Co/Cu multilayers are have been determined by low-angle x-ray reflectivity analysis. Fitting to the spectra confirms that these multilayers are of reasonably good interface quality, with small interface roughness limited to two or three monolayers, and virtually independent of individual layer

thickness and number of bilayers. The interface roughness of a Co/Cu multilayer, however, does strongly depend on deposition conditions, which are discussed in the next chapter.

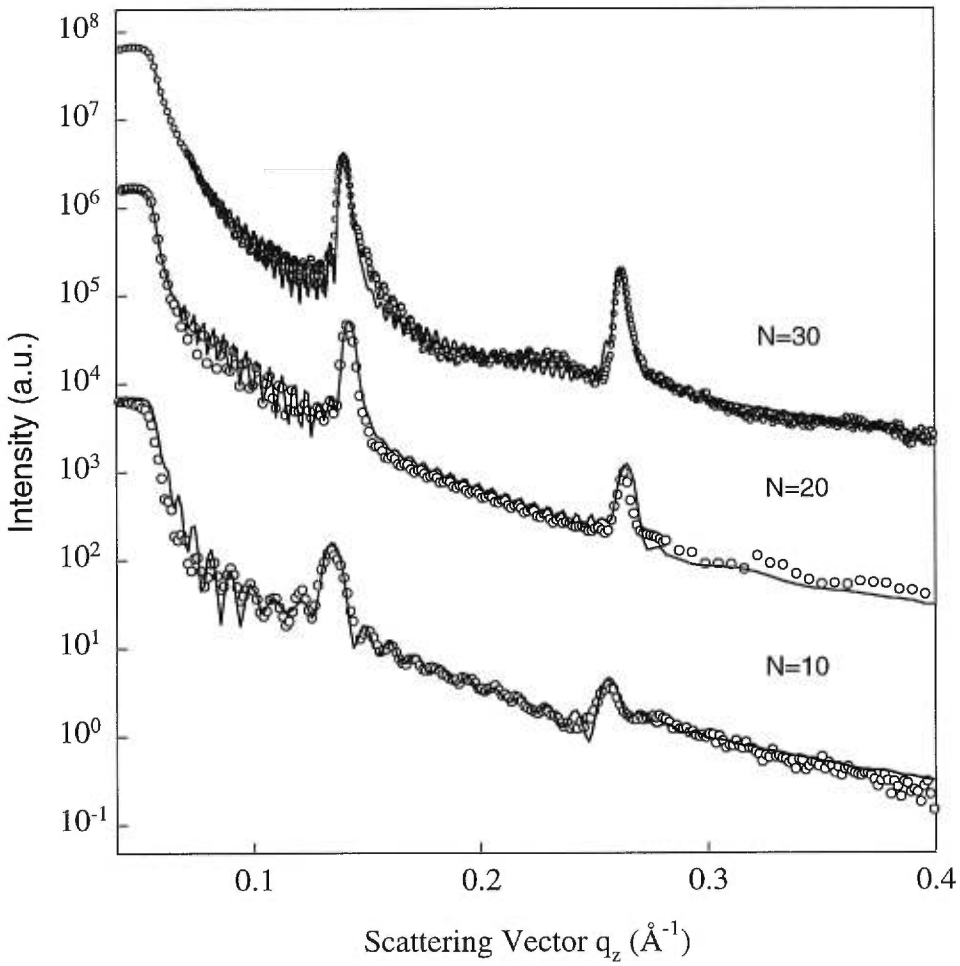


Figure 3.4. X-ray reflectivity data (circles), along with the fitted results (solid lines) for a series of [Co(17 Å)/Cu(34 Å)] ×N multilayers with different numbers of bilayer periods.

| Nominal | $t_{co}$(Å) | $t_{cu}$(Å) | $t_{o}$(Å) | $\sigma_o$(Å) | $\sigma_s$(Å) | $\sigma_I$(Å) | Δt(%) |
|---|---|---|---|---|---|---|---|
| [Co(17Å)/Cu(34Å)]×30 | 16.3±0.2 | 33.8±0.2 | 9.5±0.6 | 18.5±1.2 | 8.0±1.2 | 5.2±0.3 | 0.14±0.02 |
| [Co(17Å)/Cu(34Å)]×20 | 16.2±0.2 | 33.8±0.2 | 15.8±0.5 | 24.0±1.4 | 12.1±0.7 | 4.8±0.2 | 0.17±0.01 |
| [Co(17Å)/Cu(34Å)]×10 | 16.9±0.2 | 34.2±0.2 | 21.2±0.3 | 18.0±0.9 | 17.5±1.0 | 4.2±0.3 | 0.06±0.01 |
| [Co(10Å)/Cu(10Å)]×50 | 10.5±0.1 | 10.5±0.1 | 11.2±0.5 | 11.0±1.7 | 19.8±1.2 | 4.6±0.2 | 0.07±0.01 |
| [Co(5Å)/Cu(20Å)]×50 | 4.9±0.5 | 20.1±0.5 | 6.0±0.2 | 10.3±0.4 | 15.0±0.8 | 4.9±0.5 | 0.00±0.01 |
| [Co(15Å)/Cu(22Å)]×30 | 14.1±0.2 | 20.4±0.2 | 16.0±0.3 | 23.1±1.2 | 7.5±1.5 | 5.9±0.3 | 0.17±0.02 |
| [Co(50Å)/Cu(75Å)]×14 | 49.5±0.3 | 76.8±0.3 | 26.7±0.2 | 17.3±0.6 | 16.7±1.5 | 6.1±0.2 | 0.08±0.01 |

Table 3.1. Structural parameters extracted from the fitted results shown in Fig. 3.2-Fig. 3.4 for seven multilayer samples. $t_{co}$ is the Co-layer thickness, $t_{cu}$, the Cu-layer thickness, $t_o$, the thickness of the oxide overlayer, $\sigma_o$, the outer surface roughness, $\sigma_s$, the substrate roughness, $\sigma_I$, the interface roughness, and Δt, the percentage thickness gradient.

### 3.1.2. Non-specular Low-angle X-ray Scattering Analysis

One major limitation of specular x-ray reflectivity measurements lies in the fact that the specular field is not influenced by roughness correlations. Hence, from specular measurements, it is not possible to distinguish correlated roughness from uncorrelated roughness. In particular, specular mesurements can not distinguish "genuine" interface roughness (with large lateral correlation length) from interfacial mixing (which can be considered as interface roughness on an atomic scale). Complimentary information about interface morphology can only be acquired from non-specular measurements that record the distribution of the diffusive field in three-dimensional reciprocal space. In this work, two kinds of diffuse scattering scans have been performed to study the interface roughness correlation: offset (θ,2θ) scan and ω rocking scan.

In the offset (θ,2θ) geometry, as shown in Fig. 2.5(b), measurements are made with the film rotated a small fixed amount in order to profile the distribution of the off-specular radiation perpendicular to the film plane. For vertically correlated roughness, in reciprocal space, the diffuse intensity is concentrated in the ($q_x$, $q_y$) planes centred at $q_z=2\pi n/\Lambda$ (Bragg sheets)[58], where $q_z$ is the vertical component of scattering vector and Λ is the bilayer thickness. Thus, peaked diffuse scattering is expected at Bragg conditions.

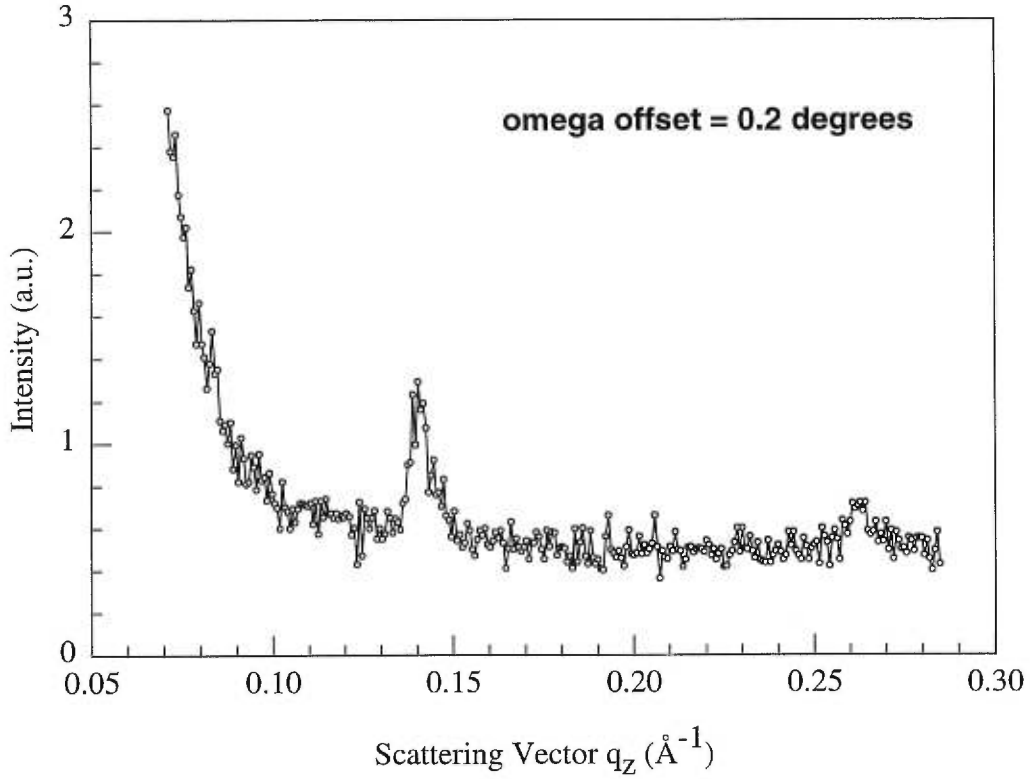


Figure 3.5. Diffracted intensity as a function of vertical scattering vector $q_z$ with a 0.2° offset angle for a [Co(17 Å)/Cu(34 Å)]×30 multilayer.

For uncorrelated roughness, diffuse intensity is spread in all directions and there is no coherency. As a result, vertically correlated roughness can be distinguished from uncorrelated roughness.

Fig. 3.5 shows the (θ,2θ) spectrum for the [Co(17Å)/Cu(34Å)]×30 film with with an offset of 0.2 °. While the diffuse intensity is much lower than the specular one, superlattice peaks are still evident and the diffuse intensity has a $q_z$ dependence similar to the specular intensity. This result indicates that, to some extent, the roughness is correlated vertically from one interface to another.

For the second type of diffuse scan, ω rocking scan, as shown in Fig. 2.5(c), the incident angle ω (between source and specimen) is varied, while the angle between the source and detector 2θ is held fixed. Through the use of a narrow entrance slit to the detector, this type of measurement profiles the angular distribution of the scattered x-rays in a cut perpendicular to the surface normal (i.e., Intensity vs. $q_x$). Fig. 3.6 shows the

rocking curves around the first-order and second-order Bragg peaks for the [Co(17Å)/Cu(34Å)]×30 multilayer. For each rocking curve in the figure, the true specular reflection appears as a spike above a slowly varying diffuse background.

Detailed quantitative analysis of rocking curves for a multilayer structure can be very complicated. For our purpose of estimating lateral correlation of interface roughness, a simple model suggested by Savage *et al.* [58] is applied. In Savage's model, for two points on a surface separated by distance $R=(X^2+Y^2)^{1/2}$, the correlation function

$$C(X,Y)=\sigma^2 \exp\left[-\left(R/\xi\right)\right]^{2h} \tag{3.7}$$

is obtained, in which $\xi$ is the lateral roughness correlation length, h is the Hurst parameter. A major simplification made by Savage's model is the assumption that h = 0.5. For Co/Cu multilayers, such an assumption is not groundless: both Bernabe *et al.*[65] and Gu *et al.* [66] have reported that for Co/Cu multilayers, h is very close to 0.5, and the latter have further reported that h is not a very sensitive parameter in the fitting. With this assumption, and supposing that, experimentally, the intensity of the scattered x-rays is detected through a sufficiently long slit along the X direction, the scattered intensity from a multilayer structure is written as

$$I(q_x,q_z)=2\pi I_0 \exp(-q_z^2\sigma_c^{\,2})/q_z^2\left[2\pi\delta(q_x)+\sum_{m=1}^{\infty}\frac{2\xi\left(q_z^2\sigma_c^{\,2}\right)^m}{m(m!)}\frac{1}{\left(1+q_x^2\xi^2/m^2\right)}\right] \tag{3.8}$$

where $q_x$, $q_z$ are the in-plane and vertical components of the scattering vector respectively. $\sigma_c$ is the correlated component of interface roughness and is related to the total rms interface roughness $\sigma$ by,

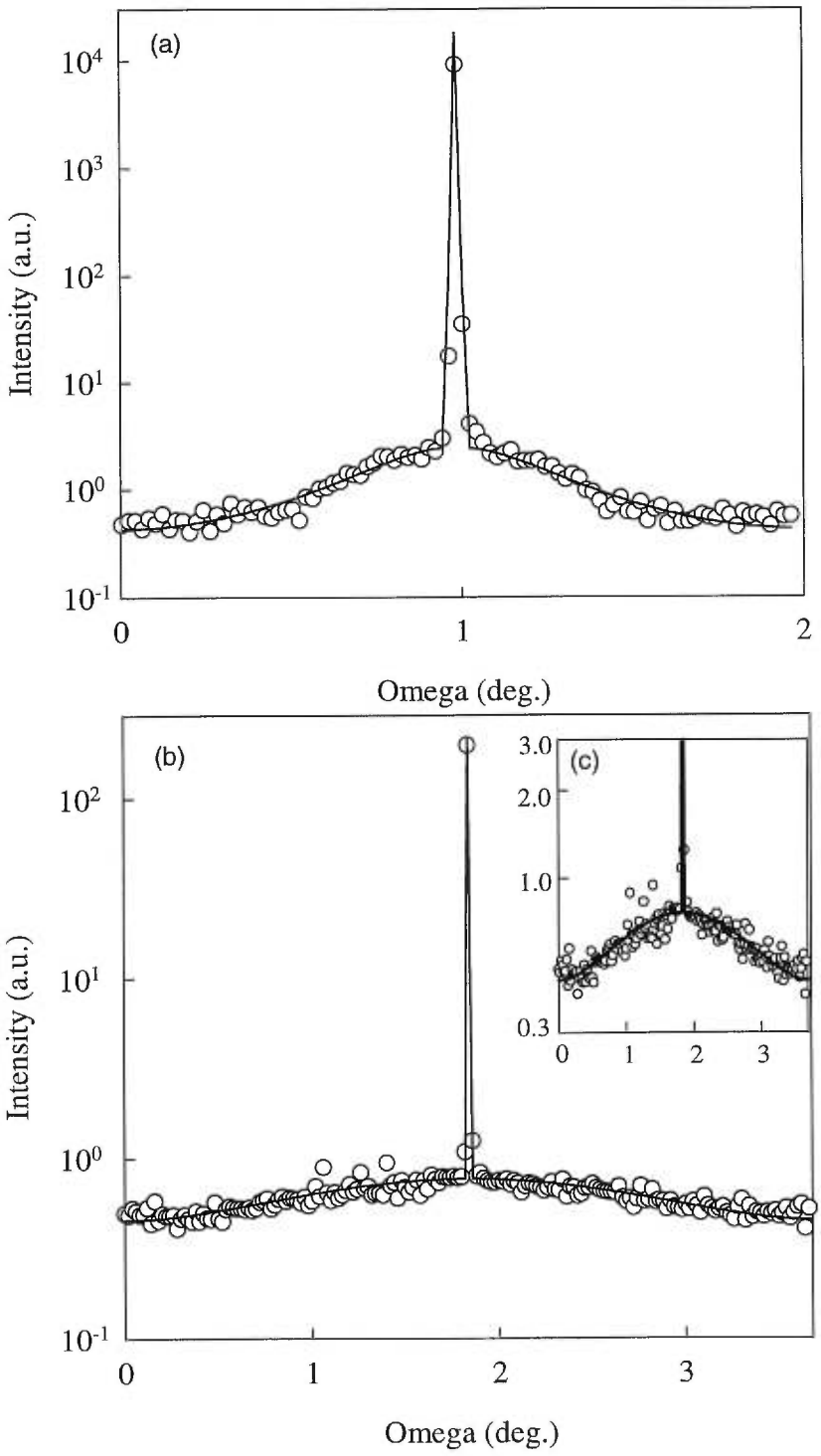


Figure 3.6. The rocking curves around the first (a) and the second (b) order superlattice peaks for a [Co(17 Å)/Cu(34 Å)]×30 multilayer. The lines are fitting curves described in the text. (c) replots (b) on an expanded vertical scale.

$$\sigma^2 = \sigma_c^2 + \sigma_u^2 \qquad (3.9)$$

where $\sigma_u$ corresponds to the uncorrelated component of interface roughness (typically, random roughness with high-frequency and short lateral correlation scale).

The intensity in Eq. 3.8 is separated into a $\delta$ function corresponding to the specular central spike in Fig. 3.6 and a diffuse component. The intensity calculated from Eq. 3.8 is then multiplied by $\sin\omega/\sin\theta$ that corrects the asymmetry effect resulting from the change in the volume of the specimen being probed as well as an envelope function that corrects for geometrical effects [58], and finally is convoluted with a function representing the instrumental broadening.

Fig. 3.7 depicts the calculated rocking curves for [Co(17Å)/Cu(34Å)]×30 multilayers with three different lateral roughness correlation lengths $\xi$ (100 Å, 500 Å, 1000 Å). It is evident that for a given $\sigma_c$, the diffuse part of the rocking curve strongly depends on $\xi$: for larger $\xi$ , the peak intensity of the diffuse component is greater and the diffuse-peak width is smaller. Therefore, by fitting calculations to experimental data, the lateral correlation length of interface roughness can be obtained.

The solid lines in Fig. 3.6 shows the fittings to the rocking curves using Savage's model. As shown, good agreement between fitted and experimental data has been obtained for both scans. Surprisingly, the parameters derived from the fittings are significantly different for the first- and second-order rocking curves (the rocking curves around the first and second superlattice peaks respectively). For the first-order rocking curve, $\sigma_c$ = 1.2 Å, $\xi$=1100±400 Å, while for the second-order rocking curve, $\sigma_c$ = 3.2 Å and $\xi$=150±20 Å. The exact origin of such an inconsistency is still unclear. Several possibilities may be considered. First, in calculating the first-order rocking curve, the envelope function used to correct geometric factors changes rapidly with $q_x$, and may dominate the shape of the rocking curve. While for the second-order rocking curve, the envelope varies much more slowly, and the rocking curve is more sensitive to the fitting parameters [58]. Secondly, the second-order rocking curve represents more of an average interfacial roughness in the entire superlattice, while the first-order curve mainly contains the information about interface roughness near the outer surface of the film and is more

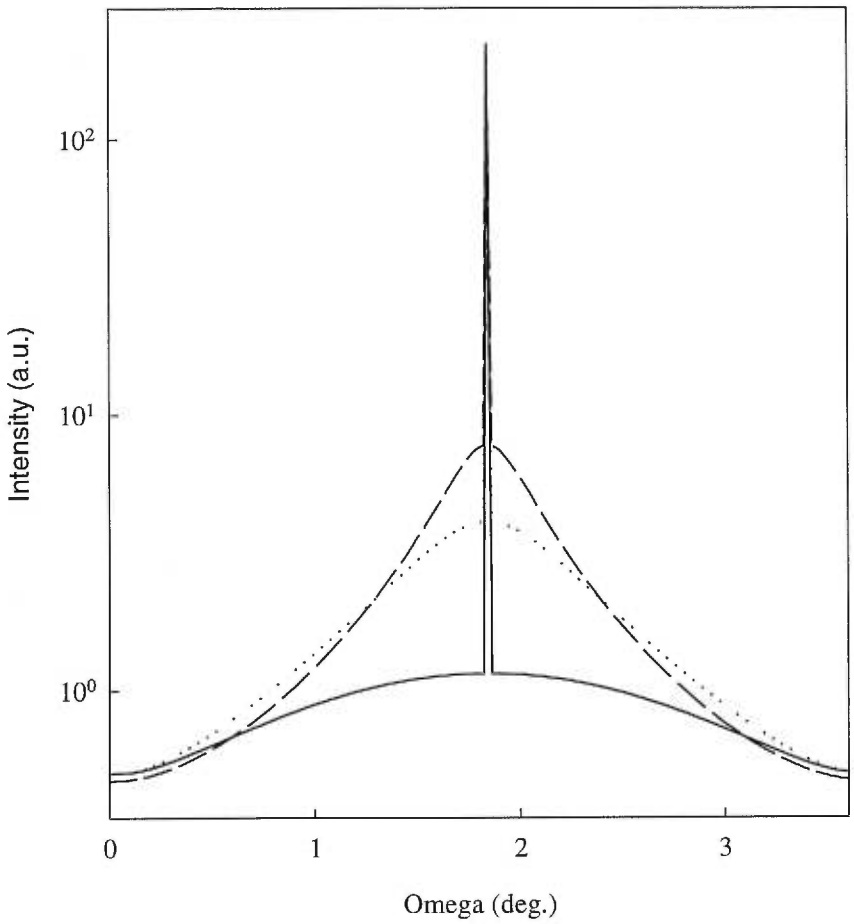


Figure 3.7. Calculated rocking curves around the 2nd superlattice peak for [Co(17 Å)/Cu(34 Å)]×30 multilayers with fixed interface roughness (5 Å) but different lateral correlation length: 100 Å (solid line), 500 Å (dotted line), and 1000 Å (dashed line).

surface sensitive. Therefore, it is considered that the parameters derived from the second-order rocking curve are better descriptions of the interface roughness in the whole multilayer structure. Large $\xi$ obtained from these fittings suggests good in-plane diffusion during film growth. Meanwhile, large $\sigma_c$ (compared to $\sigma_u$) derived from the fitting to the second-order rocking curve may suggest that interface imperfections in Co/Cu are dominated by roughness with large lateral correlation length instead of interdiffusion.

Studying interface roughness correlation by using diffuse x-ray scattering techniques has attracted a lot of attention over the past few years. Recently, Bernabe *et al.* [65] and Gu *et al.* [66] have reported a very different lateral roughness coherence length $\xi$ for similar Co/Cu multilayers. At very small angles ($2\theta=1.32^\circ$), Bernabe reported a $\xi$ of

about 6000 Å, while at large angles (2θ=4.16 °), Gu *et al.* obtained a ξ of about 20 Å. Interestingly, the ξ we derived from the first-order rocking curve (2θ= 1.84 °) is closer to Bernabe's value, while what we derived from the second-order rocking curve (2θ=3.72 °) is closer to Gu's result. At this stage, it's not clear whether such agreements are simply coincidental. Future work is still needed in at least two aspects. On the experimental side, as diffuse scattering signals are typically much weaker than specular signals, synchrotron radiation source should be applied in order to provide a better dynamic range in reciprocal space. On the theoretical side, more work is also required to obtain a more complete and reliable interpretation of the measured data.

### 3.1.3. High-Angle X-ray Diffraction Analysis

X-ray diffraction in the high-angle regime provides information about the atomic structure of a multilayer, including lattice constant, crystallographic texture, grain size, etc.

Fig. 3.8 presents the high-angle x-ray diffraction patterns of a series of Co/Cu multilayers of various thickness combinations as well as a pure Co and a pure Cu film of about 800 Å each. As shown, the pure Co film forms the hcp phase. The pure Cu film, on the other hand, exhibits a strong fcc (111) peak at 2θ=43.4° and a much weaker fcc (200) peak at 50.5°. An even weaker fcc (311) peak is barely observable around 2θ=90° (not shown). Clearly, the pure Cu film is strongly textured in the fcc (111) direction with a small fraction of fcc (200)-orientated grains. The crystalline spacing *a* obtained from the position of the (111) peak is 3.54 Å, which perfectly agrees with the bulk value of Cu. Almost all the multilayers (perhaps except for the [Co(50 Å)/Cu(75 Å)]×14 multilayer ) show similar diffraction patterns as the Cu film, with no evidence of the hcp Co line. This suggests that (1) as the Cu film, all the multilayers are highly textured, independent of layer thickness or number of periods, (ii) the Co layers in the multilayers are stabilized into metastable fcc phases by Cu layers, and the alternative Co and Cu layers grow coherently. The positions of the (111) peak of the Co/Cu multilayers are slightly shifted towards higher angles, and situate between the (111) peak of fcc Cu (at 43.4°) and the (111) peak of fcc Co (at 44.2°). For most samples, however, since the (200) and (311)

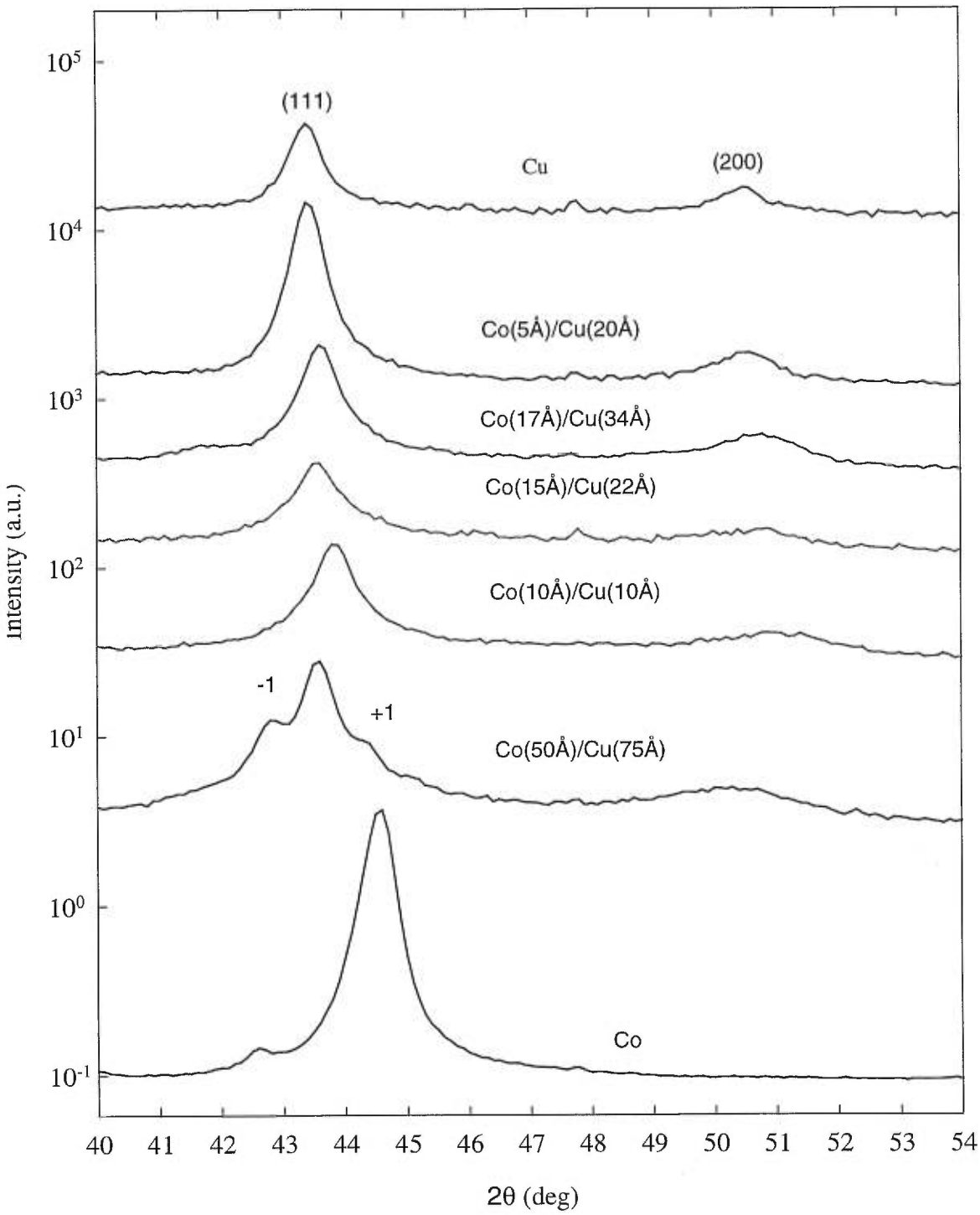


Figure 3.8: High-angle x-ray diffraction spectra for a 800 Å Co film, a 800 Å Cu film, and a series of Co/Cu multilayers with various layer thicknesses.

peaks are too weak and broad, it is difficult to determine their positions precisely. The positions of (111) peaks and the average lattice constants derived from them are summarized in Table 3.2. Roughly speaking, the average lattice constant increases as the ratio between Co-layer thickness and Cu-layer thickness increases: for the [Co(5Å)/Cu(20Å)]×50 multilayer, the lattice constant is almost the same as pure Cu, while for the [Co(10Å)/Cu(10Å)]×50 multilayer, the lattice constant is 3.60 Å which is very close to the value for fcc Co (3.61 Å).

The structural coherence length in the growth direction (or average vertical grain size) of a film can be estimated from the linewidth of the (111) Bragg Peak using Sherrer's formula [67], which gives

$$L = 0.9\lambda / \Delta(2\theta)\cos\theta, \tag{3.10}$$

where L is the coherence length, λ is the wavelength of the x-ray, and θ and Δ(2θ) are the position and measured halfwidth of the diffraction peak, respectively. The calculated values of L are also shown in Table 3.2 for the Cu film and the multilayers. As indicated, we estimate coherence lengths normal to the surface of 120 Å – 160 Å for all the multilayers which are much larger than their individual layer thicknesses. Also, the coherence length of a multilayer diminishes only slightly with decreasing individual layer thicknesses, and is always comparable to that of the pure Cu film. These observations suggest good structural coherence across the Co/Cu interfaces.

For the multilayer with the largest individual layer thicknesses, [Co(50 Å)/Cu(75 Å)]×14, two satellite peaks due to superlattice modulation are visible in the vicinity of the (111) Bragg peak. The positions of the peaks (2θ=42.8° and 2θ=44.4° respectively) agree well with the period of the superlattice (~125 Å). The appearance of the satellite peaks, resulting from both the structural coherence on an atomic scale and a well-defined interface structure, further confirms the good quality of the multilayer. For the rest of the multilayers, however, satellite peaks are not seen, despite the large coherence length estimated from Sherrer's formula. This can be explained as follows: (1), due to the very small lattice mismatch (~ 2 %) between fcc Co and Cu, the satellite peaks for a Co/Cu multilayer are expected to be very weak. (2), for the multilayers with small bilayer

periods, the satellites situate far from main Bragg peak, and are therefore less intense and hence more difficult to observe.

| Sample | 2θ | a | L |
|---|---|---|---|
| 800 Å Cu | 43.4° | 3.54 Å | 147.6 Å |
| [Co(5Å)/Cu(20Å)]×50 | 43.4° | 3.54 Å | 160.5 Å |
| [Co(17Å)/Cu(34Å)]×30 | 43.8° | 3.60 Å | 141.8 Å |
| [Co(15Å)/Cu(22Å)]×30 | 43.6° | 3.58 Å | 123.1 Å |
| [Co(10Å)/Cu(10Å)]×50 | 43.8° | 3.60 Å | 120.9 Å |
| [Co(50Å)/Cu(75Å)]×14 | 43.6° | 3.58 Å | – |

Table 3.2. The (111) diffraction peak positions (2θ), average lattice constants (a), and vertical structural coherence length (L) of a series of Co/Cu multilayers with various layer thickness combinations and numbers of periods.

## 3.2. GMR and Interlayer Magnetic Coupling of Co/Cu Multilayers

One of the primary objectives of this work is to study the correlation between the structure and the magnetotransport properties of Co/Cu multilayers. This objective can be achieved by modifying multilayer structures using various techniques and by examining the resulted effects on the magnetotransport behaviour. The first step to understanding of such effects, however, is to have a thorough characterization of the magnetic and magnetotransport properties of the as-deposited Co/Cu multilayers.

### 3.2.1. Cu Thickness Dependence of GMR and Interlayer Magnetic Coupling

Co/Cu is a particularly promising system for applications in magnetoresistive recording heads or sensors for several reasons. First, sputtered polycrystalline Co/Cu multilayers exhibit the largest GMR at room temperature[6]. Second, the GMR of Co/Cu system decreases less rapidly with temperature compared with other GMR systems. Third, the GMR of Co/Cu multilayers also saturates at relatively low magnetic fields. In

chapter 1, it has been shown that in Co/Cu multilayers, the GMR ratio is an oscillating function of Cu thickness ($t_{cu}$) with three well-defined maxima. These occur at $t_{cu} \approx 1$ nm, 2 nm and 3 nm respectively, and correspond to antiferromagnetic (AF) coupling between neighbouring Co layers.

Fig. 3.9 shows the magnetoresistance curves of Co/Cu multilayers fabricated using our sputtering system. These curves correspond to the multilayers with the Cu-layer thickness near the three oscillatory peaks. As shown, the GMR ratios at both the first and second peak are larger than 20 %. At the third peak, the GMR is relatively smaller, around 7 %. These values are similar to those reported by other groups[5] for Co/Cu multilayers with similar configurations, a fact which confirms that our multilayers are of comparable quality. Furthermore, while the GMR ratios for the first peak and second peak multilayers are close, the shapes of their MR curves are very different. At the first peak, the saturation field ($H_s$) of the MR curve is about 5 kOe and no magnetoresistive hysteresis is observed. On the other hand, at the second peak, $H_s$ is much smaller (~ 600 Oe) and a magnetoresistive hysteresis is evident with two maxima of resistivity appearing near the coercive fields. Such a difference can be understood in terms of very different interlayer AF coupling strengths ($J_{AF}$). Using the expression[68] $H_s=4J_{AF}/M_s t_M$, where $M_s$ and $t_M$ are the saturation magnetization and thickness of the magnetic layers respectively, $J_{AF}$ is estimated to be 0.3 erg/cm$^2$ for the first peak, and 0.04 erg/cm$^2$ for the second peak multilayer. These values are also comparable with those in the literature [6]. The relatively weaker interlayer exchange coupling (compared with crystalline anisotropy or other sources of hysteresis) in the second peak multilayer makes it difficult to rotate the magnetization as the field switches direction, which then results in obvious magnetoresistive hysteresis. As shown in Fig. 3.9, the MR hysteresis is even more significant for the third peak multilayer. Noticeably, however, the $H_s$ for the third peak Co/Cu is close to that of the second peak sample. It has been suggested [69] that for multilayers with thick Cu (>25 Å), some degree of magnetic disorder may occur during the magnetization reversal, and in this case, the $H_s$ of MR curve may not necessary be an appropriate indication of the AF coupling strength.

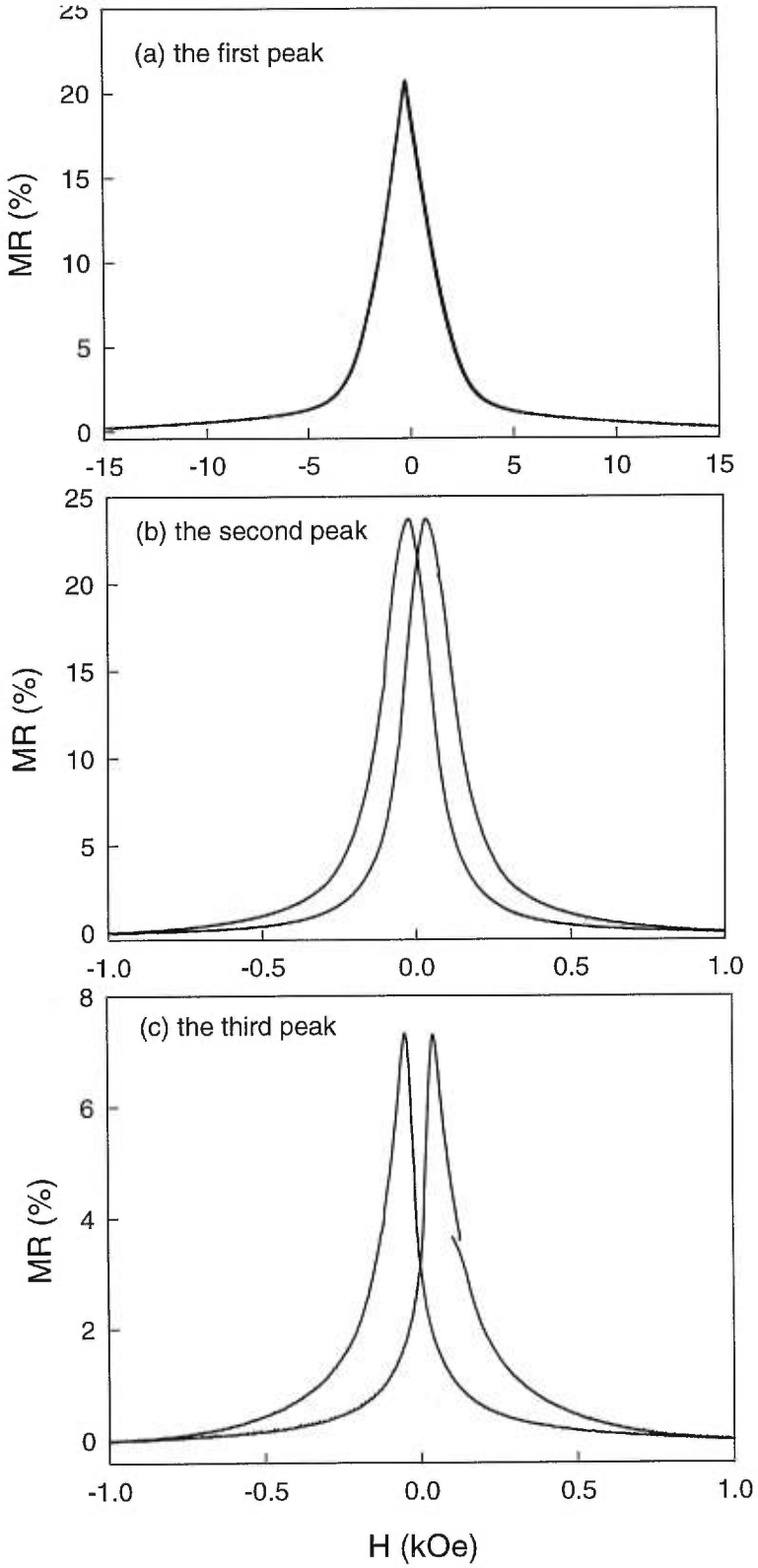


Figure 3.9. MR curves of the Co/Cu multilayers with Cu thickness at the three oscillation peaks:(a) [Co(10 Å)/Cu(10 Å)]×50, (b) [Co(17 Å)/Cu(22 Å)]×30, and (c) [Co(17 Å)/Cu(34 Å)]×30.

The magnetization curves of the above-mentioned multilayers are presented in Fig. 3.10. It is expected that perfect AF coupling in a multilayer should result in zero magnetic remanence. However, this is not the case for the magnetization curves in Fig. 3.10: the magnetization curves for the first peak and the third peak multilayers show large remanent magnetizations in low fields of about 70% of the saturation magnetizations, suggesting that the AF coupling in these multilayers is rather incomplete. Nevertheless, the saturation fields of both multilayers are clearly much larger than their coercive fields, indicating the existence of a small fraction of AF coupled regions which contribute to the GMR. For the multilayer at the second peak, much smaller magnetic remanence (~0.3) is observed. Taking $(1-M_r/M_s)$ as an estimate of the volume fraction of AF coupled regions, where $M_r$ and $M_s$ are the remanence and saturation magnetization respectively, it suggests that 70% of the volume of the second multilayer is AF coupled.

It should be stressed that the incompleteness of AF coupling is not only observed in our multilayers, but is a common characteristic of Co/Cu multilayers prepared by various groups and under various conditions [6]. This phenomenon can be ascribed to the fact that, compared with many other GMR systems (e.g., Fe/Cr, Co/Ru, etc.), the exchange coupling energy between magnetic layers is relatively small in Co/Cu multilayers. As a result, other factors, for example, domain-wall energies varying from site to site due to local defects[70], or randomly oriented magnetic easy axes associated with individual grains[71], play relatively more important roles in determining the magnetic alignments at zero applied field. Consequently, the regions of AF alignment may coexist with local regions of ferromagnetic alignment. Larger AF coupling strength may offset these effects and should favour more complete AF alignments in zero field. This is evident by comparing the magnetic curves in Fig. 3.10 for the Co/Cu multilayers at the second and the third AF peak. Nevertheless, for the multilayer with Cu thickness at the first oscillation peak, despite its large AF coupling energy, the AF coupling has been shown to be rather incomplete. This is explained in a somewhat different context: for such multilayers, as their Cu layers are extremely thin, a tiny number of pinholes through the Cu layers (perhaps at grain or twin boundaries) could easily result in large direct ferromagnetic coupling sufficient to overwhelm the indirect AF coupling. This may occur either over small regions or the whole sample depending on the distribution of the

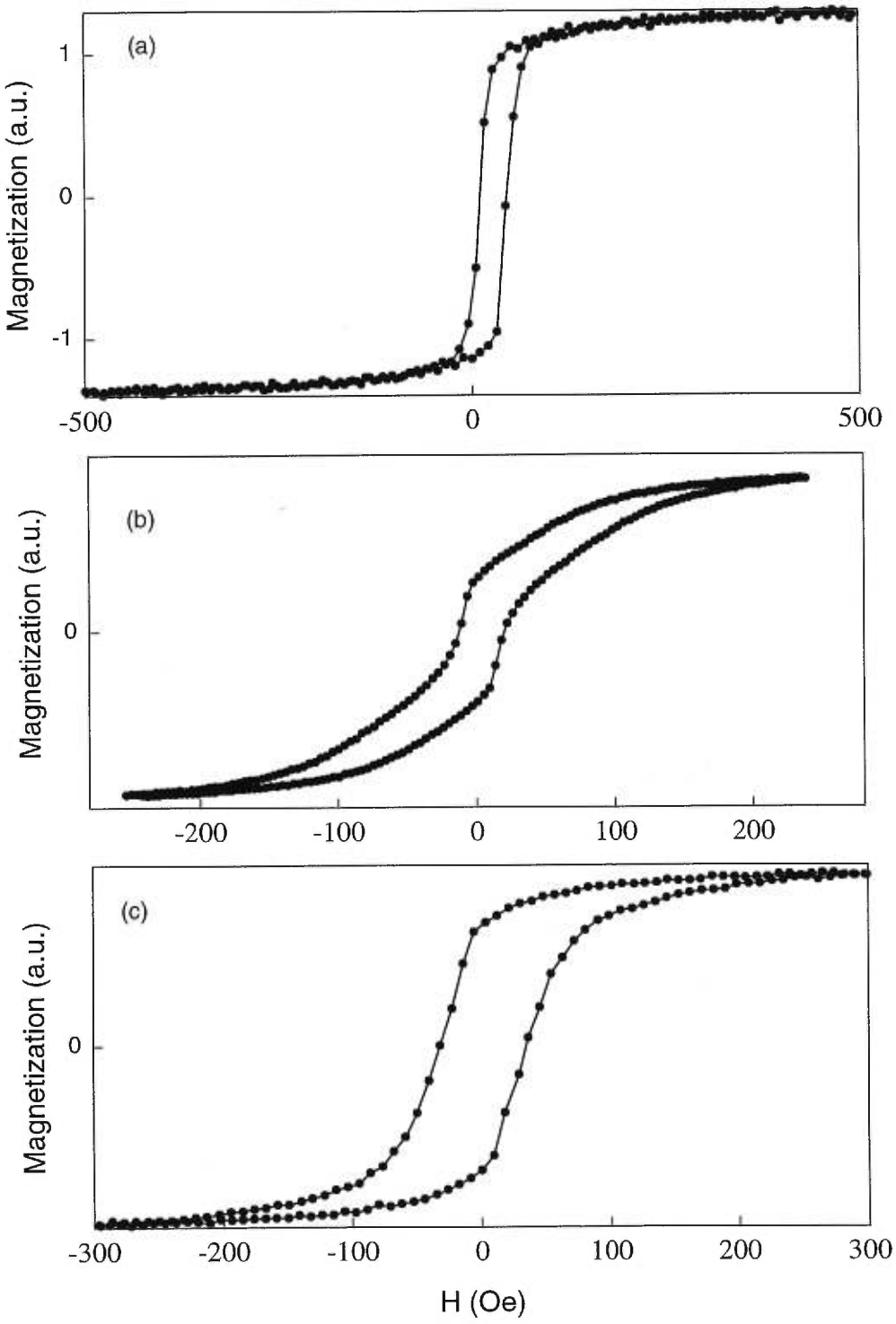


Figure 3.10. Magnetization curves of the Co/Cu multilayers with Cu thickness at the three oscillation peaks: (a) [Co(10 Å)/Cu(10 Å)]×50, (b) [Co(17 Å)/Cu (22 Å)]×30, and (c) [Co(17 Å)/Cu(34 Å)]×30.

ferromagnetic bridges. Furthermore, around the first peak, the magnetic coupling is extremely sensitive to the Cu thickness. Thus, local variations of the Cu layer thickness resulting from interface roughness may also lead to imcomplete AF coupling. Parkin *et al.*[24] have shown that sputtering Co/Cu multilayers onto an Fe buffer layer improves interface quality and leads to much more complete AF coupling at the first peak. Finally, as will be discussed in the following chapters, there is a strong correlation between the GMR and the volume fraction of AF aligned magnetic layers in zero field, which plays a key role in understanding the correlation between the structural and magnetotransport properties in Co/Cu multilayers.

Based on the above discussion, the multilayers near the second oscillatory peak show many advantages for the purpose of this work: (1). These multilayers exhibit reasonably large GMR (15%-25%). (2). AF coupling of these multilayers is more complete (~70%) so that it is possible to tune their GMR over a wide range. (3). The saturation fields of these multilayers are relatively low, which gives rise to larger GMR field sensitivty. (4). Due to relatively thick Cu layers (~22 Å), the structures of these multilayers are well defined and easy to reproduce. Consequently, the following discussions on GMR focus on such multilayers.

Fig. 3.11 shows the evolution of magnetization curves as the Cu thickness is varied around the second peak, for a series of multilayers with the Co thickness fixed at 17 Å. As expected, the saturation magnetization ($M_s$) is almost the same for all the multilayers. In contrast, the remanence ($M_r$) and saturation filed ($H_s$) change dramatically with varying $t_{cu}$. Here, the variation of $t_{cu}$ roughly ranges over one period of the oscillation. As shown, for the multilayers with $t_{cu}$=16 Å and 19 Å, the hysteresis curves are nearly square, indicating the Co-layers are ferromagnetically coupled. With increasing $t_{cu}$, the remanence decreases and the saturation field increases systematically until $t_{cu}$ reaches 22.5 Å which corresponds to the second peak of the antiferromagnetic coupling. Further increase in $t_{cu}$ increases the remanence and decreases the saturation field monotonically until $t_{cu}$ = 27 Å. Noticeably, while the mutlilayers with $t_{cu}$ = 16 Å and $t_{cu}$ = 27 Å both correspond to ferromagnetic coupling in the exchange interaction oscillation, the latter multilayer reveals much larger coecivity and saturation field. This difference can be related to the fact that, as the Cu layer is much thicker for this

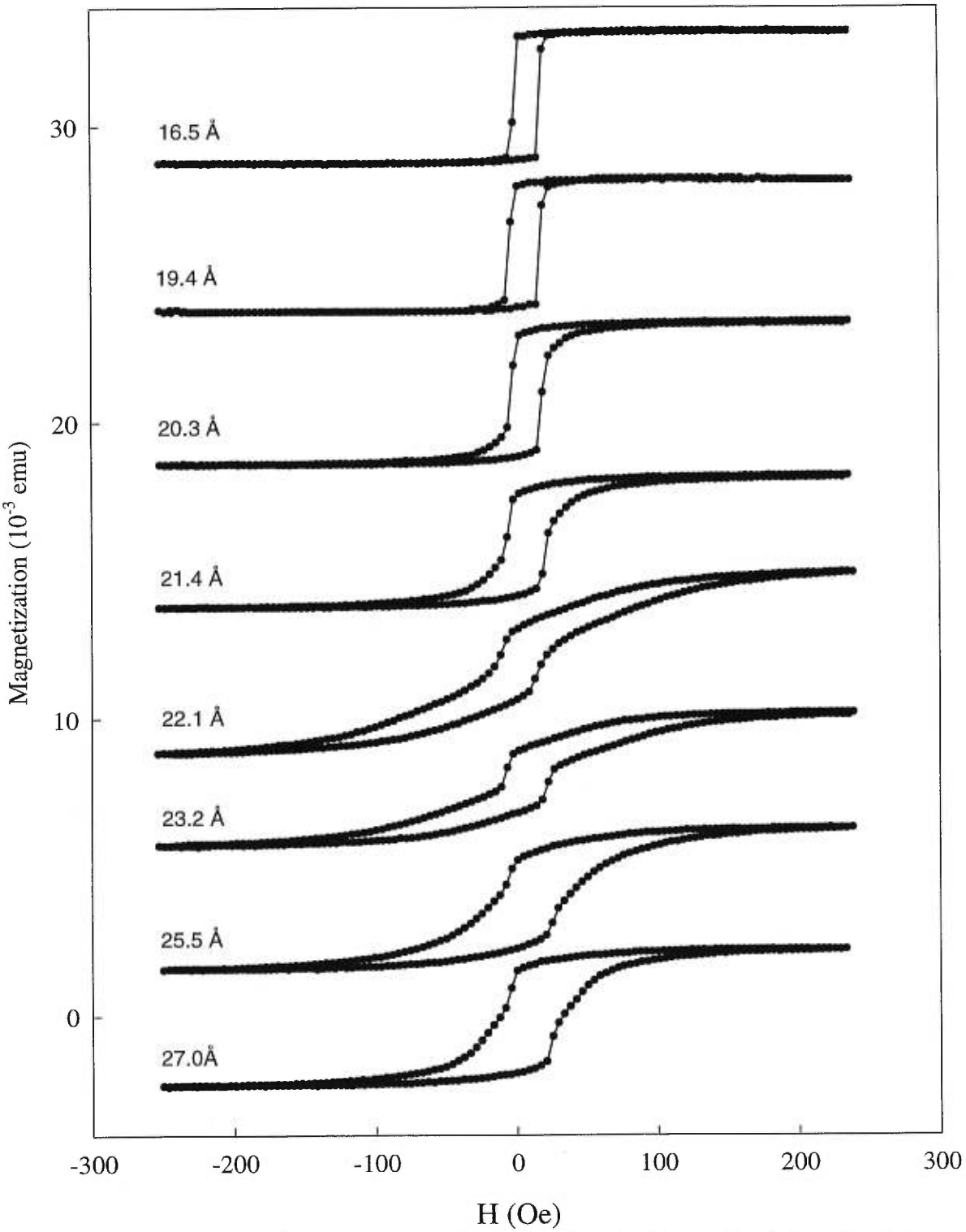


Figure 3.11. Magnetization curves of a series of [Co(17 Å)/Cu($t_{Cu}$ Å)] ×30 multilayers with $t_{Cu}$ varying from 16 Å to 27 Å. The curves have been displaced for clarity.

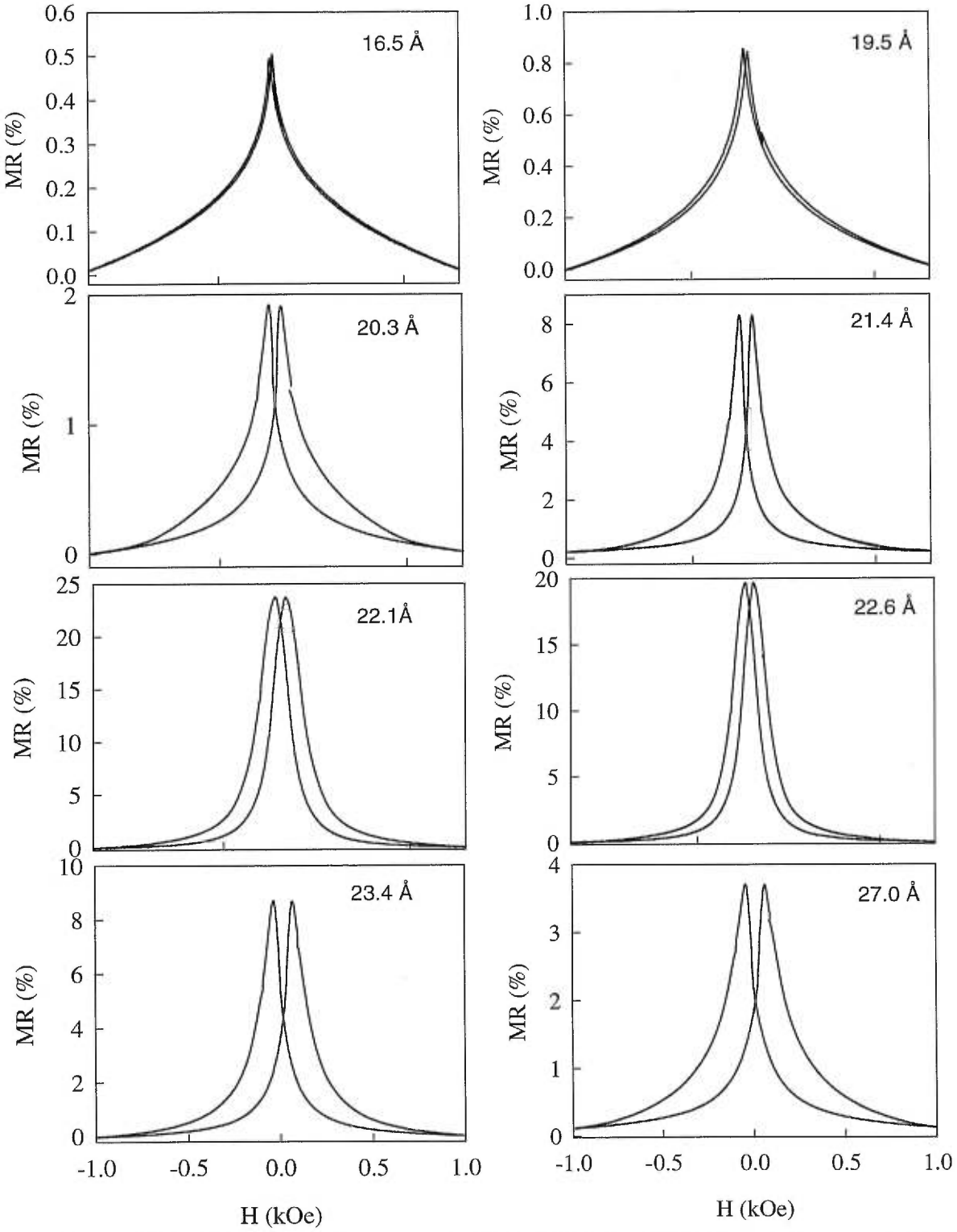


Figure 3.12. MR curves of a series of [Co(17 Å)/Cu($t_{Cu}$ Å)] ×30 multilayers with $t_{Cu}$ varying from 16 Å to 27 Å.

sample, the ferromagnetic coupling between the Co layers is weaker and parts of the Co layers may not be coupled in either way.

Fig. 3.12 shows that the GMR of the multilayers passes through a sharp maximum as the thickness is varied through the second AF peak. As shown, for ferromagnetically coupled mulitayers ($t_{cu}$=16 Å and 19 Å), the GMR ratios are negligible (<1%). With increasing $t_{cu}$, the GMR increases and starts to rise rapidly when $t_{cu}$ reaches 21 Å. A further increase of $t_{cu}$ by 1-2 Å dramatically raises the GMR to 20-25 %. The GMR ratio then decreases rapidly for $t_{cu}$ > 23 Å. Unlike the ferromagnetic coupled multilayers with small Cu thicknesses, the multilayers with $t_{cu}$ = 25 Å and 27 Å retain moderate GMR ratios. This behaviour might be associated with magnetic disorder or decoupled regions which exist in such multilayers. In addition, the shape of the MR curve also varies significantly with $t_{cu}$. As can be seen, the resistivities near the MR maximum respond sharply to applied external fields. Shifting $t_{cu}$ away from the oscillatory peak in either direction broadens the MR curve.

To conclude this section, we have successfully prepared Co/Cu mutilayers exhibiting well-defined oscillatory behaviour in both interlayer exchange coupling and GMR. It is also worth mentioning that despite the fact that the width of the second oscillatory peak is only about 2-3 Å, we have little difficulty producing reproducible multilayers with large GMR. (The fluctuation in GMR for a batch of 5-7 samples can be well controlled within 2-3%). Our later discussions on the correlation between structure and GMR can therefore be confidently based on the high quality of our samples and the repeatability of our sample preparation.

### 3.2.2. Co Thickness Dependence of GMR and Interlayer Magnetic Coupling

Though not as dramatically as the Cu thickness, the Co thickness of a Co/Cu multilayers also affects their magnetic and magnetotransport properties. Fig. 3.13 shows the magnetization curves for a series of [Co($t_{co}$)/Cu(22 Å)]×30 multilayers with $t_{co}$ ranges from 2.5 Å to 14 Å and $t_{cu}$ fixed at the second AF peak. Except for the sample with $t_{co}$ = 2.5 Å whose magnetization is too weak to measure, all the other multilayers exhibit small remanences which are indicative of AF interlayer coupling. The magnetic curves are

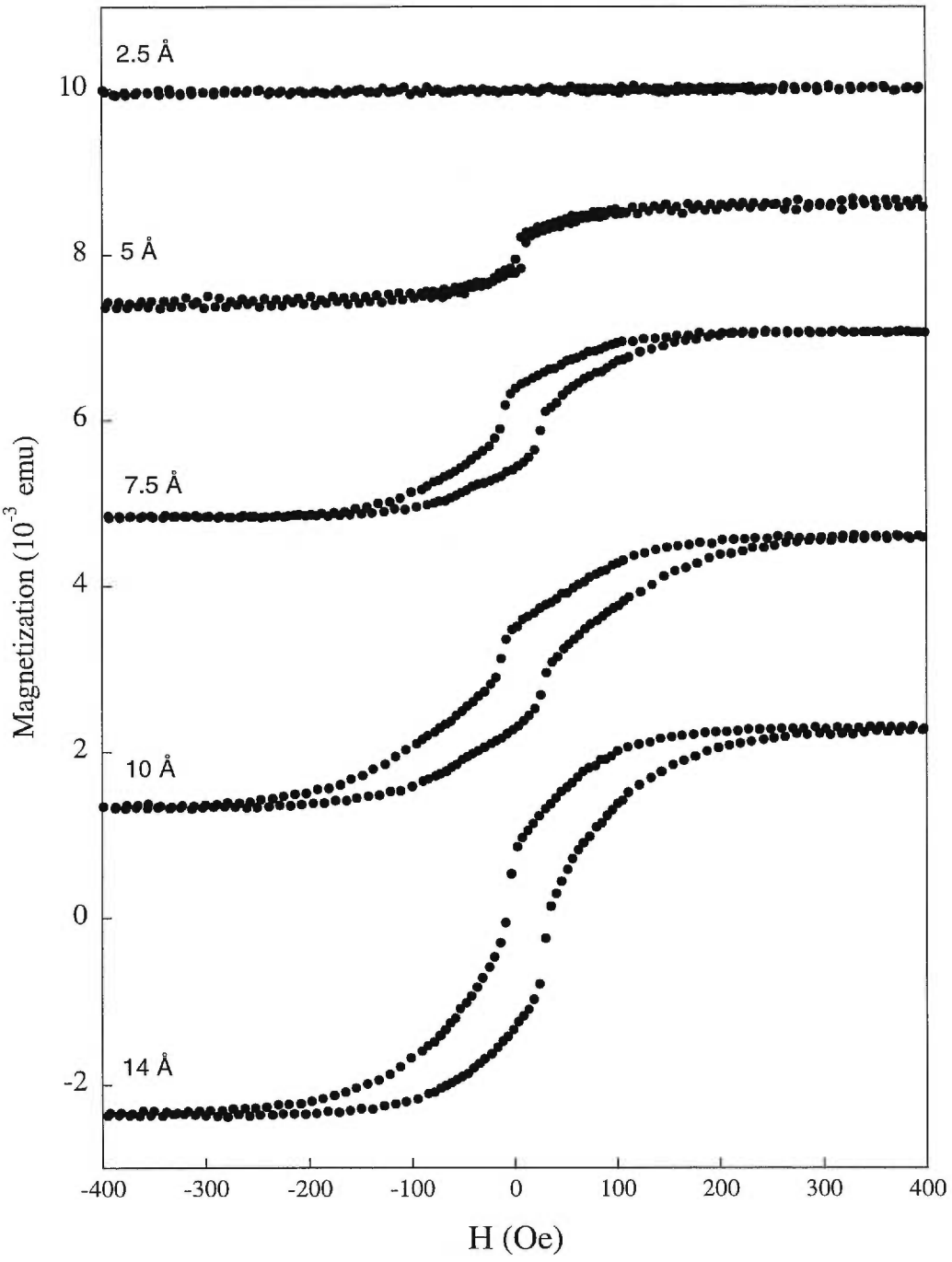


Figure 3.13. Magnetization curves of a series of [Co($t_{Co}$ Å)/Cu(22 Å)] ×30 multilayers with $t_{Co}$ varying from 2.5 Å to 14 Å.

particularly similar for the multilayers with $t_{co} \geq 7.5$ Å so that, at these thicknesses, the Co layer thickness has little effect on the interlayer exchange coupling. For the sample with $t_{co} = 5$ Å, a signification reduction in coercivity is observed. This might be related to the fact that, as the Co layer becomes thinner, the effects of crystalline anisotropy and other sources of hysteresis become less important compared with interlayer AF coupling (which does not depend strongly on the Co thickness) [72]. However, even for the 5 Å Co multilayer, the magnetization is well saturated by an external field of 400 Oe, and no sign of superparamagnetism is observed. This result confirms the layer structure for this Co thickness and is also consistent with the x-ray reflectivity data shown in Fig. 3.3.

Fig. 3.14 presents the effects of Co thickness on the MR curves for the series of multilayers mentioned above. For the sample with $t_{co} = 2.5$ Å, the MR is less than 1 % and the shape of the MR curve shows no sign of saturation even in fields of 15 kOe, characteristic of a system with very small ferromagnetic particles in a non-magnetic matrix. Given that 2.5 Å correspond to 1-2 monolayers of Co, such a result is not surprising. For the rest of the multilayers, the GMR increases monotonically with $t_{co}$ but all of them show large GMR ratios (>10%). The increase of GMR with $t_{co}$ nearly saturates after $t_{co}$ reaches 14 Å. It has been reported [50] that GMR starts to decrease with $t_{co}$ for $t_{co} > 20$ Å (probably due to reduced electron mean free path). As a result, GMR ratio is optimized for multilayers with $t_{co}$ between 10 Å and 20 Å. Most of the later discussions will therefore be focused on the multilayers with $t_{co}$ in this range.

Despite their relative small GMR ratios, the multilayers with very thin Co layers demonstrate some very interesting featues. Fig 3.14 shows that the magnetoresistive hysteresis is largely reduced for the multilayers with thin Co layers. For example, with $t_{co}$=5 Å, the hysteresis almost disappears, consistent with the magnetization curves presented in Fig. 3.13. As discussed earlier, this behavior can be attributed to the dominance of AF coupling over such factors as magnetic anisotropy or domain wall pinning. Defining the field sensitivity of GMR by $S=\Delta R/R/\Delta H_{FWHM}$, where S, $\Delta R$, R, $\Delta H_{FWHM}$ are sensitivity, total resistance change induced by external field, resistance of the multilayer, and half peak width of the GMR curve respectively, reduced hysteresis may potentially improve *S*. Unfortunately, such an effect is largely offset by the decrease

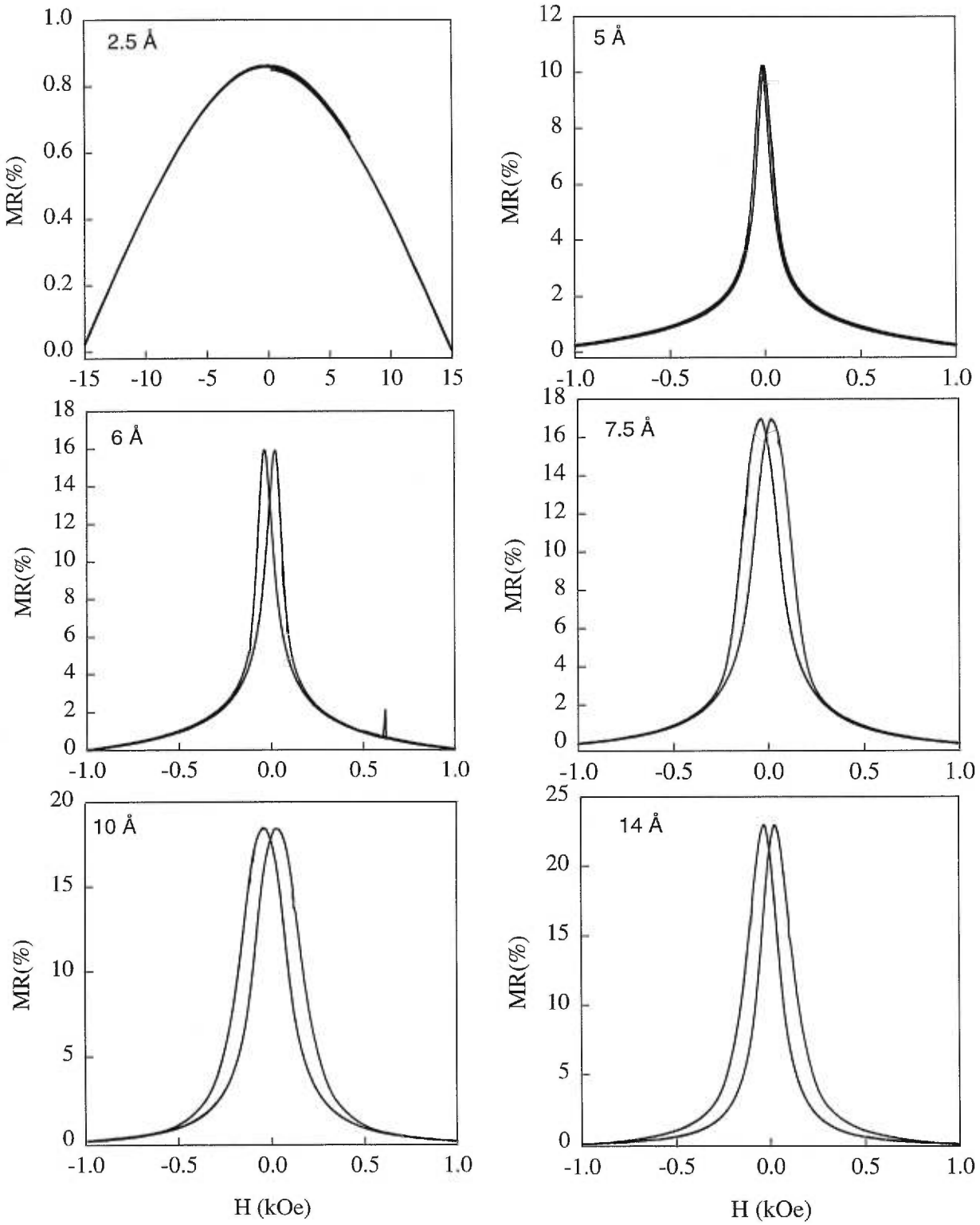


Figure 3.14. MR curves of a series of [Co($t_{Co}$ Å)/Cu(22 Å)] ×30 multilayers with $t_{Co}$ varying from 2.5 Å to 14 Å.

of GMR ratio with decreasing $t_{co}$. As calculated from the data shown in Fig. 3.14, the sensitivity for the multilayers with $t_{co}$=5 Å and 6 Å are 0.10%/Oe and 0.145%/Oe respectively, compared with 0.114%/Oe and 0.118%/Oe, respectively, for the multilayers with $t_{co}$=14 Å and 17Å.

Another feature of the multilayers with thin Co layers is the presence of significant tails in their MR curves. As shown in Fig. 3.14, the MR of the multilayer with $t_{co}$=5 Å consists of two contributions: the central peak and the slowly varying background. The central MR peak may have similar origins as the GMR observed in the multilayers with thicker Co layers. On the other hand, the tail, which accounts for about one fourth of total GMR, might be related to the discontinuous structure of the thin Co layers. With increasing $t_{co}$, the tail becomes less significant, and for the multilayers with $t_{co} > 10$ Å, it is negligible, suggesting that the Co layers in such samples are intact.

# Chapter 4: Deposition Temperature Dependence of GMR in Co/Cu Multilayers

Giant magnetoresistance (GMR) is closely correlated with the microstructure of a multilayer. A close examination of such correlation is crucial for both optimizing the effect and understanding its mechanism. To do so, it is necessary to find techniques to vary the structural properties of the multilayers in a systematic fashion. It is known that the structure of a sputtered multilayer is sensitive to the growth parameters, including sputtering pressure, power, substrate, and temperature. Among these, deposition temperature is of particular interest since it is easy to control and reproduce and its effects on the structure of a film are also relatively easy to understand. In this chapter, we will present the results for a series of Co/Cu multilayers deposited at temperatures from –40 °C to 120 °C. A detailed analysis is carried out on how the structure of the multilayer varies with the deposition temperature, and how such a variation results in the evolution of GMR and other physical properties such as resistivity and interlayer magnetic coupling.

## 4.1. Deposition Temperature Dependence of Structural Properties

Fig. 4.1 presents the low-angle x-ray reflectivity spectra of a series of multilayers deposited at various temperatures with nominal configuration [Co(16 Å)/Cu(32 Å)]×20. The nominal thicknesses are determined by the calibrations performed at room temperature with a quartz-crystal monitor, which have been further confirmed by low-angle x-ray reflectivity measurements on pure Co and Cu films (also deposited at room temperature). Fig. 4.1, however, shows that the positions of the superlattice peaks (and thus layer thicknesses) vary with deposition temperature. Specifically, for deposition temperatures between 15 °C and 120 °C, very little shift in the superlattice peak positions can be observed with temperature. However, as the deposition temperature is lowered to 0 °C, the layer thicknesses are reduced by approximately 10-20 %, as estimated from the changes in the superlattice peak positions. Lowering the deposition temperature further to -15 °C reveals little effect on the layer thicknesses and for the multilayer deposited at -40

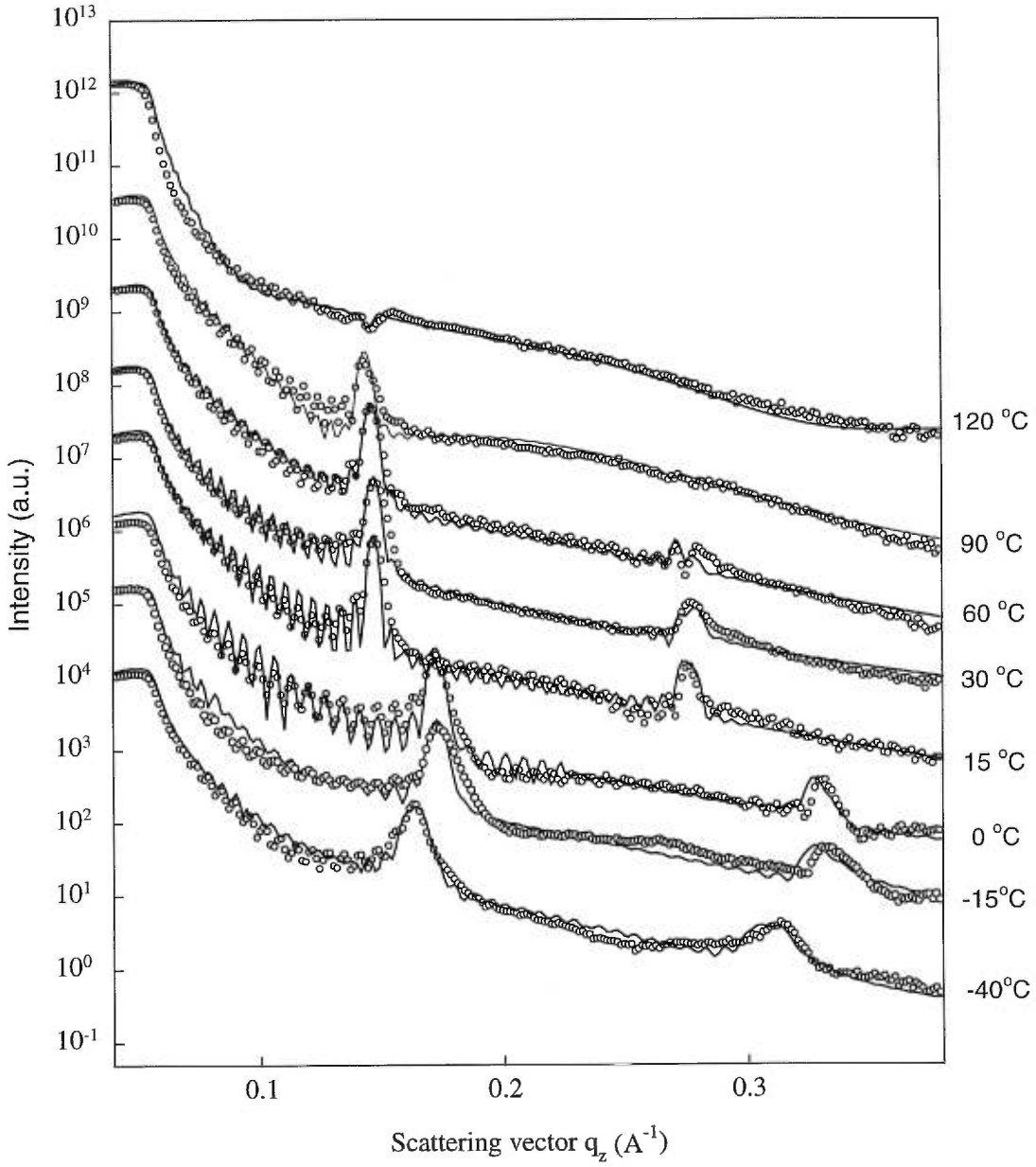


Figure 4.1. Low-angle x-ray reflectivity spectra for [Co(16 Å)/Cu(32 Å)]×20 multilayers deposited at various substrate temperatures, ranging from - 40 °C to + 120 °C. The solid lines are fitted curves. Curves have been displaced for clarity.

°C, the superlattice peaks are even shifted slightly towards low angles, indicating the layer thicknesses have increased. Such a variation seems to be rather random, but surprisingly, we find that it can be well reproduced and does not depend on the sequence of sample preparation. Of course, the variation in bilayer period might be related to the deposition temperature dependence of such factors as strain or substrate adhesion coefficient. Nevertheless, considering the dramatic change occurred as the deposition is varied by only 15 degrees from 15 °C to 0 °C, other factors must have been involved. One explanation is related to the configuration of our sputtering system described in chapter 2. For deposition temperatures below 15 °C, liquid nitrogen is circulated through the cooling tank (see Fig. 2.1), which may trap some sputtered atoms and thus reduce effective sputtering rates. As shown in chapter 3, such small variation in layer thicknesses has little effect on interface quality. However, GMR and interlayer magnetic coupling are very sensitive to Cu layer thickness, and the variations of layer thicknesses with deposition temperature should not be ignored.

Fig. 4.1 also indicates that the interface structure of a Co/Cu multilayer varies considerably with deposition temperature. The multilayer deposited at 15 °C exhibits the highest interface quality, as evidenced from the sharp and well-defined superlattice peaks in its spectrum. Clear-cut Kiessig fringes resulting from the finite total thickness of the film confirm that the substrate/film and the film/vacuum interfaces are flat. Increasing deposition temperature leads to systematic reduction in superlattice peak intensities as well as finite-size oscillations. The suppression of superlattice peaks is indicative of the deterioration in interface quality, resulting from either interface roughness or interfacial mixing. However, given the fact that Co and Cu are virtually immiscible, we ascribe the diminishing of superlattice peaks to increased interface roughness only. As the deposition temperature is elevated to 120 °C, both superlattice peaks and Kiessig fringes disappear. The former suggests the interface roughness becomes comparable to the layer thicknesses of the multilayer that disrupts the entire superlattice, while the latter shows the loss of coherence between the top and the bottom of the film. It is also worth mentioning that the intensity of the second-order superlattice peak appears to be far more sensitive to the increase in the deposition temperature than the first-order peak, thus confirming that the current evolution in superlattice peak intensities is interface-related rather than associated

with the reduction in the contrast of bulk parameters between the layers (which should suppress both superlattice peaks uniformly). On the other hand, at low temperatures, both superlattice peaks are retained. However, below 15 °C, a systematic broadening of the superlattice peaks has occurred with decreasing deposition temperature, suggesting the multilayer structure becomes less uniform. Such an effect might be connected to the reduced surface mobility at low substrate temperatures. Taken together, we conclude that the interface structure of a Co/Cu multilayer is optimized at the deposition temperature of 15 °C.

| Temperature | $t_{Co}$ (Å) | $t_{Cu}$ (Å) | $\sigma_s$ (Å) | $\sigma_I$ (Å) | Δt(%) |
|---|---|---|---|---|---|
| -40 °C | 12.0 | 27.4 | 14.0 | 4.7 | 0.25 |
| -15 °C | 11.8 | 27.5 | 11.5 | 4.7 | 0.18 |
| 0 °C | 11.8 | 26.5 | 7.5 | 4.6 | 0.14 |
| 15 °C | 14.7 | 31.8 | 8.0 | 4.6 | 0.10 |
| 30 °C | 14.9 | 31.6 | 11.8 | 4.8 | 0.10 |
| 60 °C | 15.0 | 31.8 | 20.6 | 6.1 | 0.10 |
| 90 °C | 15.8 | 31.8 | 24.4 | 10.9 | 0.10 |
| 120 °C | 15.0 | 31.8 | 30.4 | 18.3 | 0.10 |

Table 4.1. Structural parameters extracted from the fitting results shown in Fig. 4.1. $\sigma_s$ (Å) is the substrate roughness, $\sigma_I$ (Å) is the interface roughness, $t_{Co}$ (Å) is the Co layer thickness, $t_{Cu}$ (Å) is the Cu layer thickness, and Δt is the layer thickness gradient in percentage.

Fittings to the spectra based on the optical model described in chapter 3 agree with the above qualitative analysis. The solid lines in Fig. 4.1 are the fitted curves and agree well with the experimental data. The principal parameters obtained from the fittings are listed in Table 4.1. As shown, for the deposition temperatures above 15 °C, the interface roughness increases with temperature monotonically from 4.6 Å at 15 °C to 18.2 Å at 120 °C (which exceeds the Co layer thickness!). Below 15 °C, the interface

roughness seems to be independent of deposition temperature and remain between 4 Å and 5 Å. Nevertheless, in order to simulate the broadening effects of the superlattice peaks, a linear thickness gradient factor has been introduced in the fittings to the spectra of the multilayers deposited at low temperatures, as listed in Table 4.1. It should be admitted that other structural deficiencies might also cause similar effects. In particular, considering the reduced surface mobility at low deposition temperatures, non-uniformity in layer thickness over large lateral scales might be the principal reason for peak broadening. Unfortunately, in specular analysis, it is difficult to separate such a factor from other factors such as lateral thickness gradient. Due to this problem, the interface roughness obtained for the multilayers deposited at low temperatures should be accepted with caution.

The increase of interface roughness with increasing deposition temperature can be explained in terms that, since Co/Cu are immiscible, higher growth temperature may enforce phase segregation in the vicinity of an interface and suppress structural coherence across an interface. However, Fig. 4.2, which presents the x-ray reflectivity spectra of pure Cu (~ 800 Å) deposited at various temperatures, reveals another possibility. Even for the pure Cu film, the finite-size oscillation peaks have completely disappeared when the deposition temperature is raised to 100 °C, indicating the film is extremely rough. In contrast, moderately lowered deposition temperature (e.g., -15 °C) enhances the finite-size oscillations, suggesting the film is smoother. Such results can be understood only by taking into account the interaction between the film (Cu) and the substrate (Si). Transmission electron microscopy analysis by Parkin *et al.* [24] has demonstrated that strong interaction between Cu and Si results in rumpling the Cu layer as it grows onto a Si substrate. This effect is expected to be enhanced as the growth temperature is increased. For a Co/Cu multilayer, large substrate/bottom interface roughness resulting from such an interaction can be propagated throughout the rest of the film and hence increase the roughness of Co/Cu interfaces as well as that of the top surface of the multilayer.

The high-angle x-ray diffraction spectra of the [Co(16 Å)/Cu(32 Å)]×20 multilayers in Fig. 4.3 show significant changes in the crystallographic structure with deposition temperature. First, the multilayer film deposited at -40 °C is almost perfectly

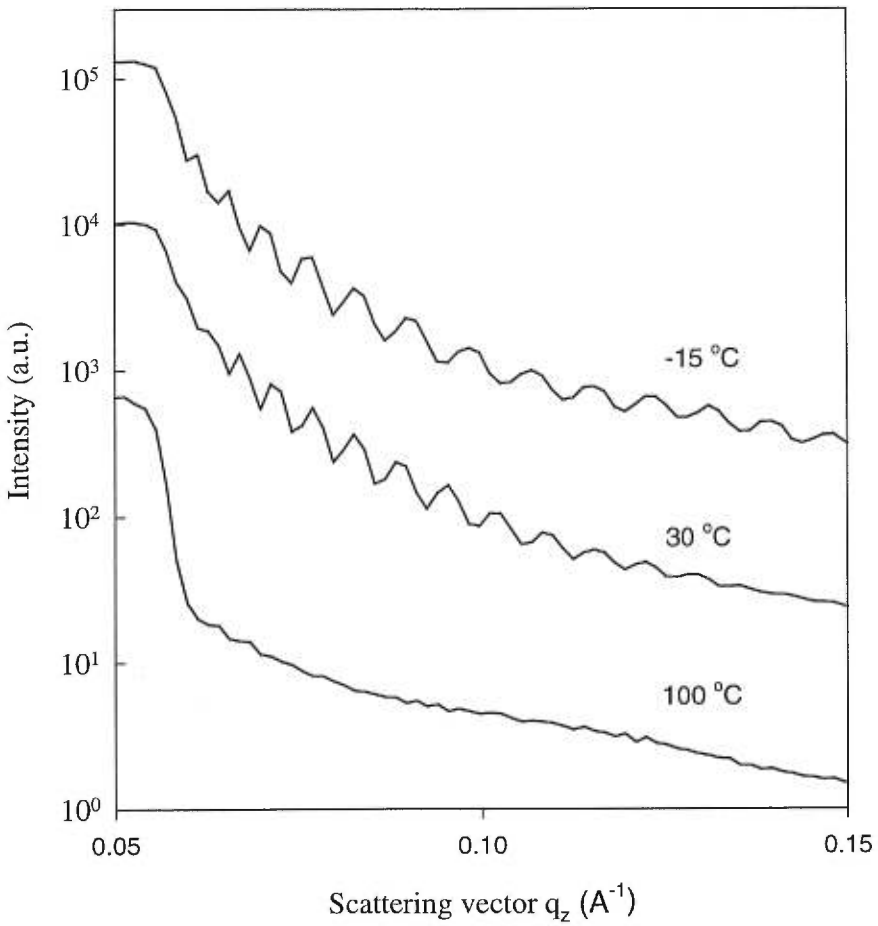


Figure 4.2. Low-angle x-ray reflectivity spectra of pure Cu films (~800 Å) deposited at -15 °C, 30 °C, and 100 °C respectively. Curves have been displaced for clarity.

textured in the fcc (111) direction. As the deposition temperature is increased, the fcc (200) peak appears and its intensity is progressively enhanced, indicating a gradual loss of (111) texture. For the multilayer deposited at 120 °C, the intensity of the (200) is approximately half of the (111) peak intensity, while other peaks, for example, (311) peak, are still nearly invisible. This shows the multilayer is dominated by both vertically (111) and (200)-orientated grains. Second, the (111) intensity varies non-monotonically with deposition temperature. The maximum intensity is observed for the multilayer deposited at 15 °C, while for the multilayers deposited at higher temperatures, the reduction in the (111) peak intensity is compensated by the increase of the intensity of (200) peak. The sharp decrease of (111) peak intensity for the multilayer deposited at low

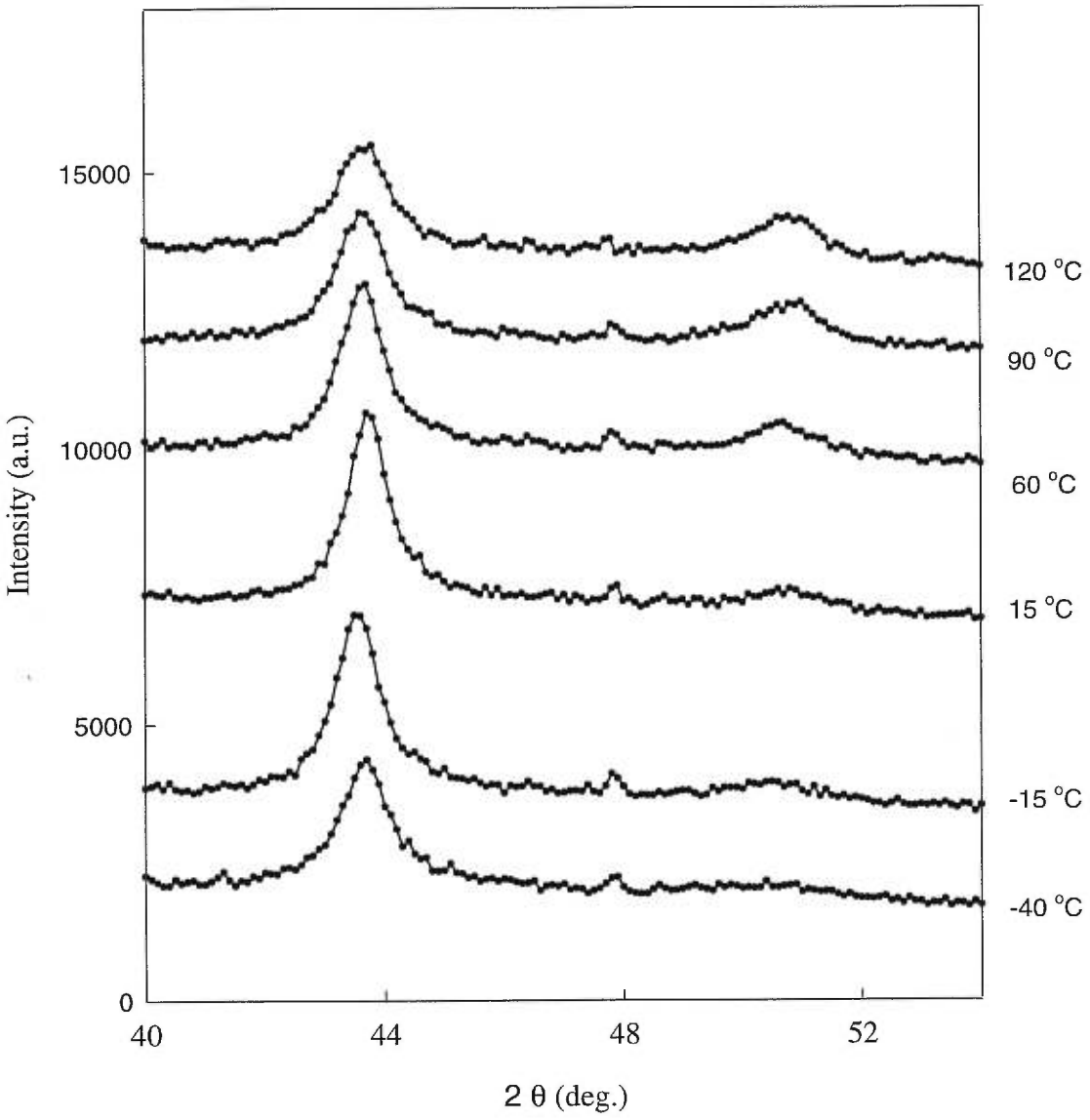


Figure 4.3. High-angle x-ray diffraction spectra for [Co(16 Å)/Cu(32 Å)]×20 multilayers deposited at various substrate temperatures, ranging from -40 °C to +120 °C. Curves have been displaced for clarity.

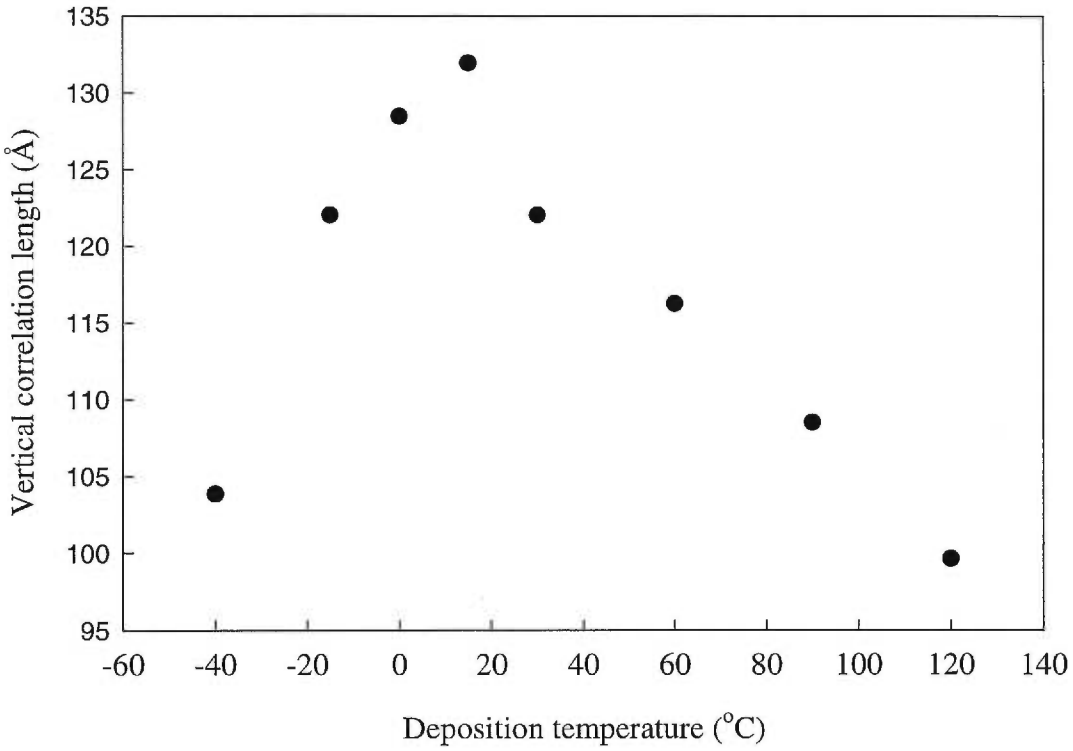


Figure 4.4. Variation of vertical structural coherence length of [Co(16 Å)/Cu(20 Å)]×20 multilayers with deposition temperature.

temperature (-40 °C ) can only be explained by poor crystallinity due to the prohibition of grain growth at low substrate temperature. Finally, the linewidth of the (111) peak also changes non-monotonically with deposition temperature. As the deposition temperature increases from -40 °C, the linewidth initially decreases, reaching a minimum at 15 °C before it starts to increase systematically. Fig. 4.4 shows the variation of the vertical crystalline coherence length (calculated from the linewidth by using Shearrer´s formula) as a function of deposition temperature. The vertical coherence length exhibits a maximum of 130 Å at the deposition temperature of 15 °C and then decreases with either increasing or decreasing deposition temperature. The decrease in coherence length at low temperatures, again, can be explained by poor crystallinity. On the other hand, the decrease in coherence length at high temperatures might be associated with increased disorder in the atomic distribution and phase segregation which suppress interface coherency. Nevertheless, it should be noted that, at all the deposition temperatures, the

vertical coherence lengths are near or above 100 Å which is much larger than the bilayer periods of the multilayers. Thus, a good degree of structural coherency is maintained for all of these multilayers.

## 4.2. Deposition Temperature Dependence of Mangetic and Magnetotransport Properties

Section 4.1 has shown that the multilayer structure of a Co/Cu superlattice is optimized at the deposition temperature of 15 °C, as characterized by small interface roughness, good layer thickness uniformity, and large vertical structural coherence length. In this section, we show how the variations of multilayer structure influence the interlayer magnetic coupling and GMR of a Co/Cu multilayer.

To investigate this question, we have prepared a series of Co/Cu multilayers with the nominal configuration of [Co(16 Å)/Cu(20 Å)]×20 at various deposition temperatures. Since the actual deposition rates may vary with temperature, in order to make the comparison meaningful, at each temperature, the sputtering period for Cu has been carefully varied with very small steps around that corresponding to the second GMR peak; subsequently, the multilayer with the largest GMR is selected. This procedure ensures that all the multilayers have a Cu layer thickness close to the second GMR oscillatory peak. On the other hand, it was shown in chapter 3 that small changes in the Co layer thickness does not significantly affect AF coupling and GMR. As a result, for deposition temperatures higher than 15 °C, the sputtering period for Co has been fixed at the value determined by the calibration performed at room temperature. For lower deposition temperatures (0 °C, -15 °C, -40 °C), the change in the deposition rate becomes more significant, and the Co sputtering period has been adjusted according to the thickness analysis by using x-ray reflectivity measurements on pure films and multilayers deposited at corresponding temperatures. Finally, the layer thicknesses of selected multilayers in the above series have been checked by low-angle x-ray reflectivity measurements, and the deviations from the nominal values have been found to be within 5 %.

Fig. 4.5 presents the magnetization curves for the series of multilayers deposited at different temperatures. All multilayers exhibit very close saturation magnetic moments. It is known[73] that intermixing between Co and Cu introduces magnetically inactive layers that should reduce the saturation magnetic moments of a multilayer. As this is not observed in Fig. 4.5, it suggests that no significant interfacial mixing is induced over this deposition temperature range, consistent with the fact that Co and Cu are immiscible in the equilibrium state and with the assumption that the variation of interface structure within the current deposition temperature range arises mainly from the variation of interface roughness. The magnetization curve for the multilayer deposited at 15 $^{o}$C exhibits the most significant AF interlayer coupling features, as is evidenced by its small residual magnetic moments in zero field and high magnetic saturation field. Interestingly, the same deposition temperature also leads to the highest structural quality of a multilayer. At lower deposition temperatures, significant AF coupling is retained, although the magnetic remanence is slightly increased with decreasing deposition temperature, suggesting the AF coupling becomes a bit less complete. This effect can be accounted for by the increased non-uniformity induced by low deposition temperatures.

In contrast, increasing deposition temperature (above 15 $^{o}$C) results in a much more dramatic suppression in the interlayer AF coupling. As shown, magnetic remanence increases and the saturation field decreases rapidly with increasing deposition temperature, indicating both the net AF coupling fraction and the AF coupling strength are substantially reduced. The increase of interface roughness with increasing deposition temperature might be responsible for such an evolution. First, interface roughness breaks the in-plane translational invariance [7]. Second, interface roughness causes local variations (fluctuations) of the spacer thickness which may smooth out the magnetic coupling oscillation that varies from antiferromagnetic to ferromagnetic with a period of only about 10 Å . Third, large interface roughness may also generate direct magnetic bridging which favors ferromagnetic coupling between the Co layers. This last reason may account for the complete loss of AF coupling in the multilayer deposited at the highest temperature (120 $^{o}$C). As indicated by x-ray reflectivity (Table 4.1), the interface roughness of this multilayer has become comparable to the layer thicknesses.

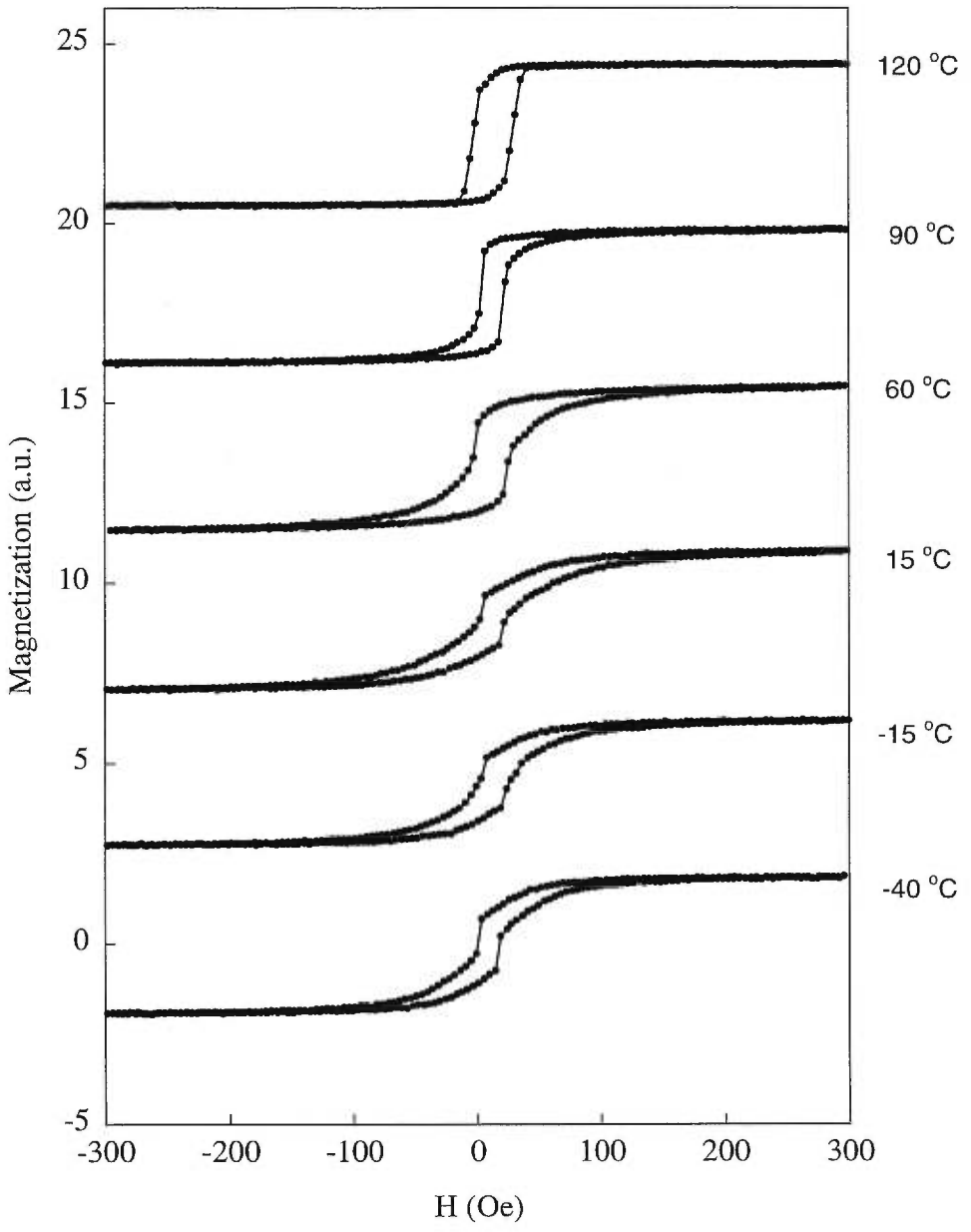


Figure 4.5. Room temperature magnetization curves for [Co(16 Å)/Cu(20 Å)]×20 multilayers deposited at various substrate temperatures, ranging from -40 °C to +120 °C. Curves have been displaced for clarity.

Finally, it is noticed that the change of crystallographic texture shown in Fig. 4.3 may also affect the interlayer magnetic coupling. Studies have shown that both interlayer magnetic coupling strength and oscillation period are strongly dependent on the film texture. Although it has been reported that the (100)-textured Co/Cu multilayers exhibit stronger AF coupling than those textured in the (111) direction, the coexistence of grains oriented in both directions may introduce two different oscillation periods and thus flatten the oscillatory peaks. As a result, the possibility cannot simply be excluded that the presence of a significant amount of (200)-oriented grains in a mainly (111)-textured Co/Cu multilayer may suppress AF coupling. However, given the dramatic change in AF coupling as the deposition temperature is increased from 15 °C to 60 °C, and the very subtle increase in the (200) peak intensity observed over the same temperature interval, it is hardly convincing that the suppression of AF coupling observed here is dominated by the change in film texture. In addition, no direct parallel between the AF coupling and the film texture can be drawn from the current results: the best AF coupling is observed in the multilayer with small amounts of (200)-oriented grains instead of the multilayers deposited at low temperatures with nearly perfect (111) texture.

Fig. 4.6 presents the variations of (a) the saturation resistivity $\rho_s$, (b) the change of resistivity $\Delta\rho$, and (c) the GMR ratio ($\Delta\rho/\rho_s$) as functions of the deposition temperature. Here we concentrate on the saturation resistivity $\rho_s$ in order to eliminate the magnetoresistive contribution due to the antiferromagnetic ordering in zero field. Since in these multilayers, the electron mean free path is comparable to the layer thickness, their resistivities provide valuable information about the interface electron scattering and interface structures. Fig. 4.6 shows that indeed the resistivity varies non-monotonically with the deposition temperature, similar to the evolution of interface quality. However, the smallest resistivity is found in the multilayer deposited at 60 °C, rather than the one with the highest interface quality. This variation suggests that interface scattering is not the only factor governing the change of resisitivity. Other structural imperfections (grain boundaries, local defects, etc.) may also be influenced by the deposition temperature and contribute to the variation of resistivity. In particular, higher deposition temperature may promote grain growth and thus increase the average lateral grain size. Larger grain size means lower grain boundary density and reduced probability of electron scattering at

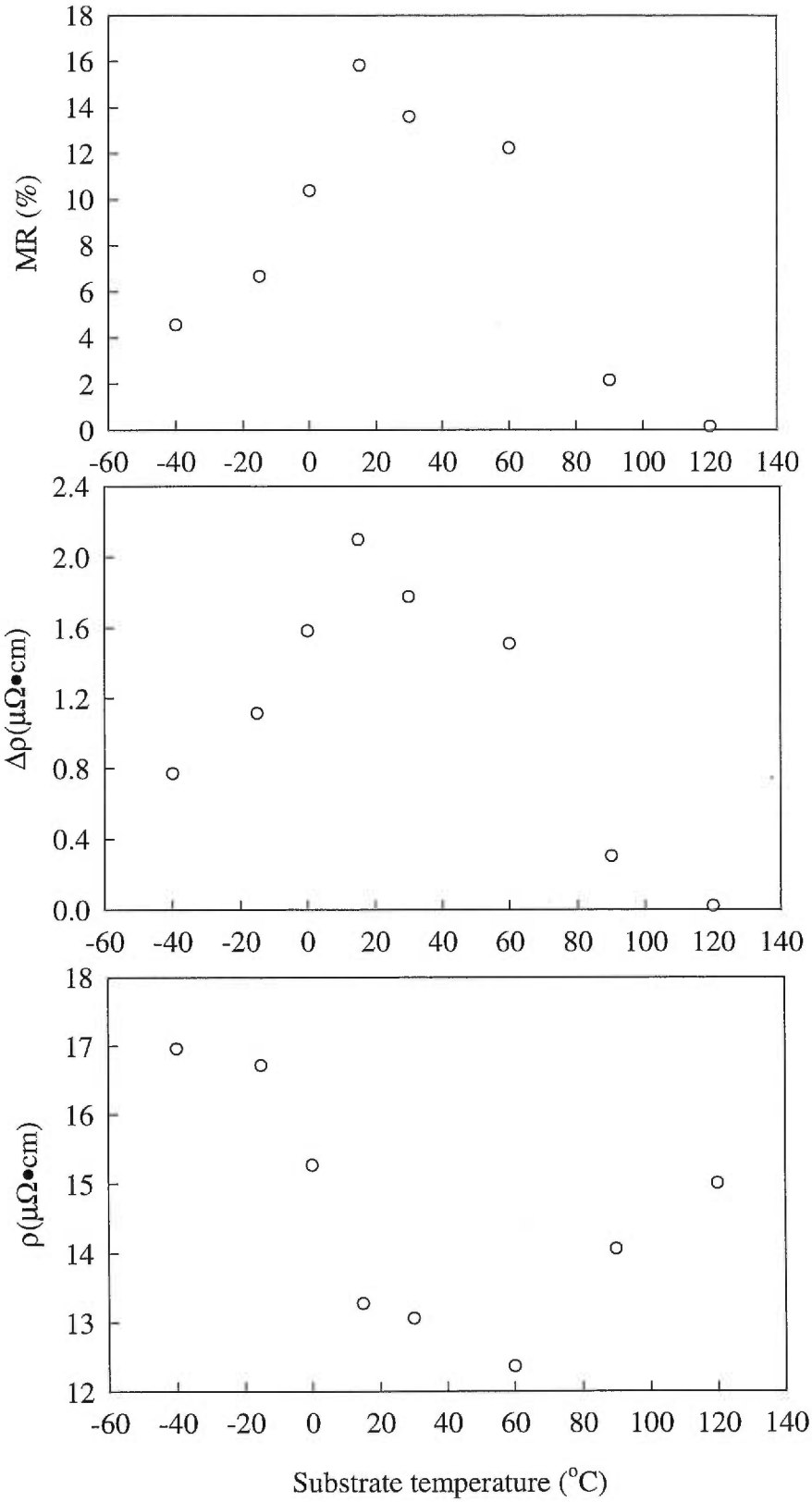


Figure 4.6. (a) Resistivity, ρ, (b) change in resistivity, Δρ, and (c) MR ratio of [Co(16 Å)/Cu(20 Å)]×20 multilayers as functions of deposition temperature.

grain boundaries. This may explain the shift of minimum resistivity towards higher deposition temperature. On the other side, film growth at lower temperatures might be involved with smaller grain size, more point defects such as vacancies and interstitial atoms, increased number of dislocations, as well as higher densities of interfacial atomic steps with large lateral scales. All these kinds of imperfections may explain the rapid increase of resistivity with decreasing deposition tempearture below 15 °C, despite the fact that the *rms* interface roughness obtained from the fittings to the x-ray reflectivity spectra seems to be rather insensitive to the deposition temperature in this region.

On the contrary, as shown in the (b) and (c) of Fig. 4.6, both the largest $\Delta\rho$ and GMR ratio are found in the multilayer deposited at 15 °C which has the optimized interface quality, underlining the importance of interface structure on GMR. From the current results, the increase in GMR is correlated with the improvement in the qualities of the interfaces, in agreement with the earlier work of Thomson *et al.*[43] However, their conclusion was drawn by comparing only two samples. Fig. 4.6 shows that both increasing deposition temperature above 15 °C and decreasing deposition temperature below 15 °C reduces GMR considerably, although reasonably large GMR ( >10%) can be obtained for deposition temperatures between 0 °C and 60 °C. At higher temperatures, the decrease of GMR can be explained at least partially by the accompanied suppression of interlayer AF coupling due to the increase in interface roughness. In contrast, the sharp decrease of GMR at lower temperatures can not be understood by the change in AF coupling, as all these multilayers remain AF-coupled to a large extent. It seems that the decrease of GMR in these multilayers originates from the enhancement of electron scattering, as revealed by their high resistivities. As mentioned, this can be associated with all sorts of imperfections located at interfaces, grain boundaries, or even within the grains, although it is impossible to separate these contributions and evaluate their relative importance solely from the current results. However, no matter which mechanism prevails, it is certain that the vast number of scattering processes introduced by lowering deposition temperature are *spin-independent*. Such processes not only reduce the GMR ratio directly through increasing $\rho_s$, but also reduce the opportunity a conduction electron may travel through successive Co layers with anti-parallel magnetic alignments and thus

reduce $\Delta\rho$. As clearly indicated in Fig. 4.6(b), $\Delta\rho$ decreases significantly with decreasing deposition temperature and is the dominant contribution to the decrease in the GMR ratio

To complete this section, Fig. 4.7 presents the MR curves of the above multilayers. As shown, the hysteresis of the MR curves increases systematically with increasing deposition temperature (except for the one deposited at the highest temperature whose MR is almost two orders of magnitude smaller that of the others). The multilayer deposited at -40 °C exhibits sharp resistivity peaks and a very low MR saturation field, while for the multilayers deposited at higher temperatures, the peaks become wider, and the MR saturation fields increase systematically. This behaviour indicates that the deposition temperature has a considerable effect on the magnetic reversal process of the Co layers which is closely related to such factors as magnetic domain structures and local pinning mechanisms. In addition, the MR of all the multilayers except that deposited at 120 °C is well saturated at the external field of 1 kOe. It can be concluded that the MR of all the multilayers originates from the AF interlayer coupling only and that other MR mechanisms (for example, MR due to granular effects, which is not expected to saturate at low fields) have negligible contributions.

In summary, it is found that the multilayer structure and the electrical and magnetic properties of Co/Cu multilayers can be optimized by varying the deposition temperature. Technically, in order to obtain Co/Cu multilayers with reasonably large GMR, the deposition temperature should be held between 0 °C and 60 °C. The highest GMR is observed in the multilayer with the optimized interface quality, and various kinds of structural imperfections may reduce the GMR through either suppressing AF interlayer coupling or introducing *spin-independent* electron scattering. On the other hand, the variation of deposition temperature affects many aspects (interface roughness, structural uniformity, grain size, texture, defects, etc.) of the structure of a multilayer simultaneously. The layer thicknesses might also vary slightly from sample to sample and hence influence the GMR as well. Since it is difficult to separate these factors, other techniques are required to provide further insight into the correlation between the structural properties and the GMR in Co/Cu multilayers. We will discuss this issue in the following chapters.

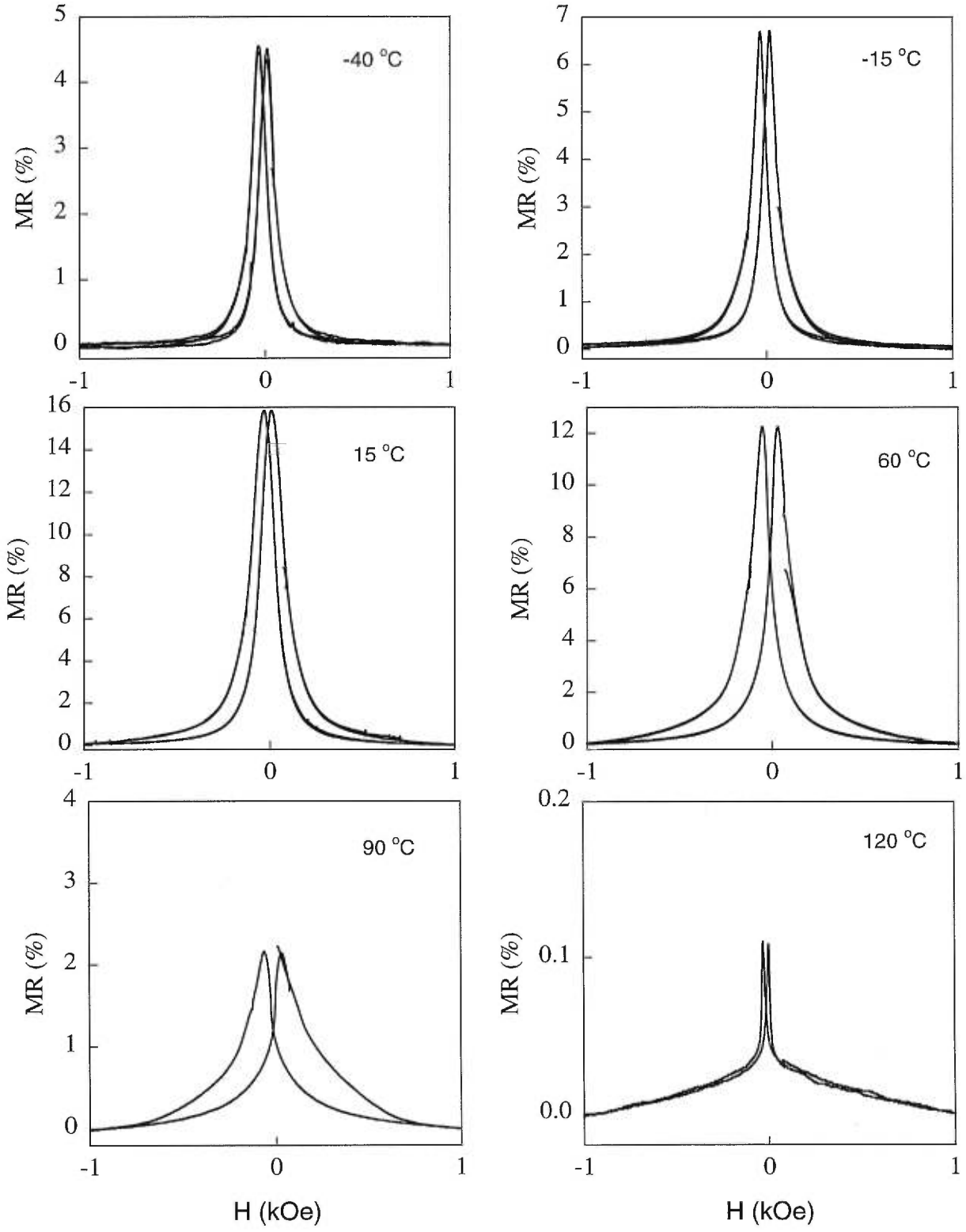


Figure 4.7. MR curves for [Co(16 Å)/Cu(20 Å)]×20 multilayers deposited at various substrate temperatures, ranging from -40 °C to +120 °C.

# Chapter 5: Ion Beam Irradiation of Co/Cu Multilayers

In Chapter 4, it has been shown that GMR and interlayer magnetic coupling of Co/Cu multilayers are very sensitive to structural parameters. By varying substrate temperature during deposition, both GMR and magnetic properties can be modified dramatically. Nevertheless, it has also been shown that substrate temperature influences various structural properties (for example, interface roughness and film texture) simultaneously. Since all these factors may have profound effects on GMR, it is difficult to assess their relative importance. In general, any *in-situ* technique aiming at modifying interfaces, including varying the deposition parameters, co-deposition at interfaces, or inserting third elements within the interface regions, also affects the growth of the subsequent layers and therefore the crystallography of a film. Moreover, with these techniques, for every new interface condition, a new sample has to be made, and random sample-to-sample variations (for example, Cu layer thickness, which also has drastic influence on GMR) are unavoidable. Therefore, direct comparison between different samples is often inconclusive. To clarify the role of interfaces in GMR, it would be desirable to find a technique that is able to modify the interface structure in a systematic manner in a *single* existing multilayer. In this chapter, we will show ion beam irradiation is a very promising candidate for this purpose.

The motivation of this study is twofold. First, the ion-beam irradiation technique is applied to modify the interfaces of Co/Cu multilayers to study the correlation between GMR and interface structure. Second, structure evolution of the Co/Cu multilayer under irradiation is of interest by itself. The Co/Cu system has a large positive heat of mixing, and Co and Cu are strongly immiscible in equilibrium. On the other hand, it has been reported that metastable CoCu alloys can be obtained by using non-equilibrium techniques such as low temperature codeposition[74]. It is interesting to examine whether similar alloys can be achieved by irradiating Co/Cu multilayers, and if so, how the positive heat of mixing will affect the mixing process. Up to now, although ion-beam irradiation effects have been studied extensively for many bilayer/multilayer systems[75], very few data have been published for Co/Cu. In part, this might be due to the fact that the atomic contrast between Co and Cu is very low, a fact which makes it difficult to

apply conventional methods such as Rutherford backscattering spectrometry (RBS) to probe the structure evolution under irradiation (especially for very low ion doses). In this chapter, however, we take advantage of the fact that the magnetic and magnetotransport properties of Co/Cu multilayers are extremely sensitive to the interface structure, and show that measurements of these properties provide valuable information about the interface modification induced by ion-beam irradiation at low doses that are barely detectable by other techniques.

The rest of this chapter is organized as follows. In 5.1, a brief review is given about ion-beam mixing processes in layered structures. In 5.2, the effects of ion-beam irradiation will be discussed for multilayers with very thin Co layers to examine the possibility of the formation of CoCu alloys and the nature of ion-beam mixing in this system. In 5.3, for a multilayer with thick Co and Cu layers, by combining x-ray reflectivity analysis and magnetization measurements, the ion-beam mixing width is estimated as a function of ion dose, and the ion mixing rate is obtained and compared with existing models. Finally, section 5.4 will focus on ion irradiation effects on the magnetic and magnetotransport properties of GMR multilayers. The correlation among the variations of these properties under irradiation will be addressed and the role of interface structure in interlayer antiferromagnetic coupling and GMR will be discussed.

## 5.1. Ion-beam Mixing in Layered Structures

Ion-beam mixing refers to the atomic intermixing and alloying that occur at the interfaces of a layered structure due to atomic rearrangement induced by ion irradiation. This phenomenon was first observed in 1972 by Lee *et al.* [76] in the Pd/Si system. Subsequently, it has been found [77] that many metastable as well as equilibrium phases can be obtained by ion-beam mixing.

The simplest model for ion-beam mixing is the ballistic mixing model [78], which takes into account only the purely ballistic aspects of atomic collisions, such as the atomic mass and density. As an energetic ion collides with a target atom, the target atom is displaced from its lattice site and is relocated. If this process takes place at an interface, interface mixing results.

There are two primary processes associated with ballistic mixing: recoil mixing and cascade mixing. In recoil mixing, atom relocation occurs only by single-collision events and is highly directed. Recoil mixing is effective when the collision between the incident ion and the target atom is head-on. With such collisions, the target atoms recoil far from their initial location. However, a head-on collision is rare, and by far the greatest number of collisions are glancing angle collisions with much smaller energy transfer and relocation range. For example, it has been shown that for 100 keV Ar ions on Pt, a Pt recoil at 89° will be nearly $2 \times 10^{15}$ as likely as a Pt recoil by a head-on collision. Therefore, the number of target atoms contributing to mixing by the mechanism of recoil implantation will be small.

Cascade mixing refers to the multiple relocations of target atoms resulting from a single incident ion. In the multiple displacement process, an initially displaced target atom (primary recoil) continues the knock-on-atom processes, producing secondary recoil atom displacements which in turn displace additional atoms. In a typical collision cascade, the displaced atoms have kinetic energies much smaller than the incident ion energy and, after many generations of collision cascades, they move in nearly random directions. The displacements of these atoms can therefore be described approximately by random walks. Sigmund and Gras-Marti [78] show that with cascade mixing, the spread of intermixing varies linearly with $\Phi^{1/2}$, where $\Phi$ is the ion dose. This relationship has been confirmed in a great number of systems [77].

The number of cascade-induced displacements per atom, or dpa, is another important parameter in determining the nature of ion-beam mixing. Dpa indicates the statistical average of the fractional number of lattice atoms that have experienced a lattice displacement. The dpa resulting from a given ion dose is written as[79],

$$dpa = \frac{0.4 F_D \phi}{E_D N_0} \tag{5.1}$$

where $E_D$ is the average minimum displacement energy, $F_D$ is the energy deposited per unit path length at the interface, $\phi$ is the ion dose, $N_0$ is the atomic density. At low doses, dpa is small and the interfacial reaction is considered to be composed of many localized

volumes of reaction. With increasing dose, dpa increases, and the collision cascades overlap to form a continuous mixed layer at the interface. This situation typically occurs at ion doses equivalent to about one-tenth of a monolayer (about $10^{14}$ ions/cm$^2$).

In many cases, however, the simple ballistic mixing model fails to predict the ion mixing rate. To explain very different mixing rates observed for systems with similar ballistic parameters (atomic density, atomic number, and atomic mass), thermodynamic effects in ion mixing must be taken into consideration. It has been found [77] that chemical driving forces play important roles in ion mixing. One of the most important thermodynamic aspects that needs to be taken into consideration is the heat of mixing which is a measure of the attractiveness between two different elements relative to their attractiveness to themselves. If A and B are the two elements, the heat of mixing is negative when the bond strength of A-B is greater than A-A or B-B. The more negative the heat of mixing, the greater the tendency to form an A-B alloy. It has been suggested that the effects of the heat of mixing on the ion mixing rate can be expressed as [75],

$$\frac{4Dt}{\phi} = \frac{4D_0 t}{\phi}\left(1 - \frac{2\Delta H_{mix}}{k_B T}\right) \tag{5.2}$$

where D, $D_0$ are diffusion coefficients with and without the effect of mixing heat taken into account respectively, $\Delta H_{mix}$ is the heat of mixing, $\phi$ is the ion dose, $k_B$ is Boltzmann's constant, and T is the local temperature in the collision cascade (not the average temperature of the specimen). As indicated by Eq. 5.2, with negative heat of mixing, there is a driving force to form an interface alloy during ion irradiation. Positive heat of mixing, on the other hand, reduces the ion-mixing rate, and at elevated temperatures, may even cause back-diffusion (demixing) of the mixed layer into its components.

Finally, it has been found [75] that, for many systems, at low temperatures, the ion-mixing rate is relatively insensitive to the sample temperature during irradiation, while above a critical temperature $T_c$, the mixing rate increases rapidly with increasing temperature. Such a temperature dependence is related to the so called "radiation-enhanced diffusion" process which occurs as follows: after collision cascades, the volume

affected by collision cascades can contain a non-equilibrium amount of vacancies and interstitial defects, since typical recombination times for these defects may significantly exceed the cascade duration of $10^{-10}$ s. When these defects become mobile at a high enough ambient temperature, thermally activated defect migration can occur and contribute to mixing during the relaxation or delayed stage. The transition temperature $T_c$, above which the radiation induced diffusion becomes important has been found to be correlated with the cohesive energy by the linear relationship[80] $T_c(K) \cong 95.2\ \Delta H_{coh}$ (eV atom$^{-1}$). In the Co/Cu system, as $\Delta H_{coh}$ is around 4 eV for both Co and Cu, $T_c$ is estimated to be around 350 K. Therefore, this diffusion process is not considered to be important for our irradiation experiments which were performed at 77 K.

## 5.2. Irradiation of Co/Cu Multilayers with Very Thin Co Layers.

This chapter will focus on the ion-irradiation effects on the GMR and interlayer magnetic coupling in Co/Cu multilayers. The first step towards investigating such effects, however, is to have a thorough characterization of the structure modifications. In 5.1, we have discussed the intermixing induced by ion beams. Nevertheless, it should be noted that ion-beam mixing is by no means the only effect induced by ion irradiation. Other effects, such as local defects, demixing, or phase segregation may also play important roles. The relative importance of these effects depends on many factors such as ion mass, ion energy, dose, temperature and the nature of the system. For example, while ion-beam mixing has been observed for many binary systems with negative heat of mixing, it has also been found that for systems with very large positive heat of mixing (e.g., Co/Ag), the two constituents segregate completely upon ion-beam bombardment [81].

As mentioned in Chapter 4, Co and Cu are strongly immiscible. With moderately large positive mixing heat (~ +13 kJ/g) [82], no equilibrium phases exist in the Co-Cu binary diagram [83]. However, with non-equilibrium techniques such as evaporation [84], melt-spinning [85], low-temperature co-deposition [74], metastable CoCu alloys with extended solubility are attainable. The magnetic properties of such alloys have been reported [74].

The question thus arises whether ion-beam bombardment can produce similar CoCu alloys. To investigate this possibility, a series of [Co($t$ Å)/Cu(17 Å)]×50 multilayers with $t$ ranging from 2.5 Å to 12.5 Å has been grown and subjected to 1 MeV $Si^+$ ion irradiation at 77 K with ion doses up to $1 \times 10^{17}$ ions/cm$^2$. The Co layers were chosen to be very thin in order to achieve steady mixing states at relatively low ion doses. Despite the thin Co layers, the compositional modulation of these multilayers before irradiation has been clearly evidenced by low-angle x-ray reflectivity measurements for Co thickness down to at least 5 Å (Chapter 3). In addition, the Cu layer thickness (17 Å) was explicitely chosen to be far from any antiferromagnetic (AF) interlayer coupling peak in order to avoid the complexity introduced by such coupling. The rest of this section will be devoted to a comparison of the structural, magnetic and transport properties of such multilayers before and after irradiation at various ion doses.

### 5.2.1. Crystalline Structures

High-angle x-ray diffraction spectra of a [Co(5 Å)/Cu(17 Å)]×50 multilayer at different ion doses are plotted in Fig. 5.1. The as-deposited multilayer is principally textured in the fcc (111) direction; other fcc peaks, such as (200), (311) and (222) are also visible but much weaker. Since the region between 55° and 75° is dominated by substrate (Si) peaks, it has been omitted from the figure. It is interesting to note that, upon irradiation, no evident change is observed in either the intensities or the linewidths of the peaks, which precludes significant grain growth induced by ion beam. The relative intensities between the peaks are also essentially unaffected and the film maintains a high degree of texture in the fcc (111) direction. At all doses, the Bragg peaks are sharp and well-defined, indicating that significant lattice coherence remains upon irradiation. This observation can be ascribed to fact that the lattice constants of fcc Co and fcc Cu are very close. Finally, irradiation at relatively low ion doses ($<5\times10^{15}$ ions/cm$^2$) shifts the peaks toward higher angles. This behaviour might be explained by the mixing of Co into Cu that slightly reduces the average lattice constant of the Cu matrix. Irradiation at high doses ($>1\times10^{16}$ ions/cm$^2$), on the other hand, shifts the peaks toward lower angles. The exact reason for such a shift is still not clear, but can be understood in terms of the voids

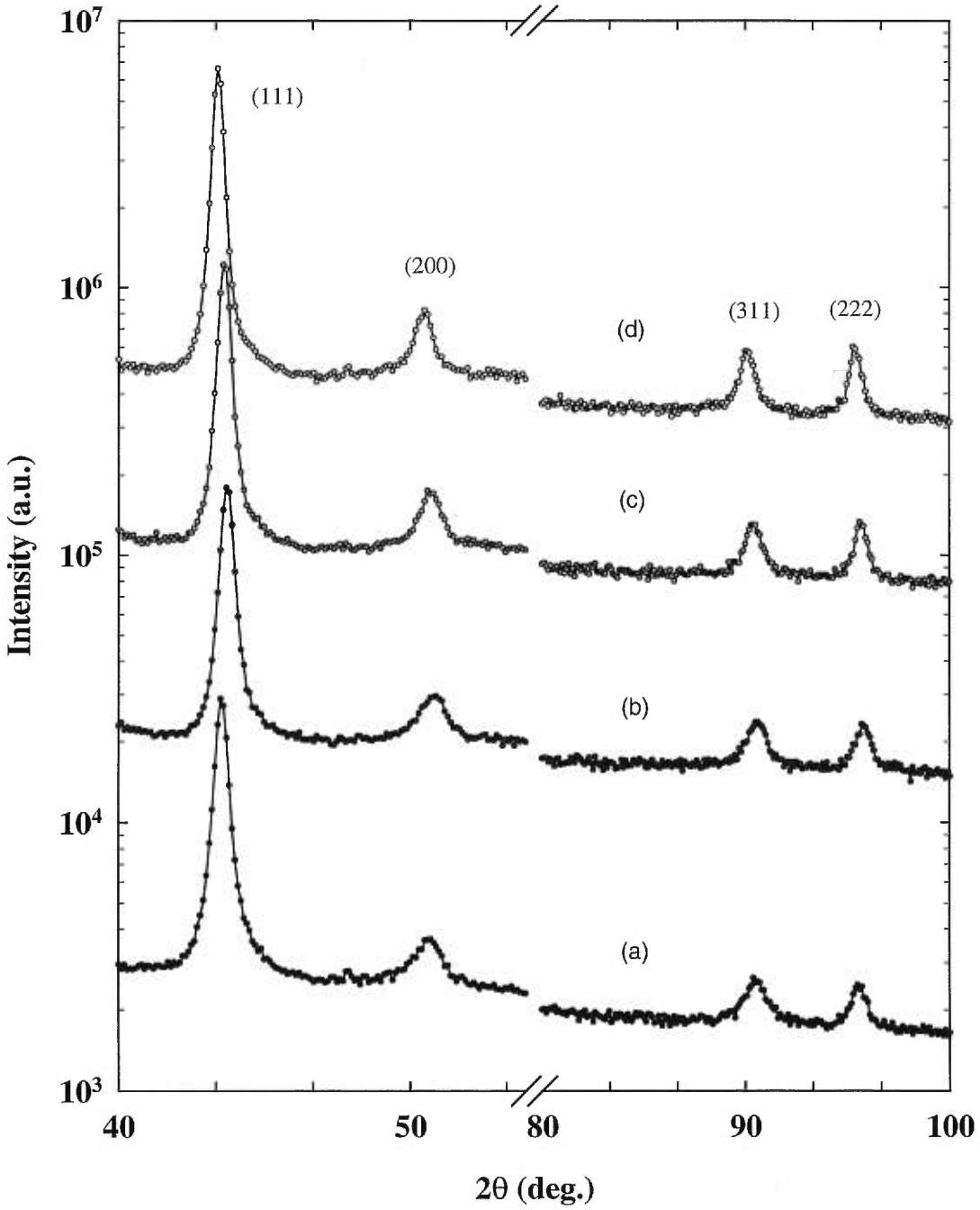


Figure 5.1. High-angle x-ray diffraction spectra for a [Co(5 Å)/Cu (17 Å)]×50 multilayer: (a) as-deposited, (b) after irradiation at $1\times10^{15}$ ions/cm$^2$, (c) $5\times10^{15}$ ions/cm$^2$, and (d) $1\times10^{16}$ ions/cm$^2$.

and inclusions produced by the implantation, as suggested by Schelp *et al.*[86]. Noticeably, however, all these peak shifts are rather insignificant.

The above observation confirms that, over a wide dose range, the crystallographic changes induced by 1 MeV $Si^+$ ion irradiation on the Co/Cu system are small, in sharp contrast to the changes generated by many other techniques, such as deposition temperature or co-deposition, and reveals one of the major advantages of ion-beam irradiation as a tool to investigate the correlation between interface structure and GMR. With the morphology unchanged under irradiation, any change in the GMR of a multilayer can be ascribed to the variation of the interface structure.

### 5.2.2. Magnetic Properties

Owing to the coherency of the Co and Cu lattices, high angle x-ray diffraction has limited effectiveness for investigating intermixing or the existence of very small Co clusters dispersed in Cu matrix. On the other hand, magnetic properties of Co-Cu films have been found to be very sensitive to the atomic distribution of Co [87]. Depending on the sizes and the separations of the Co particles, the Co-Cu system may exhibit ferromagnetic, paramagnetic, superparamagnetic or spin-glass behaviors. As a result, the magnetic properties of this heterogeneous system provide valuable information about its atomic structure.

Fig. 5.2(a) presents the magnetization curves of the [Co(5 Å)/Cu(17 Å)]×50 multilayer measured at 300 K at ion doses up to $5\times10^{15}$ ions/cm$^2$. Before irradiation, a large part of the magnetization saturates at very low magnetic field (<50 Oe), indicating that the Co layers are continuous or consist of islands with large lateral sizes. A small tail of the magnetization, that saturates at relatively high field, is also observed, arising from a small fraction of the multilayer that is antiferromagnetically coupled, or a small number of Co clusters coexisting with the continuous Co layers. Upon irradiation, two major features of the magnetization remain unchanged: first, all the magnetization curves exhibit marked hysteresis; second, all the magnetization curves are well saturated at a magnetic field of 1 kOe. For all ion doses, no sign of superparamagnetic behavior is observed, so that a significant presence of small Co clusters can be ruled out.

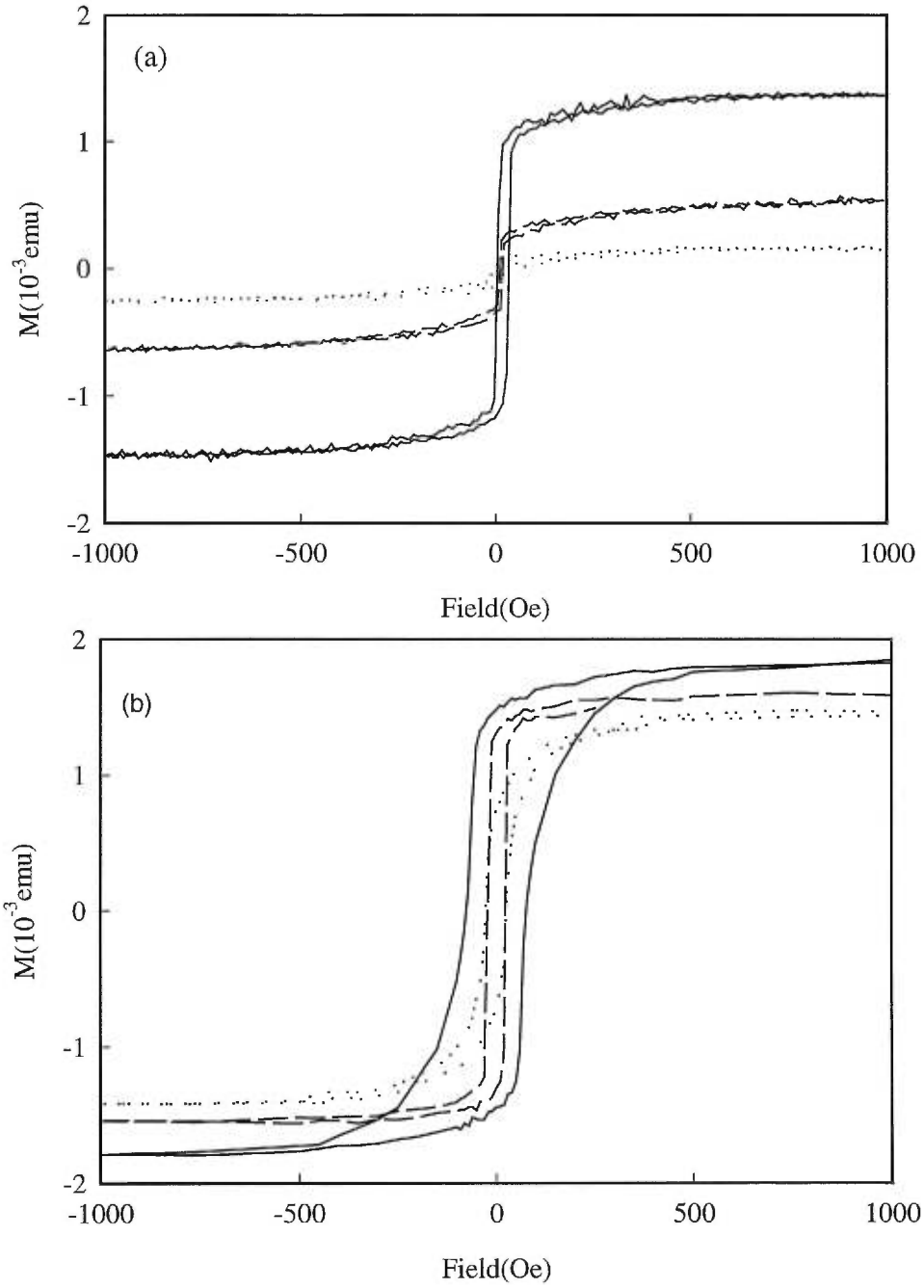


Figure 5.2. Magnetization curves of [Co(5 Å)/Cu(17 Å)]×50 multilayers measured at (a) 300 K and (b) 50 K before irradiation (solid line), after a dose of $1\times10^{15}$ions/cm$^2$ (dashed line), and a dose of $5\times10^{15}$ ions/cm$^2$ (dotted line).

The most noticeable effect of ion irradiation on the magnetization is the reduction in saturation level which decreases progressively with ion dose to 10% of the as-deposited value at 300 K.

For comparison, the corresponding magnetization curves of the same multilayer measured at low temperature (50 K) are shown in Fig. 5.2(b). Although ion irradiation produces significant changes in the magnetic remanence and coercivity of the multilayer, in contrast to the room temperature results, the saturation magnetization is only slightly reduced by irradiation. Such a contrast strongly suggests that the irradiation with ion dose of $5\times10^{15}$ ions/cm$^2$ has reduced the magnetic transition temperature to between 50 K and 300 K.

To investigate this effect, the magnetization of the multilayer has been measured as a function of temperature from 5 K to 300 K, at an external field of 40 Oe. The results are shown in Fig. 5.3. For the as-deposited multilayer, both ZFC and FC data show little variation with temperature, which are characteristic of continuous Co layers or large Co particles with a Curie temperature well above 300 K. However, after irradiation at a dose of $5\times10^{15}$ ions/cm$^2$, the FC and ZFC curves drop sharply when the temperature is raised about 100 K, indicating a Curie transition around 190 K. In fact, the temperature dependence of magnetization for the irradiated multilayer has been found to be very close to that of CoCu alloys with similar compositions obtained by low-temperature co-deposition [74]. Furthermore, the Curie temperature estimated above is also consistent with the magnetic phase diagram of fcc CoCu alloy [74]. Such an agreement points to the conclusion that metastable CoCu alloys can be formed by low temperature irradiation with 1 MeV $Si^+$ ions. The main difference between the magnetic behavior of the irradiated Co/Cu multilayer and that of a co-deposition alloy lies in the absence of a spin-glass transition at low temperature for the multilayer. We suggest that such a difference is connected to the fact that small amounts of dispersed Co particles remain ferromagnetic at low temperatures. The existence of such Co particles in a heavily irradiated multilayer is indicated by the residual magnetization at room temperature.

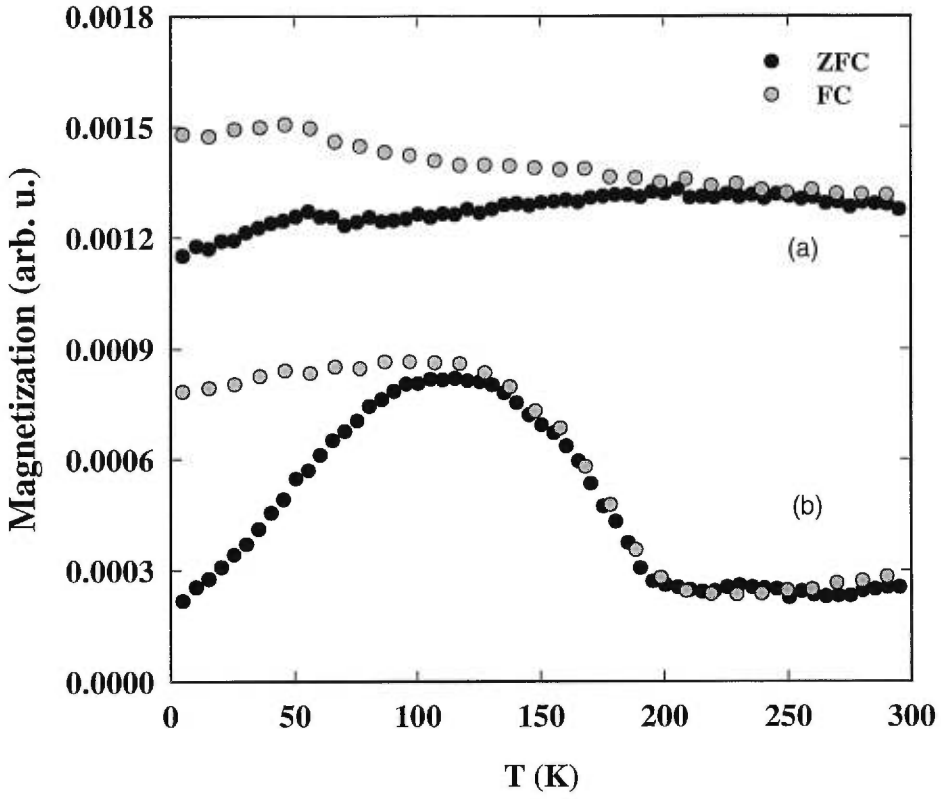


Figure 5.3. The zero-field-cooled curves (ZFC) and field-cooled curves (FC), with the external magnetic field $H_{ext}$=20 Oe, for [Co(5 Å)/Cu (17 Å)]×50 multilayer (a) as-deposited and (b) after irradiation with a dose of $5\times10^{15}$ ions/cm$^2$.

Finally, to show how the magnetic moment depends on the Co concentration in ion-beam prepared CoCu alloys, a series of Co/Cu multilayers with various nominal average compositions and very thin layers (<15 Å) were deposited and were irradiated at a high ion dose of $10^{17}$ ions/cm$^2$. For these multilayers, low-angle x-ray reflectivity measurements have confirmed that the compositional modulation is completely destroyed at an ion dose of $5\times10^{15}$ ions/cm$^2$. Moreover, the saturation magnetization ($M_s$) of these multilayers changes only slightly with increasing ion dose above $5\times10^{16}$ ions/cm$^2$. Thus, it is expected that an ion dose level as high as $10^{17}$ ions/cm$^2$ should lead to a steady-state of intermixing. In Fig. 5.4, the normalized magnetic moment ($M/M_{bulk}$) is shown as a function of nominal Co concentration, where M is the magnetic moment per Co atom for

a heavily irradiated multilayer and $M_{bulk}$ is the bulk magnetic moment of Co as estimated from a 1000 Å Co film. For a nominal composition smaller than about 25% Co, the mixed films are nearly nonmagnetic. The magnetic moment then increases with increasing Co concentration, and for nominal composition greater than about 50% Co, the average Co magnetic moment in the irradiated films is only slightly (~10%) smaller than the bulk value. These data are particularly useful in estimating the interfacial mixing width induced by ion irradiation, as will be discussed in section 5.3.

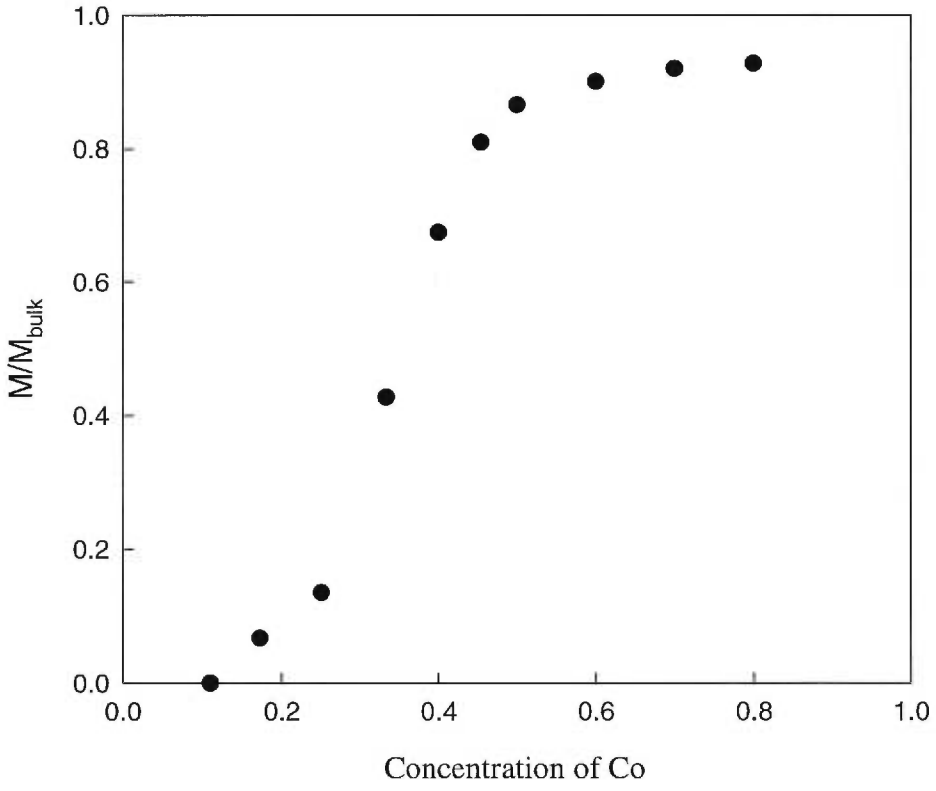


Figure 5.4. Normalized magnetization ($M/M_{bulk}$) of a series of [Co($t_{Co}$<15 Å)/ Cu($t_{Cu}$ < 15 Å)] ×50 multilayers as a function of nominal Co concentration [$t_{Co}/(t_{Cu}+t_{Co})$] after irradiation at $1\times10^{17}$ ions/cm$^2$. $M_{bulk}$ is the bulk magnetic moment of Co obtained from a 1000 Å pure Co film.

### 5.2.3. Transport Properties

The electrical transport properties of Co/Cu multilayers also change dramatically upon ion irradiation. Fig. 5.5(a) shows the resistivity of the [Co(5 Å)/Cu(17 Å)]×50 multilayer as a function of ion dose. For doses lower than $1\times10^{15}$ ions/cm$^2$, the resistivity increases moderately but monotonically with ion dose, but for doses between $10^{15}$ and $10^{16}$ ions/cm$^2$, a sharp increase is observed. At the dose of $10^{16}$ ions/cm$^2$, the resistivity of the film reaches 75 μΩ·cm which is roughly three times greater than that of the as-deposited multilayer. For higher doses, the increase in resistivity with ion dose reveals a sign of saturation. In contrast, the resistivity of pure 1000 Å Co or Cu films (22 μΩ·cm and 4.5 μΩ·cm respectively) changes only slightly (< 15%) upon irradiation at these doses. Consequently, we suggest that the large increase in resistivity of the multilayer is associated with ion-beam mixing. At low doses (<$10^{15}$ ions/cm$^2$), ion bombardment promotes local atomic mixing near interface regions which, in turn, increases the resistivity of the multilayer by reducing the electron transmission coefficient at Co/Cu interfaces. As the ion dose further increases, Co atoms are dispersed deeply into the Cu layers due to multiple displacements. Such Co impurities in the Cu matrix greatly enhance electron scattering in these regions and raise the resistivity sharply. This trend continues until a steady mixing state is achieved at the ion dose of $10^{16}$ ions/cm$^2$. At this stage, the resistivity of the film is found to be very close to that of a homogeneous CoCu alloy (with similar nominal composition) fabricated by low temperature codeposition [18]. Further irradiation only increases the resistivity slightly through the creation of crystalline defects. Should high ion doses lead to phase segregation into large clusters, as is observed in the Co/Ag system [81], the resistivity is expected to drop with increasing ion dose. Such a drop, however, is not observed for the Co/Cu, so such a scenario can be ruled out.

Fig. 5.5(b) and (c) present Δρ (change in resistivity induced by magnetic field) and the MR ratio of the multilayer as functions of ion dose. As mentioned earlier, the Cu thickness of this multilayer was explicitely chosen to be far from any antiferromagnetic (AF) interlayer coupling peak. In this case, a small MR ratio of about 2% primarily originates from the random orientations of Co moments at zero field, due to some degree

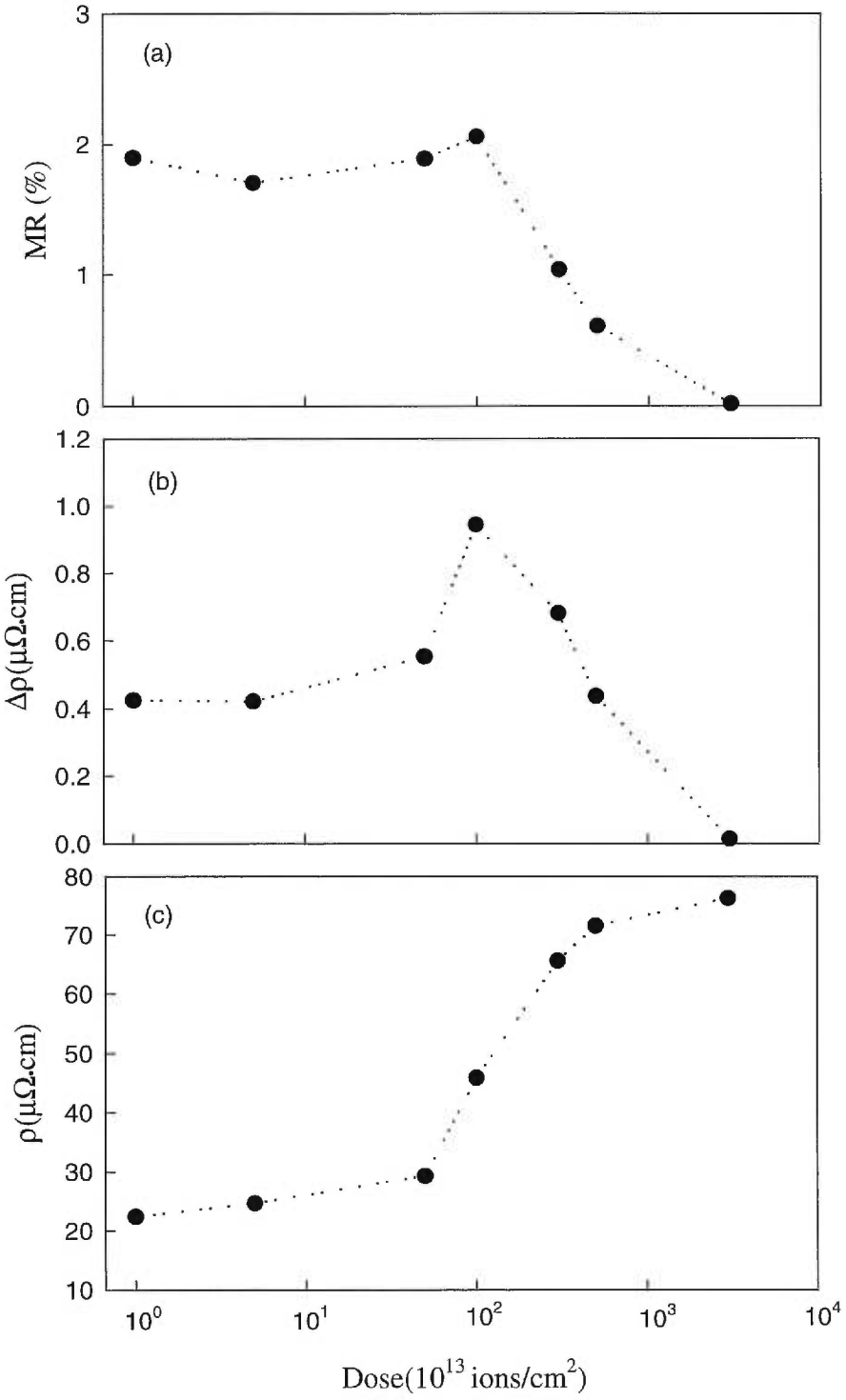


Figure 5.5. (a) MR ratio, (b) change of resistivity, Δρ, and (c) Resistivity, ρ, of a [Co(5 Å)/Cu(17 Å)]×50 multilayer as functions of ion dose.

of discontinuity of thin Co layers, which are eventually saturated in the field direction by external field. Ion irradiation with doses lower than $10^{15}$ ions/cm$^2$ leads to a slight increase in MR ratio, as a result of sharp increase in $\Delta\rho$ compensated by equally large increase in $\rho$. As discussed, increase in $\rho$ is related to enhanced impurity scattering due to ion mixing, while increase in $\Delta\rho$ might be related to the breakdown of continuous layers which enhances the chances that the Co moments are misaligned at zero field. Noticeably, the $\rho$ and $\Delta\rho$ start to rise sharply at similar doses (~$10^{15}$ ions/cm$^2$), which also coincides with the dose at which the magnetization of the multilayer starts to drop. Such doses may correspond to the region the layer structure begins to be disrupted. Further irradiation reduces both MR ratio and $\Delta\rho$. The magnetoresistance disappears completely as the film becomes nonmagnetic at room temperature after being irradiated at doses greater than $10^{16}$ ions/cm$^2$.

Of particular interest is the evolution of the shapes of the MR curves with ion dose. Fig. 5.6 depicts the MR curves measured with field in the TMR and PMR configurations (see 2.4.1). As shown, for the as-deposited multilayer, there is a large difference between TMR and PMR curves. Such a difference is a characteristic of a layered structure and can be ascribed to demagnetizing factor. It therefore shows that, before irradiation, Co forms continuous or quasi-continuous layers (islands with large in-plane dimensions). The double maxima in the PMR curve might be explained as follows. As the external field is applied in the perpendicular direction, depending on local environments, some Co moments can be rotated into the perpendicular direction at relatively low fields, which leads to the initial increase in resistivity. As the rest of the Co moments are also aligned in the perpendicular direction, the resistivity starts to drop. As shown in Fig. 5.6, the difference bewteen TMR and PMR is systematically suppressed with increasing ion dose, and at doses above $5\times10^{15}$ ions/cm$^2$, the magnetotransport behavior of the film becomes isotropic, as is typical for inhomogeous systems with very small magnetic particles embedded in magnetic matrix. Hence, it is concluded that the Co is dispersed into the Cu layers upon irradiation. The MR, however, is much smaller than that reported for CoCu granular systems with similar composition. This difference can be understood in terms that, as Co atoms are dispersed by the ion-beam, only those clustered into small particles contribute to GMR. As these atoms are further dispersed with higher

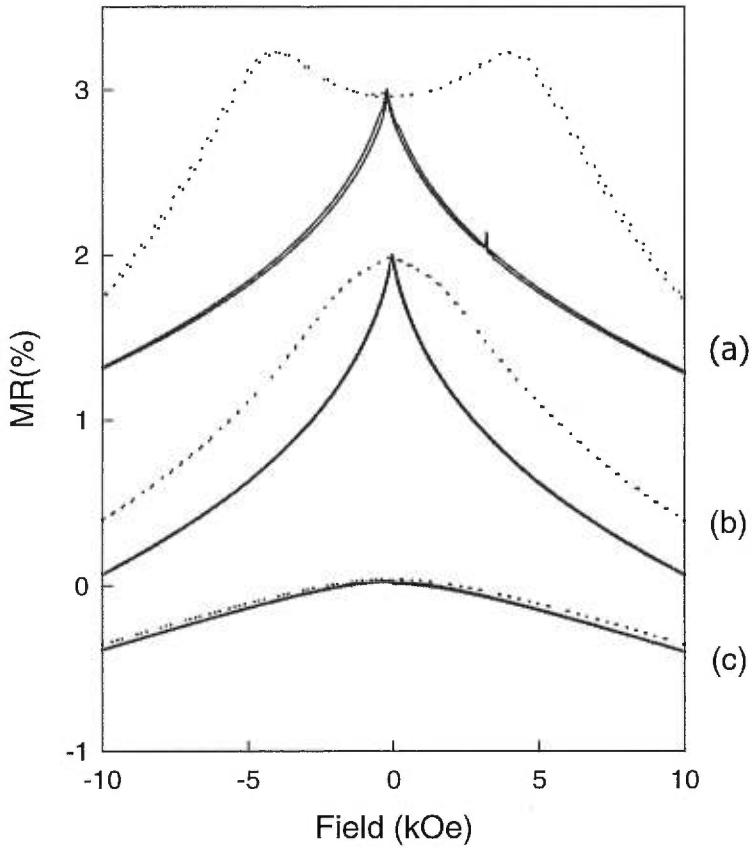


Figure 5.6. TMR (solid lines) and PMR (dotted lines) curves for a [Co(5 Å)/Cu(17 Å)]×50 multilayer (a) as-deposited, (b) after irradiation at $1\times10^{15}$ ions/cm$^2$, and (c) after irradiation at $5\times10^{15}$ions/cm$^2$ . The curves are shifted for clarity.

ion dose, GMR continues to decrease. As the dose reaches $10^{16}$ ions/cm$^2$, MR no longer exists indicating the proportion of Co atoms remaining in such clusters is negligible.

To conclude section 5.2, both magnetic and transport measurements point to a picture in which the Co atoms in a Co/Cu multilayer with thin Co layers are dispersed into Cu matrix upon irradiation. The metastable alloys formed by ion irradiation have magnetic and electrical properties similar to those of the CoCu alloys fabricated by other non-equilibrium methods. While 1 MeV $Si^+$ induces the intermixing between Co and Cu, no accompanied dramatic changes in crystallographic morphology (including grain size, texture etc.) are observed.

## 5.3. Ion Beam Mixing Efficiency

In order to correlate the structural modification induced by ion bombardment and the variation in interlayer magnetic coupling and GMR of Co/Cu multilayers, quantitative information about the structural evolution under ion irradiation is necessary. In this context, one of the most important parameters is the interfacial mixing width and its variation of interfacial mixing width as a function of ion dose determines the ion-beam mixing efficiency, Moreover, a direct comparison between the mixing efficiencies obtained from experiments and theoretical models may shed further light onto the mixing mechanisms under the current experimental conditions.

Conventional methods to obtain information on ion-beam mixing include Rutherford backscattering spectrometry (RBS), secondary ion mass spectrometry (SIMS), and Auger electron spectroscopy. However, the composition wavelength of a GMR multilayer is typically less than 10 nm and significant change in GMR can be associated with angström spreads of mixed regions. Probing such subtle mixing effects using the above-mentioned methods is usually very difficult, especially for mulilayers with little atomic contrast (such as Co/Cu). Nevertheless, the x-ray diffraction technique offers unique advantages for working at such small-scales, including high spatial sensitivity, high penetration and nondestructive capability. At high-angles, x-ray diffraction yields structure information on a crystallographic scale. Ion-beam mixing in textured grains is mainly reflected in the change of relative intensities of superlattice satellite peaks. By fitting such changes, the thickness of ion-beam mixed regions can be determined with angström accuracy for many multilayer systems [88]. However, a major difficulty of applying this method to Co/Cu system lies in the fact that the lattice mismatch between fcc Co and fcc Cu is very small (less than 2%), which makes the satellite peaks typically very weak and not well-defined. On the other hand, at low angles, x-ray reflectivity measurements are sensitive to the average profiles of electronic density and absorption coefficient in a multilayer structure, and don't rely on contrast in the lattice constant. Despite the fact that Co and Cu are very similar in many aspects, we have shown that the large contrast in absorption coefficient between Co and Cu [65] provides low-angle x-ray reflectivity measurements with sufficient sensitivity to detect subtle changes in interface

structures of Co/Cu multilayers. Furthermore, by modeling the interfacial structure of a multilayer and comparing the calculated x-ray reflectivity spectra of the modeled structures with experimental data, quantitative information about interface evolution upon ion irradiation can be obtained.

To study the ion-beam mixing effects over a wider range of ion dose or intermixing width, we focus in this section on a *single* multilayer ( [Co(50 Å)/Cu(75 Å)]×14, designated as Co50/Cu75 hereafter) with thicker individual layers. Superlattice peaks up to the sixth order in the low angle x-ray reflectivity spectrum can be observed, so it is possible to quantify the interfacial mixing width accurately. The multilayer is irradiated successively with ion doses ranging from $10^{13}$ ions/cm$^2$ to $10^{16}$ ions/cm$^2$. After each irradiation, the structure of the multilayer is characterized by a variety of x-ray scattering techniques including high-angle x-ray diffraction, specular low-angle x-ray reflectivity, and low-angle rocking curve measurements. The ion-beam-mixed interface structure is modeled by a sequence of slices whose compositions are determined by an error function profile, and the mixing width at each dose is then determined by fitting to the experimental data. In parallel, the saturation magnetization of the multilayer is also measured after each irradiation, and the mixing width is estimated as a function of ion dose from the variation of the saturation magnetization. The ion-beam mixing efficiencies estimated from these two approaches are then compared, and finally the experimental results are compared to the mixing efficiency predicted by the ballistic ion-beam mixing model.

### 5.3.1. High-angle X-ray Analysis

Fig. 5.7 presents high-angle x-ray diffraction spectra of the Co 50/Cu 75 multilayer at various doses up to $1\times10^{16}$ ions/cm$^2$ (at which point the multilayer structure is destroyed as indicated by low-angle x-ray reflectivity mesurements). The spectrum of the as-deposited multilayer has been described in chapter 3: in brief, the multilayer is highly textured in the fcc (111) direction and the superlattice satellite peaks near the (111) main peak are visible but very weak due to the small lattice mismatch between fcc Co and fcc Cu.

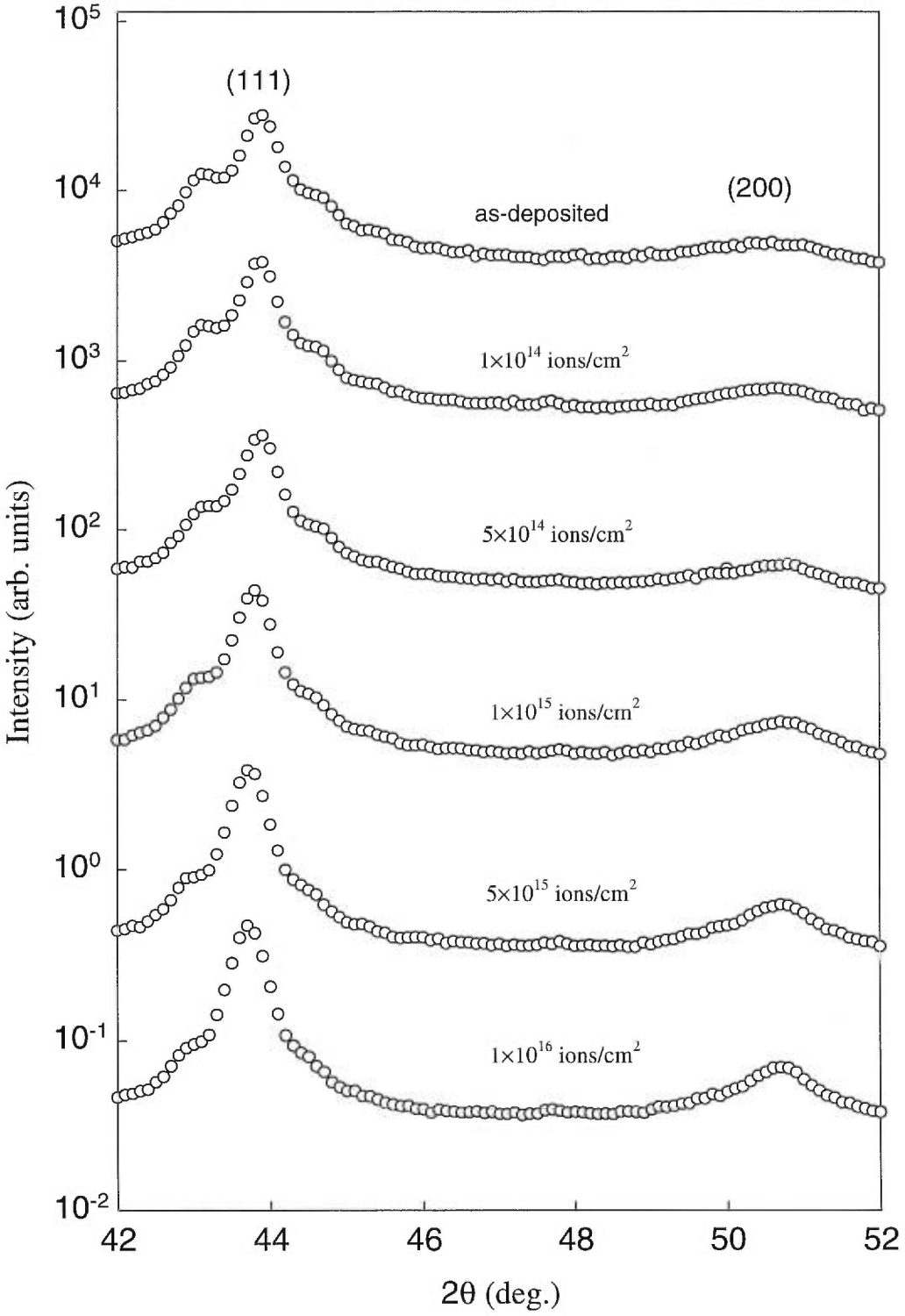


Figure 5.7. High-angle x-ray diffraction spectra for the [Co(50 Å )/Cu(75 Å) ] ×14 multilayer as a function of ion dose.

The most noticeable effect of ion irradiation is the progressive reduction in the superlattice satellite peaks with increasing ion dose, in agreement with the picture that the interfaces are systematically blurred by ion mixing. At $1\times10^{16}$ ions/cm$^2$, the satellite peaks are almost invisible. However, since the satellite peaks are rather weak even for the as-deposited multilayer, fitting these spectra for quantitative information about the mixing width is not feasible.

Other effects are also visible. For example, at high doses ( $> 10^{15}$ ions/cm$^2$ ), the (111) linewidth is slightly reduced upon irradiation, which is not observed for the multilayers with thin Co layers (see section 5.2). This change might be related to subtle grain growth due to the annealing of crystalline defects or grain boundaries during irradiation, as has been widely observed in other systems [89]. However, it should be noticed that, due to the existence of satellite peaks, it is difficult to determine the variation in grain size (linewidth) precisely from these data. Also, upon irradiation, the (111) peak shifts slightly towards smaller angles. However, the corresponding change in average lattice constant is less than 1%, which is in contrast to the observations made for multilayers such as Au/Ni[89], or Ag/Cu[90], where pronounced shifts of the Bragg peaks upon irradiation have been recorded. Such a difference is not surprising, since neither the mixing of Co into the Cu matrix nor the mixing of Cu into the Co matrix is expected to change atomic spacing significantly. Again, the satellite peak intensity masks the exact position of the main Bragg peak, so that the precise peak shift cannot be determined reliably. Nevertheless, Fig. 5.7 shows that the changes in grain size or lattice constant are not considerable, especially at low doses. Finally, at doses greater than $10^{15}$ ions/cm$^2$, the (200) peak is enhanced slightly. Such an effect, however, is hardly visible at low doses, and even at the largest dose ($> 10^{16}$ ions/cm$^2$), a high degree of (111) texture is still maintained.

### 5.3.2. Specular Low-angle X-ray Reflectivity Analysis

Fig. 5.8 shows low-angle x-ray reflectivity spectra of the Co 50/Cu 75 multilayer before and after irradiation at various doses. For the as-deposited multilayer, clear superlattice peaks are observed up to the sixth order, which confirms that the Co/Cu

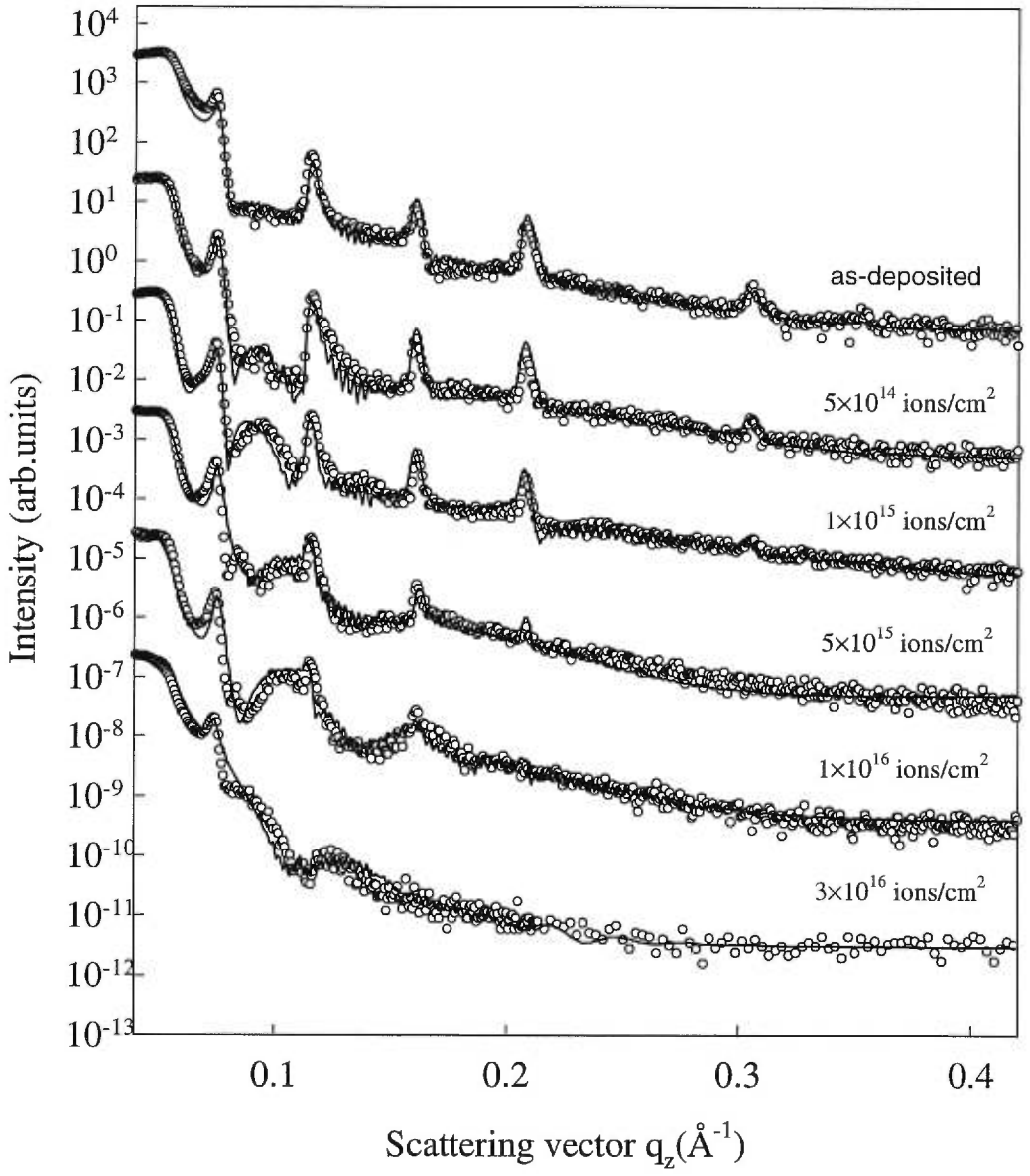


Figure 5.8. Experimental (circles) and simulated (line) specular low-angle reflectivity spectra for a [Co(50 Å )/Cu(75 Å) ] ×14 multilayer at various ion doses.

interfaces are well-defined. Upon ion irradiation, the positions of the superlattice peaks remain the same, indicating the modulation period of the multilayer is not changed. On the other hand, the intensities of the superlattice peaks are progressively reduced as the ion dose increases. At an ion dose of $3\times10^{16}$ ions/cm$^2$, only a weak first-order peak is observed, signaling that the superlattice structure is almost completely destroyed. Given the fact that the intensities of the specular superlattice peaks are indications of interface sharpness and smoothness in a multilayer structure, interface blurring induced by ion irradiation is clearly revealed by these measurements.

To quantify the effect of the ion irradiation, the x-ray spectra have been fitted with the standard optical model described in chapter 3. In order to include interfacial mixing, an error function composition profile at the interface [75] is assumed, and is written as

$$C(x) = \frac{1}{2} + \frac{1}{2} \times erf\left(\frac{x - x_0}{2\sqrt{Dt}}\right) \qquad (5.3)$$

where C(x) is the concentration of impurity atom at depth x, $x_0$ is the position of the original interface and $2\sqrt{Dt}$ characterizes the amount of mixing at the interface. This interface profile is treated as a sequence of slices (~ 1 ML), each with constant composition. For the *i*th slice, the impurity concenetion $c_i = C(x_i)$, where $x_i$ is the depth of the slice in the vertical direction. The index of refraction of the slice is deduced from its average electron density and linear absorption coefficient, and is then applied to the appropriate matrix. The entire interface region is characterized by the product of the matrices of the individual slices. For simplicity, a cutoff condition is introduced so that the slices with impurity concentration of less than 5 % are treated as pure layers. It has been found that discarding such mixing tails has little effect on the fitting. In addition, as a global roughness factor has also been incorporated into the calculation, as mentioned in chapter 3. Model calculations are fitted to the data using the nonlinear least-squares procedure described in section 3.2.

In all calculations, bulk values are used for electronic densities and absorption coefficients of Co and Cu. The modulation wavelength of the multilayer is obtained from

the peak positions for the as-deposited spectrum, and is kept constant when calculating all spectra corresponding to various doses. The remaining parameters are obtained from the fittings. The solid lines in the Fig. 5.8 are the fitted curves for the spectra, and are in very good agreement with the experimental data. The structural parameters extracted from the fittings are listed in Table 5.1. In order to explain the extra oscillatory feature induced by ion beam, an oxide overlayer has to be considered whose thickness varies with ion dose. As shown in the figure, the extra oscillation appears between the first and second order superlattice peaks at a dose of $1\times10^{15}$ ions/cm$^2$, and corresponds to an overlayer of thickness 71 ± 3 Å. Such an effect is commonly observed for intermediate ion doses, and may probably be ascribed to the damage made by the ion-beam that promotes the diffusion of oxygen. With further irradiation, this feature is shifted towards higher angles, indicating that the thickness of the overlayer decreases, probably because of ion-beam sputtering. As well, the overall profile of a spectrum is hardly changed upon irradiation (except for the highest dose). This behaviour indicates that the overlayer roughness is not changed with ion dose. From our fittings, this roughness is estimated to be around 15 Å.

| dose(ions/cm$^2$) | $2\sqrt{Dt}$ (Å) | $\sigma_I$(Å) | $\sigma_c$(Å) | $t_o$(Å) | $\xi$(Å) | $\sigma_o$(Å) |
|---|---|---|---|---|---|---|
| 0 | 0 | 6.10 | 1.56 | 17.3 | 4500 | 14.7 |
| $5\times10^{14}$ | 3.8 | 6.02 | 1.20 | 22.4 | 3100 | 15.5 |
| $1\times10^{15}$ | 6.5 | 6.08 | 1.48 | 71.0 | 3000 | 15.8 |
| $5\times10^{15}$ | 14.5 | 6.32 | 2.26 | 60.5 | 2350 | 15.9 |
| $1\times10^{16}$ | 20.2 | 6.51 | 2.75 | 60.7 | 1600 | 16.7 |
| $3\times10^{16}$ | 41.8 | 10.1 | 8.20 | 33.6 | 1500 | 20.2 |

Table 5.1. Structural parameters extracted from the fitted results shown in Fig. 5.8 and Fig. 5.10 for a [Co(50 Å)/Cu(75 Å)] × 14 multilayer at various ion doses. $2\sqrt{Dt}$ characterizes the ion mixing width, as defined in Eq. 5.3, $\sigma_I$, the overall interface roughness, $\sigma_c$, the correlated part of interface roughness, $\sigma_o$, the oxide overlayer roughness, $t_o$, the oxide overlayer thickness, and $\xi$, lateral roughness correlation length.

Interface mixing width and interface roughness suppress the superlattice peak intensities. Unfortunately, in specular mesurements, their effects are rather similar and therefore it is difficult to distinguish interfaces which are truly diffuse from those which contain genuine roughness. As previously mentioned, this problem can be partially solved by decomposing the interface roughness into correlated roughness and uncorrelated roughness. The correlated roughness typically has a large lateral correlation length, while uncorrelated roughness may not be strictly distinguishable from intermixing (which is commonly regarded as random roughness with a lateral correlation length shorter than 15 Å ). Based on this assumption, we treat the uncorrelated part of the interface roughness as a constant for all spectra, while any actual change of such roughness upon irradiation is incorporated into the interface mixing. As will be discussed in the next section, the correlated part of interface roughness is obtained from the diffuse scattering measurements around superlattice peaks and thus, can be well separated from interface mixing.

Fitting the spectra using the model described, the interface mixing width is obtained as a function of ion dose and is plotted in Fig. 5.9. Up to a ion dose of $1\times10^{16}$ ions/cm$^2$, the square of ion beam mixing width (4Dt) varies linearly with ion dose, as predicted by the cascade model of ion-beam mixing. For the spectrum with the highest dose ($3\times10^{16}$ ions/cm$^2$), the mixing width exceeds the thickness of the Co layer, and the above analysis breaks down. From Fig. 5.9, the ion beam mixing efficiency d(4Dt)/dϕ is found to be about 400 Å$^4$. This can be compared with the theoretical value calculated using the formula developed by Sigmund and Gras-Marti for ballistic ion beam mixing [78] which is in the form,

$$\frac{d(4Dt)}{d\Phi} = \frac{2}{3}\Gamma_0 \xi \frac{F_D R_c^2}{\rho E_d} \qquad (5.4)$$

where $\Gamma_0$=0.608, $\xi=[4m_1m_2/(m_1+m_2)^2]^{1/2}$ where $m_1$ and $m_2$ are the masses of the atoms involved in collisions, $R_c$ is the mean-square range of a displaced atom taken to be 1 nm [91], and $E_d$ is the average minimum displacement energy, ρ is the average atomic density and $F_D$ is the energy deposited per unit path length at the interface. Taking $E_d$=21 eV ( the

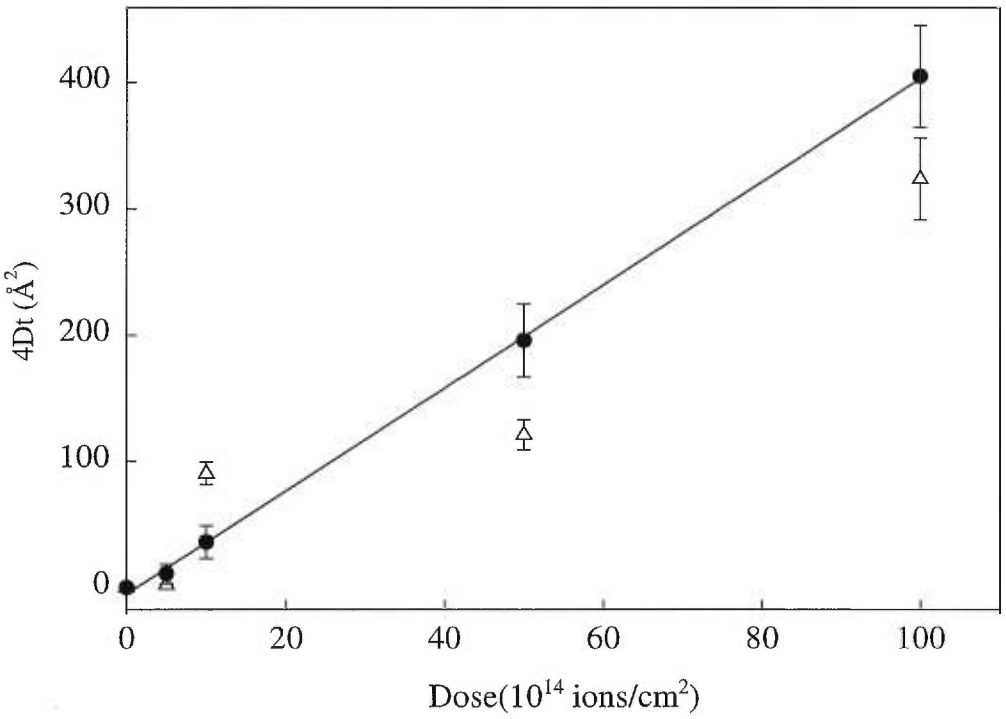


Figure 5.9. The square of mixing width (4Dt) as a function of ion dose obtained from x-ray reflectivity spectra fitting ( •) and saturation magnetization measurements (Δ).

average of Co and Cu [91]), and $F_d$=35 eV/ Å (as obtained from TRIM simulations), Eq. 5.4 predicts a mixing efficiency of 794 Å $^4$. This value is comparable to that obtained from our x-ray reflectivity fitting, suggesting that the ballistic mixing is the principal mixing mechanism of the multilayers at low temperature. On the other hand, the difference between theoretical and experimental values of mixing efficiency might be related to the effect of thermal spike mixing which may reduce the mixing efficiency in an immiscible system, as suggested by Eq. 5.2.

### 5.3.3. Rocking Curve Analysis

Nonspecular reflectivities from x-ray scattering measurements contain information about the magnitude and lateral (height-height) correlation length of the roughness variation. Fig. 5.10 shows the results of rocking scans around the first-order superlattice peak for the Co50/Cu75 multilayer after irradiation at various doses. For the

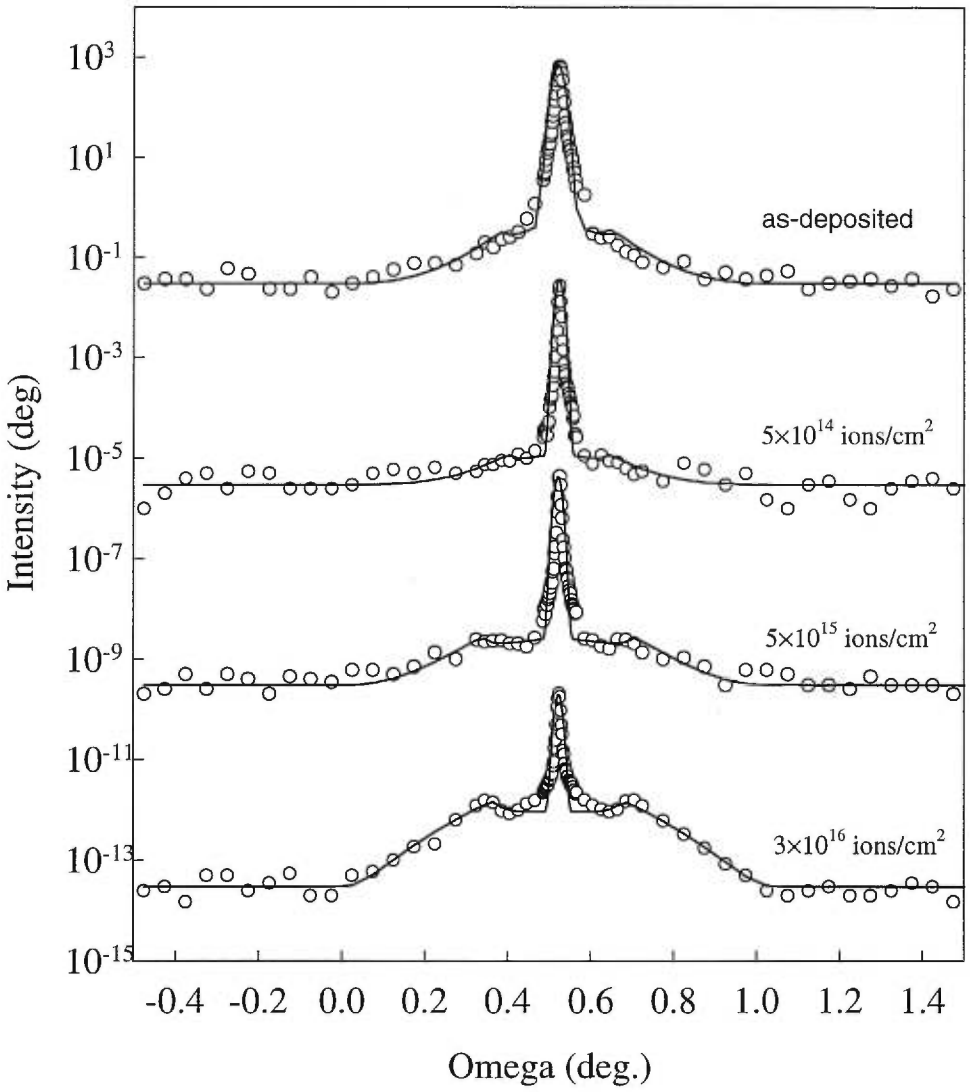


Figure 5.10. Experimental (circles) and simulated (lines) diffuse low-angle spectra for a [Co(50 Å )/Cu(75 Å) ] ×14 multilayer at various ion doses.

as-deposited multilayer, the spectrum consists of a central specular spike and a relatively weak and slowly varying diffuse background in its vicinity. Irradiation at low doses slightly reduces the background, suggesting the layers become smoother. For ion doses larger than $5\times10^{14}$ ions/cm$^2$, the diffuse signal systematically increases with ion dose. At high doses, the so-called "Yoneda wings" (broad maxima corresponding to critical angle

after which the diffuse intensity drops rapidly) are clearly seen. Such observations indicate an increase in interface roughness induced by ion irradiation at high doses. In addition, the shape of the diffuse background also varies with ion dose.

The rocking curves at various ion doses are fitted using Savage's model described in chapter 3. However, it should be mentioned that this model is based on the Born approximation under which "Yoneda wings" can not be reproduced. To reproduce "Yoneda wings", a distorted-wave Born approximation (DWBA) has to be used to refine the Savage model. As shown by Sinha *et al.* [92], the main effect of introducing DWBA is to introduce a prefactor $|T(k_1)|^2| T(k_2)|^2$ to the scattering intensity calculated within the Born approximation. Here $k_1$ is wave-vector of the incident x-ray, $-k_2$ is the time reversed state for the incident beam. T(k) is the transmission coefficient of x-rays with incident wave-vector k, and can be calculated from the Fresnel theory. This prefactor from DWBA is introduced into our calculations to simulate diffuse scattering near critical angles. The fitting curves are presented by the solid lines in Fig. 5.10. As shown, all rocking curves are well reproduced by our calculations. The interface roughness and its lateral correlation length obtained from our fitting are plotted in Fig. 5.11, as well as listed in Table 5.1, as functions of ion dose. Upon initial irradiation, the correlated interface roughness decreases slightly from 1.6 Å to a value of 1.2 Å at $5\times10^{14}$ ions/cm$^2$. At higher doses, the interface roughness continuously increases reaching 8.2 Å at a dose of $3\times10^{16}$ ions/cm$^2$. As mentioned in the previous section, such variation of correlated roughness with ion irradiation has been taken into account when fitting specular spectra. It should also be noted that, except for the highest dose, the range of variation of correlated roughness is within about 2 Å, and thus should not have significantly affected the fitting to specular spectra. Also shown in Fig. 5.11, the lateral coherence length is about 4500 Å before irradiation, which is close to that obtained by de Bernabé *et al.* [65] in their Co/Cu multilayers. This large correlation length typically reflects good diffusion during film growth. As the ion dose increases, the average lateral coherence length decreases monotonically to about 1500 Å at maximum ion dose.

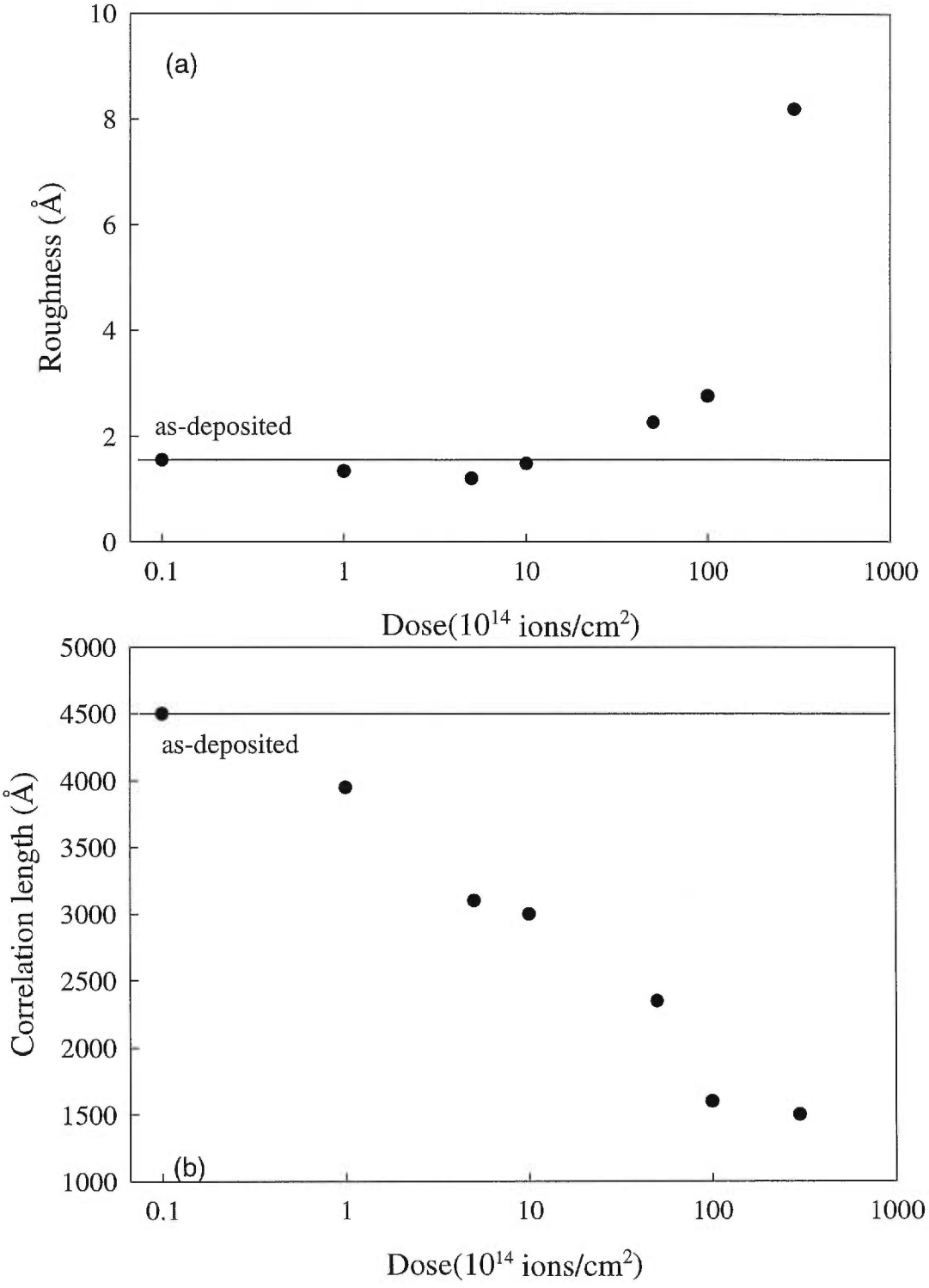


Figure 5.11. (a) Interface roughness and (b) lateral roughness correlation length as functions of ion dose obtained from diffuse low-angle spectra fitting. The horizontal lines represent the as-deposited values.

### 5.3.4. Saturation magnetization ($M_s$)

In Co/Cu multilayers, it has been reported [73] that intermixing between Co and Cu forms magnetically inactive regions and leads to a decrease in the saturation magnetization ($M_s$). Therefore, measuring $M_s$ as a function of ion dose provides another probe to study the mixing effect induced by the ion beam in such a magnetic/nonmagnetic structure. The results of our measurements are shown in Fig. 5.12. As can be seen, a clear drop of $M_s$ is observed for ion doses above $10^{15}$ ions/cm$^2$, falling approximately 20% at a dose of $3\times10^{16}$ ions/cm$^2$. This variation provides clear evidence that intermixing has been induced by ion beam irradiation.

Using a very simple model, the intermixing width can be estimated from these data: first, an error function composition profile is introduced at each interface, the same as used in modeling small-angle x-ray reflectivity fitting ; then, this interface region is divided into many thin slices (~ 1ML) and the average composition of each slice is calculated from the error function; finally, the total $M_s$ of the multilayer is evaluated by summing up the contributions of all slices,

$$M_s = \Sigma\, m(c_i) n_i \qquad (5.5)$$

where $n_i$ is the number of Co atoms in the ith slice, $c_i$ is the Co concentration in the ith slice. The $m(c_i)$ are the average magnetic moments per Co atom related to the cobalt concentration, as estimated from Fig. 5.4.

The dotted line in Fig. 5.12 shows the dependence of $M_s$ on ion dose calculated from the ion-mixing width obtained from x-ray reflectivity fitting. The result agrees with the experimental data. Similarly, $M_s$ measured from experiments can be used to estimate the ion-mixing width at various doses using Eq. 5.5. The results are shown in Fig. 5.9. As can be seen, the ion beam mixing width extracted from x-ray measurements and magnetic measurements are consistent.

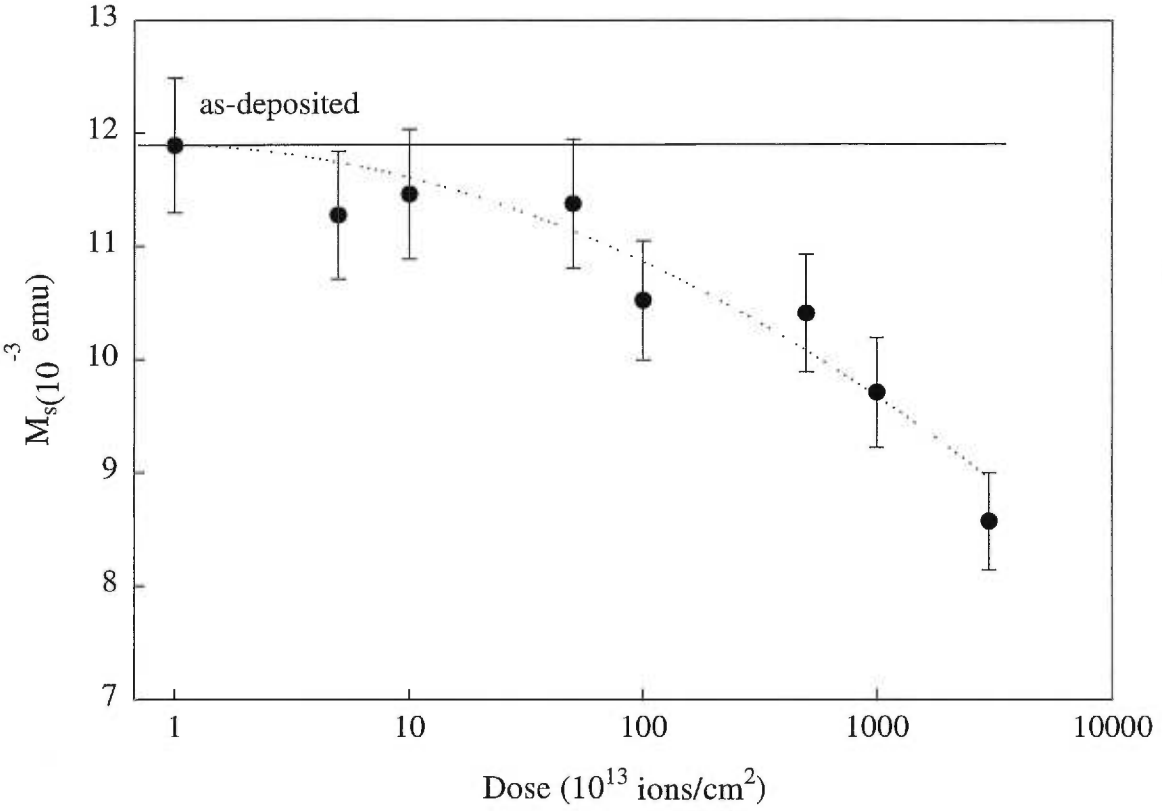


Figure 5.12. Saturation magnetization of a [Co(50 Å )/Cu(75 Å)] ×15 multilayer as a function of ion dose: (a) experimental data, and (b) calculation using the mixing widths obtained from the specular low-angle reflectivity spectra fitting.

## 5.4. Effects on the GMR and Interlayer Antiferromagnetic Coupling

In section 5.2, it has been shown that ion irradation with 1 MeV $Si^+$ leads to intermixing between Co and Cu in a Co/Cu multilayer, and section 5.3 has further derived the ion-beam mixing efficiency between Co and Cu under our experimental conditions. For those discussions, we have deliberately selected Co/Cu multilayers with little or no GMR to focus on the structural aspects and avoid the complexities introduced by interlayer magnetic coupling. In this section, however, we will concentrated on the ion irradiation effects on the GMR multilayers, including the multilayers with Cu layer thickness at the three GMR oscillatory peaks. The magnetic properties and GMR of these multlayers before irradiation have already been discussed in Chapter 3.

### 5.4.1. Ion Irradiation Effects on GMR

Fig. 5.13 shows the variations of the GMR with ion dose for three multilayers: [Co(10 Å)/Cu(10 Å)]×30, [Co(17 Å)/Cu(22 Å)]×30 and [Co(17 Å)/Cu(34 Å)]×30. The Cu-thickness of the first sample is close to the first oscillation peak of GMR, while the other two samples correspond to the second and the third peaks of GMR, respectively. For all three samples, no change in GMR is observed for ion dose below $10^{13}$ ions/cm$^2$. Above that level, GMR decreases progressively with increasing dose. For the multilayer near the first peak, the drop of GMR is particularly abrupt, probably due to very thin Cu layers, whereas GMR falls more gradually for the other two multilayers. The rest of the discussion focus mainly on the multilayers at the second and third peaks.

The decrease of GMR upon irradiation is partially due to the increase in resistivity ($\rho$), as will be shown in Fig. 5.16. However, most of the decrease of GMR is caused by the reduction of $\Delta\rho$ (the field-induced change in resistivity). For these multilayers, no increase in $\Delta\rho$ upon irradiation is observed at any dose level. It is interesting to note that in Fe/Cr multilayers, Kelly *et al.* [31] found that ion irradiation led to an increase in $\Delta\rho$ in spite of a significantly reduced AF coupling. Such behavior was explained in terms of the enhanced spin-dependent electron scattering at the Fe/Cr interfaces. In contrast, for the AF-coupled Co/Cu multilayers discussed here, no increase in $\Delta\rho$ upon irradiation is

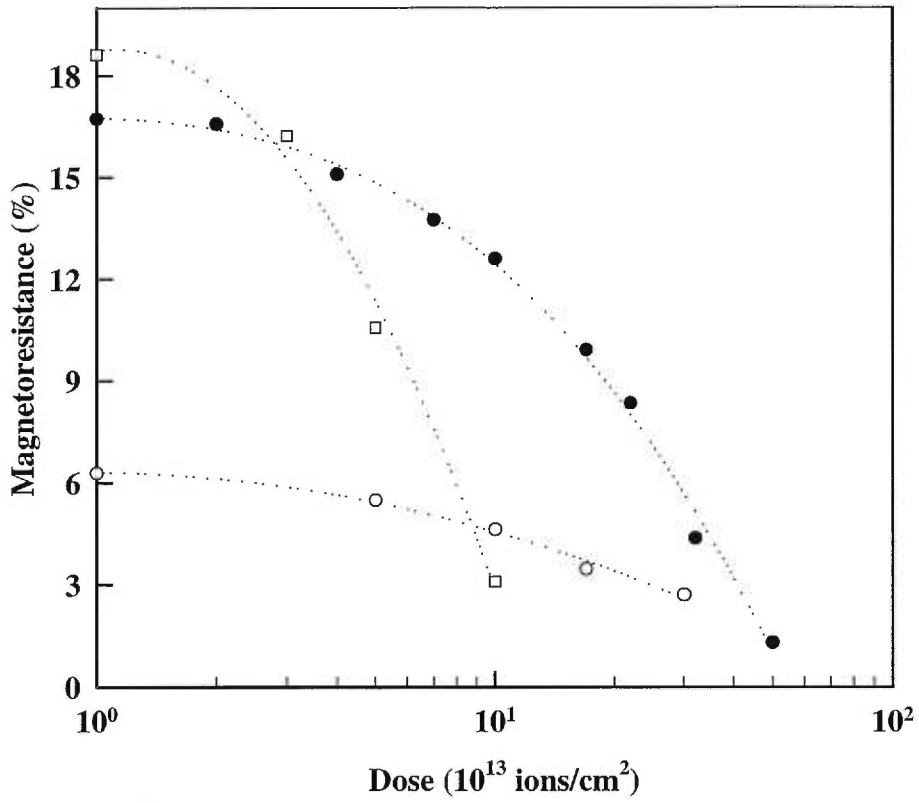


Figure 5.13. GMR ratios of [Co(10 Å)/Cu(10 Å)]×30 multilayer (open squares), [Co(17 Å)/Cu(22 Å)]×30 multilayer (solid circles), and [Co(17 Å)/Cu(34 Å)]×30 multilayer (open circles) as functions of ion dose.

observed at any dose level. This behavior suggests that the role of interface scattering in the GMR might be quite different for Co/Cu and Fe/Cr multilayers. This point will be discussed further.

Fig. 5.14 shows the GMR of a series of multilayers near the second peak before irradiation and after irradiation with a dose of $2\times10^{14}$ ions/cm$^2$. (The GMR of the sample at the oscillation peak is a bit larger than that of the sample described in Fig. 5.13, due to slightly different deposition conditions and a 50 Å Cu cap layer added to the latter sample.) The GMR of all multilayers have decreased upon irradiation. A closer look, however, reveals that the multilayers with Cu thickness slightly less than the peak position are particularly sensitive to the irradiation. In contrast, the multilayers on the other side of the peak exhibit much less drop of GMR at the same dose. This leads to a

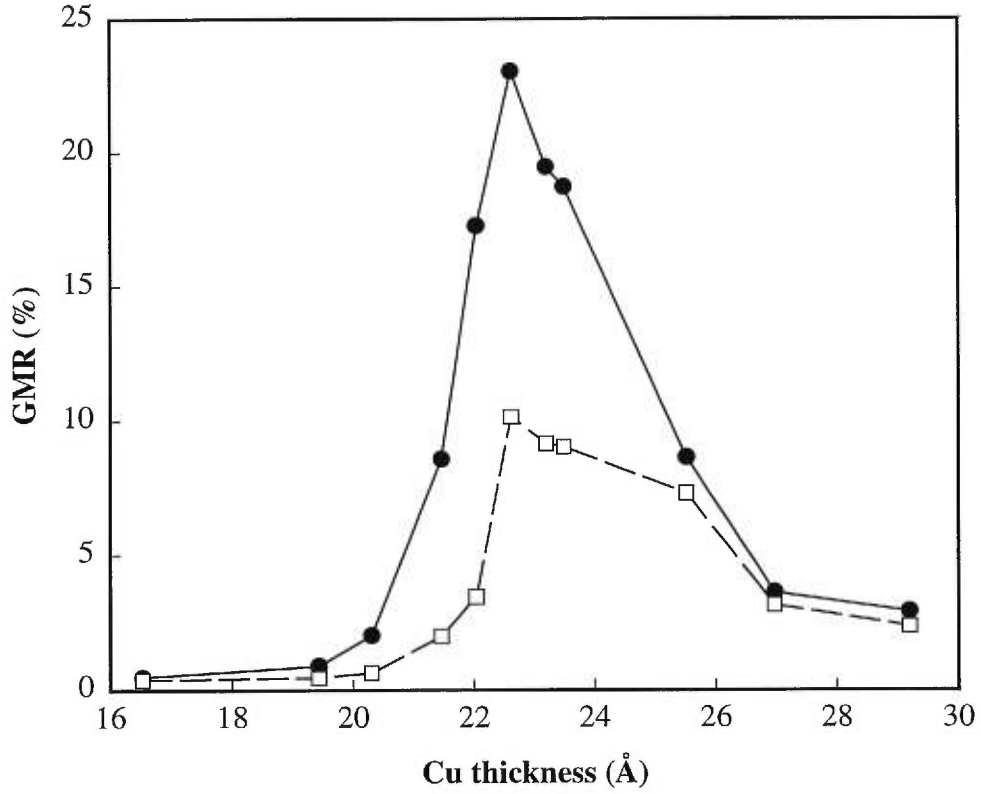


Figure 5.14. The GMR ratios of a series of [Co(17 Å)/Cu(t Å)]×30 multilayers with 16 Å < t < 30 Å before irradiation (solid circles), after irradiation with a dose of $2\times10^{14}$ ions/cm$^2$ (opens squares)

plateau of GMR for a Cu-layer thickness between 23 Å and 27 Å. Such an asymmetry seems a bit surprising, given the fact that the half width of the original peak is only about 4 Å. Some factors might be responsible for this behavior. First, intermixing may reduce the effective thickness of nonmagnetic spacers; second, the mixing of Co into Cu may contract the Fermi surface of the Cu, which in turn, alters the oscillation period of the interlayer exchange coupling [93]. These factors may shift the peak around and complicate the thickness dependence of GMR in irradiated samples. Unfortunately, at this point, it is difficult to separate such effects.

Noticeably, the drop of GMR occurs at very low ion doses. For the [Co(10 Å)/Cu(10 Å)]×30 multilayer, the GMR is quenched at the dose of $10^{14}$ ions/cm$^2$, while for the other multilayers, the GMR have completely disappeared when the dose is

increased to about $5\times10^{14}$ ions/cm$^2$. These ion doses typically correspond to the initial stages of ion-beam mixing which occurs mainly near interfaces [94, 88, 86]. The ion-beam mixing efficiency revealed in Fig. 5.9 suggests that these low ion doses lead to intermixing widths on the order of only a few ängströms. In order to examine closely the effects of ion irradiation at these low dose levels on a multilayer with relatively small wavelength, Fig. 5.15(a) presents the small-angle x-ray spectra of a [Co(17 Å)/Cu(34 Å)]×30 multilayer, (a) as-deposited, (b) after irradiation with a dose of $2\times10^{14}$ ions/cm$^2$. The as-deposited multilayer shows clear first- and second-order superlattice peaks. After irradiation, both peaks are retained. This clearly confirms that the multilayer structure is intact. On the other hand, the intensities of the superlattice peaks are reduced, due to a blurring of the interfaces. The fitted curves to the spectra are shown by the solid lines in the same figure. Considering the low dose (and thus low dpa) involved, instead of using an error function profile, only two extra slices are introduced at each interface in our simulation, corresponding to a Co-rich region ($Co_{1-x}$ $Cu_x$, where $x<0.5$) and a Cu-rich region ($Cu_{1-x}Co_x$, where $x<0.5$), respectively. Taking advantage of the fact the x-ray measurements have been taken on a single multilayer sample before and after irradiation, other parameters, such as the layer thickness and roughness are kept fixed for simplicity. While it is found that the intermixing width and x are somehow correlated, for fixed x in the range from 0.1 to 0.3, (which is comparable to dpa), the intermixing width varies from 6 Å -11 Å, all of which are small compared with the wavelength of the multilayer. This analysis leads us to conclude that the principal structural effect has been to blur the Co/Cu interface over a range of approximately 10 Å without significantly altering the periodic structure of the multilayer.

Interfacial mixing can affect the GMR in two principal ways: the introduction of additional spin-dependent electron scattering centers which would be a direct effect on the GMR; or the modification of the interlayer magnetic coupling, an indirect effect. In order to understand the effects of ion irradiation on GMR, these two aspects need to be examined.

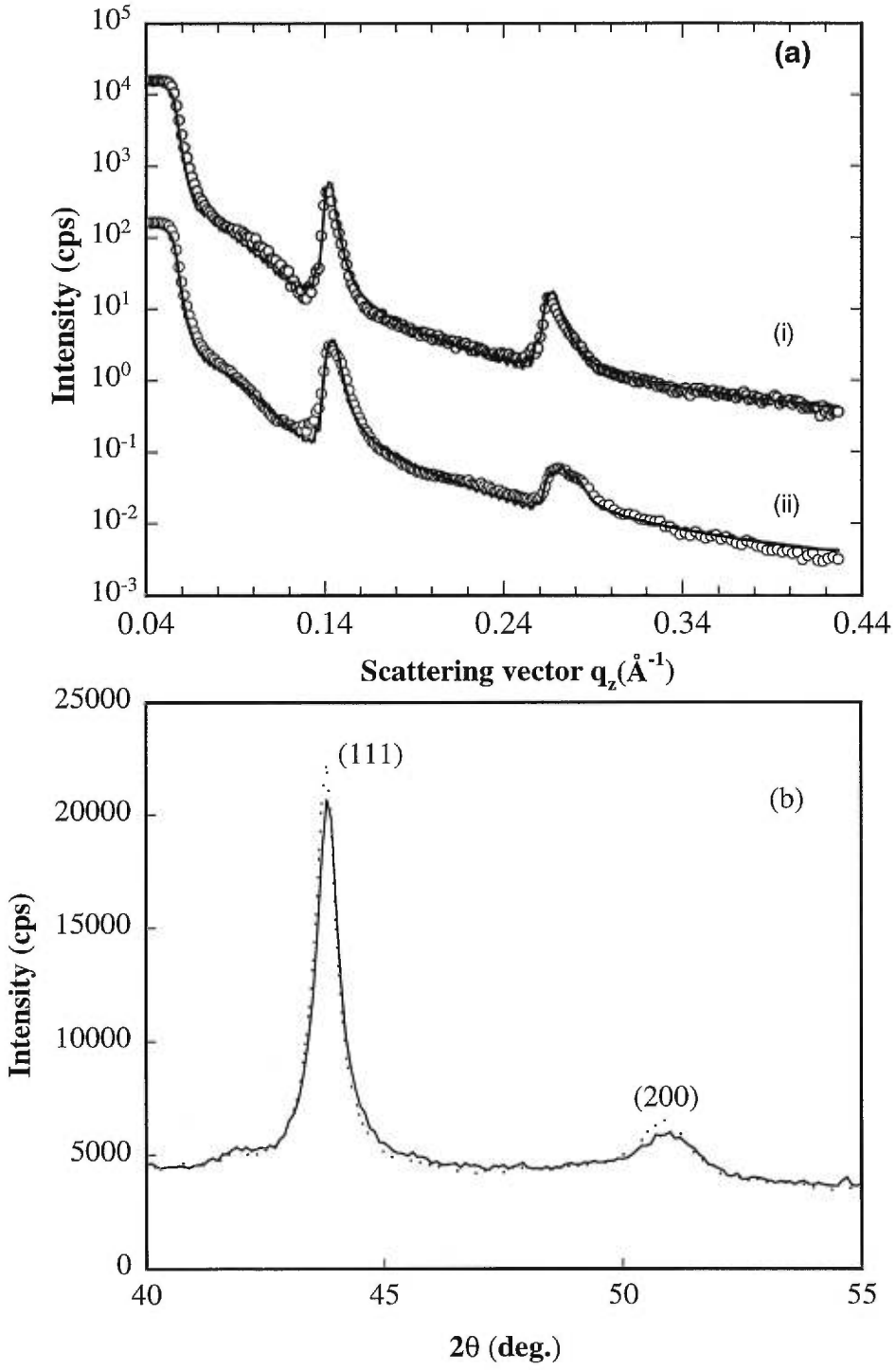


Figure 5.15.(a). Low-angle x-ray reflectivity spectra for a [Co(17 Å)/Cu(34 Å)]×30 multilayer (i) as-deposited and (ii) after irradiation at $2\times10^{14}$ ions/cm$^2$. The solid lines are fitted curves. (b). High-angle x-ray diffraction spectra for a [Co(17 Å)/Cu(22 Å)] ×30 multilayer before irradiation (solid line), and after irradiation at $2\times10^{14}$ ions/cm$^2$ (dotted line).

### 5.4.2. Ion Irradiation Effects on Electron Scattering

Fig. 5.16 presents the variations of the saturation resistivities ($\rho_s$) with ion dose for a [Co(17 Å)/Cu(22 Å)]×30 and a [Co(17 Å)/Cu(34 Å)]×30 multilayer; also shown are the corresponding variations of the resistivities of 1000 Å Cu and Co films. Here we concentrate on $\rho_s$ to eliminate GMR contribution. For ion-beam doses up to $10^{13}$ ions/cm$^2$, no change in the resistivity of the multilayers is observed. At ion doses higher than $10^{13}$ ions/cm$^2$, the resistivity of the multilayers increases noticeably, well beyond that measured for pure films. We therefore suggest that the present large increase of resistivity in the Co/Cu multilayers is connected with enhanced interface electron scattering resulting from ion-beam mixing across the interfaces.

In order to convert the increase in resistivity of a multilayer to the enhancement in electron scattering near its interfaces, we adopt the semiclassical method, initially worked out by Camley and Barnas [9], which is based on the Boltzmann equation in the relaxation time approximation. Suppose the electrical field **E** is applied in the film plane, along the x-axis, and the z-axis is normal to the film plane, the Boltzmann equation is written as,

$$\frac{\partial g}{\partial z}+\frac{g}{\tau v_z}=\frac{eE}{mv_z}\frac{\partial f_0}{\partial v_x} \tag{5.6}$$

where g(v,z) is the deviation of the electron distribution from the equlibrium Fermi-Dirac distribution $f_0(v)$. Then g is further divided into two parts: one for electrons with positive $v_z$, $g_+(v,z)$, and another one for negative $v_z$, $g_-(v,z)$. The general solution of the Eq. 5.6 is,

$$g_{\pm}(z,v)=\frac{eE\tau}{m}\frac{\partial f_0(v)}{\partial v_x}\left[1\pm F_{\pm}(v)\exp\left(\frac{\mp z}{\tau|v_z|}\right)\right] \tag{5.7}$$

where $F_{\pm}(v)$ are the functions of the electron velocity v, which are to be determined from the boundary conditions at an interface described as follows,

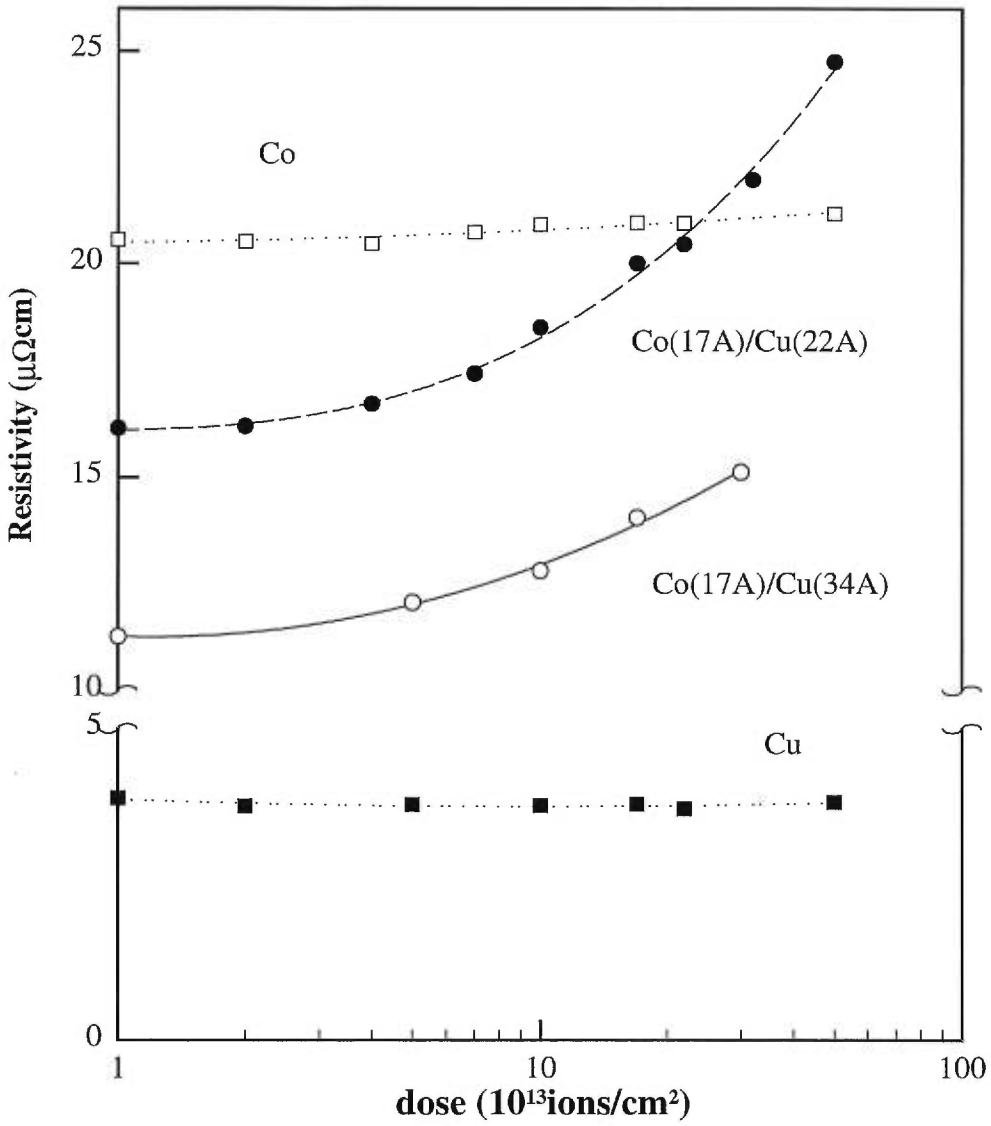


Figure 5.16. Resistivities of a [Co(17 Å)/Cu(22 Å)]×30 multilayer (solid circles) and a [Co(17 Å)/Cu(34 Å)]×30 multilayer (open circles) as well as of 1000 Å Cu (solid squares) and Co (open squares) films as functions of the ion dose.

$$g_{-}(A) = Tg_{-}(B) + Rg(A) \tag{5.8}$$

$$g_{+}(B) = Tg_{+}(A) + Rg(B) \tag{5.9}$$

where A and B represent the two layers separated by the interface, T is the transmission coefficient at the interface and is related to the probability of electron scattering at the interface D by 1-T, and R represents the reflection coefficient at the interface and is negligible for Co/Cu interface. By replacing Eq. 5.7 into the boundary conditions, $F_{\pm}(v)$ and thus $g_{\pm}(v,z)$ are obtained. The current density in the direction of the field is then calculated by,

$$J(z) = \int v_x g(v,z) d^3v \tag{5.10}$$

Finally, the current in the entire structure is found by integrating J(z) over the coordinate z. It is then simple to find the effective resistivity of the entire structure.

Using the above method, the resistivity of a multilayer is calculated with a few parameters characterizing the probabilities of electron scatterings within layers or near interfaces. These include $\lambda_{Co}$ and $\lambda_{Cu}$, the electron mean free paths for bulk cobalt and copper respectively, and the electron transmission coefficient at interfaces (T). Reversely, if $\lambda_{Co}$ and $\lambda_{Cu}$ are given, the transmission coefficient (T) can be estimated from the electrical resistivity. It should be pointed out that, however, in ferromagnets such as Co, electron transport properties should be better described by the two-channel picture, corresponding to spin-up and spin-down electrons, respectively. Unfortunately, little information on the scattering asymmetry of the two current channels can be obtained solely from the resistivity data. As a result, only the average values for all the parameters over the two spin channels are considered. Bearing this simplification in mind, we were able to obtain the as-deposited values of $\lambda_{Co}$, $\lambda_{Cu}$ and T by fitting the Cu-layer thickness dependence of the multilayer resistivity for a series of [Co(17 Å)/Cu($t_{Cu}$ Å)]×30 multilayers with $t_{Cu}$ ranging from 10 Å to 50 Å. From the fitting (not shown), the interface tranmission coefficient before irradiaiton is found to be around 0.8, and the $\lambda_{Co}$ and $\lambda_{Cu}$ obtained are 30 Å and 150 Å respectively, which are very close to those of our pure 1000 Å Co and Cu films. Next, since the resisitivity of pure Co or Cu films does not change upon irradiation, the $\lambda_{Co}$ and $\lambda_{Cu}$ are fixed as constants

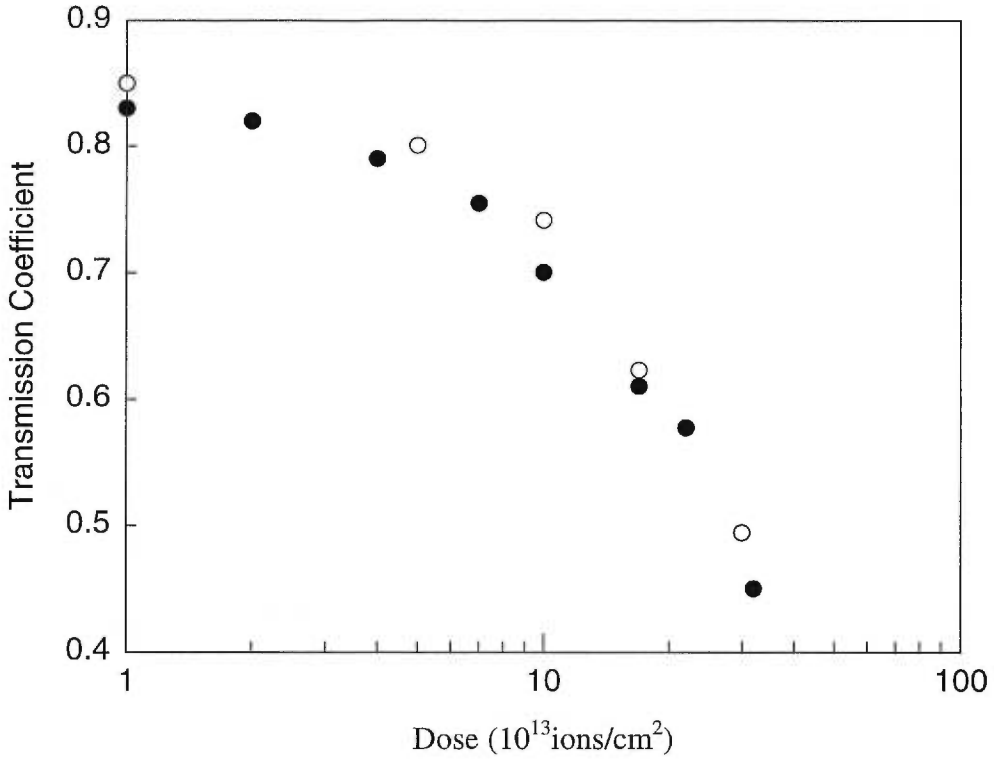


Figure 5.17. Interface transmission coefficient as a function of the ion dose for a [Co(17 Å)/Cu(22 Å)]×30 ( •) and a [Co(17 Å)/Cu(34 Å)]×30 ( o ) multilayer.

and the transmission coefficient T at each ion dose is estimated from the corresponding resistivity data shown in Fig. 5.16. The results are presented in Fig. 5.17 for the [Co(17 Å)/Cu(22 Å)]×30 and a [Co(17 Å)/Cu(34 Å)]×30 multilayers respectively. As can be seen, the transmission coefficients for the two multilayers are very close and follow similar variations upon irradiation: each is reduced by a factor of two as the ion dose reaches $5\times10^{14}$ ions/cm$^2$. This reveals a large enhancement of diffuse electron scattering near the interfaces as they are blurred by ion irradiation.

Despite the fact that the above analysis confirms a strong increase in interface electron scattering upon irradiation, no increase in either $\Delta\rho$ or GMR ratio is ever observed for any AF-coupled Co/Cu multilayer at any dose level. Such a result is inconceivable if the GMR in Co/Cu multilayers is dominated by spin-dependent impurity scattering at interfaces. Therefore, we find no evidence that interface scattering dominates GMR in Co/Cu multilayers. As far as this point is concerned, our results agree

with those obtained from artificial interface mixing through codeposition [47] and appear to support the conclusion that the scattering centers causing the GMR are in the Co layers. However, such a conclusion can not be drawn without caution. As mentioned in Chapter 1, the possibility of interface origin of GMR in Co/Cu multilayers has been suggested by early experiments of planar doping. While the major effect of ion irradiation is to introduce intermixing, the interface origin of GMR may be associated not only with spin-dependent impurity scattering due to intermixing, but also with other mechanisms. For example, the importance of "geometrical" interface roughness in GMR has been pointed out by Hood *et al.*[15]. Recently, Stiles has noted [16] that spin-dependent reflection from interfaces resulting from the band structure of bulk Co may also contribute to a large GMR through the channeling effects, even if there is no spin-dependent defect scattering. The existence of such contributions particularly can not be excluded from our results. Nevertheless, our results suggest that if the GMR in Co/Cu multilayers is interface related, it is more likely related to some mechanisms other than the intermixing based impurity scattering. Obviously, further investigation is still needed to clarify the roles of various mechanisms in the GMR of Co/Cu multilayers, and the possible interplay among these mechanisms.

### 5.4.3. Ion Irradiation Effects on Antiferromagnetic Interlayer Coupling

Another aspect to be considered is the interlayer AF coupling. As the GMR in these multilayers originates from the interlayer AF coupling, any effect on the magnetic coupling will influence the GMR. Indeed, the variation of GMR upon ion irradiation is accompanied by a variation in the interlayer magnetic coupling. Fig. 5.18 shows the magnetization curve for a [Co(17 Å)/Cu(22 Å)]×30 multilayer before irradiation and after irradiation with a dose of $2.6\times10^{14}$ ions/cm$^2$. Initially, the magnetization curve exhibits a small remanence and a slow approach to saturation, which are indicatives of significant interlayer AF coupling. After irradiation, the magnetization curve becomes characteristic of ferromagnetic (FM) coupling, with high remanence and rapid saturation. Fig. 5.19 further details the increase in $M_r/M_s$ and the decrease in the normalized saturation field $H_s/H_{s0}$ (where $H_{s0}$ is the saturation field before irradiation) as a function

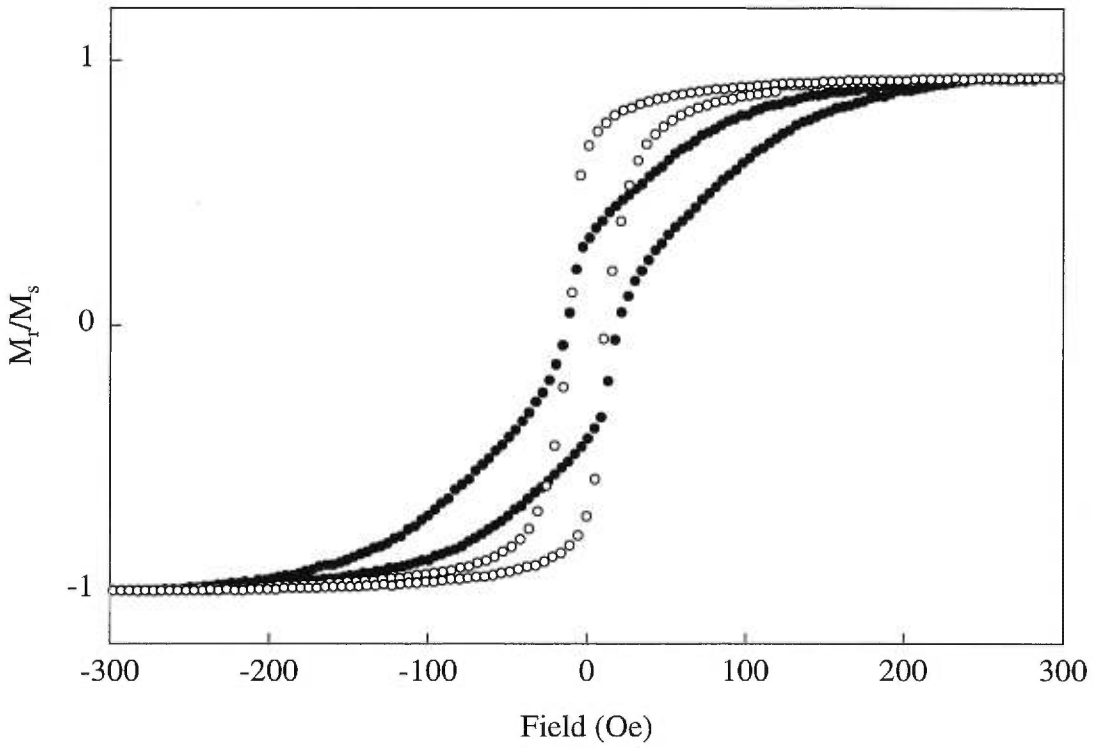


Figure 5.18. The magnetization curve for a [Co(17 Å)/Cu(22 Å)]×30 multilayer before irradiation (solid circles) and after irradiation with a dose of $2.6\times10^{14}$ ions/cm$^2$ (open circles).

of ion dose. As discussed, these parameters are usually related to the degree of AF coupling between magnetic layers. Taking (1- $M_r/M_s$) as an estimate of the volume fraction of AF coupled regions and $H_s$ as indicative of the AF coupling strength, these results suggest that both the net AF coupled fraction and the AF coupling strength are systematically reduced by irradiation.

It has been reported that, in sputtered Co/Cu multilayers, a change in crystallographic texture has profound effects on interlayer magnetic coupling. However, at the present low ion doses, high-angle x-ray diffraction after each irradiation reveals only a subtle increase in the intensity of (200) peak. While this change indicates an increase in the number of (200)-oriented grains, it cannot explain the dramatic suppression of AF coupling upon irradiation: first, the change in texture is too subtle (see Fig. 5.15b) considering the dramatic change in AF coupling; second, previous studies show that [26], in Co/Cu, the AF coupling is weakened as the grains are textured in the

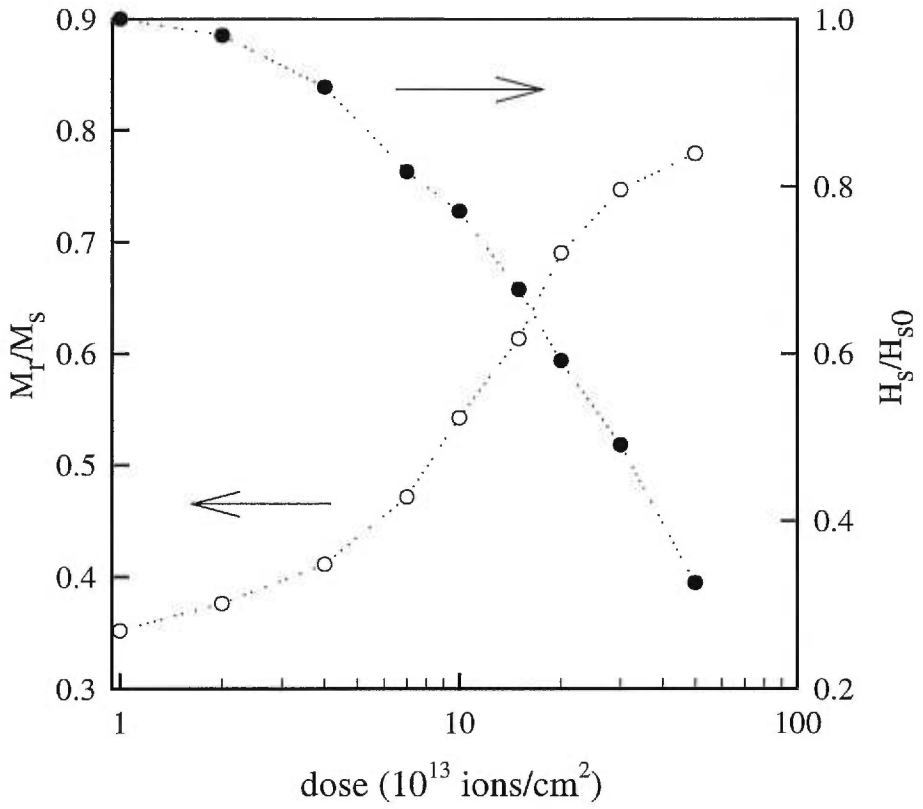


Figure 5.19. The remanence magnetization ratio ($M_r/M_s$), left scale, and the normalized saturation magnetic field ($H_s/H_{s0}$), right scale, for a [Co(17 Å)/Cu(22 Å)]×30 multilayer as functions of the ion dose. $H_{s0}$ is the saturation field of the as-deposited multilayer.

(111) direction and that the presence of (200)-oriented grains enhances AF coupling rather than suppresses it.

Interfacial mixing may also account for the change in interlayer magnetic coupling either indirectly or directly. Indirectly, the mixed interfacial layer effectively adds to the thickness of the non-magnetic (Cu) spacer layer, at the expense of the magnetic (Co) layers (or *vice versa*). While this possibility cannot be totally ruled out, Fig. 5.14 shows that the GMR decreases systematically for all the multilayers in the entire range of Cu thicknesses around the second AF-coupling peak with no shift in its position. This observation indicates that the shift in magnetic coupling period is at least not the dominant mechanism for the reduction in AF-coupling with ion dose. On the other hand, AF interlayer coupling can be suppressed directly by the disorder near

interfaces. Through a first-principle calculation, Kudrnovsky *et al.* [95] concludes that a small amount of interfacial mixing may sharply reduce the AF coupling strength due to the strong disorder present in the Co-Cu alloy system, in particular, between Cu and down-spin Co states. This kind of disorder is expected to be generated when Co and Cu are metastably mixed by a non-equilibrium technique such as ion-beam irradiation. Furthermore, with weaker AF coupling, it is more difficult to nucleate a perfect AF alignment throughout a superlattice in zero magnetic field. Consequently, a decrease in AF coupling strength reduces the volume fraction of the AF coupled regions, as is indeed observed in Fig. 5.19.

For the samples discussed here, it is interesting to note that the decrease of MR occurs at similar ion doses as the suppression of AF magnetic coupling, as is evident from Fig. 5.19 and Fig. 5.13, and suggests that the current reductions in GMR and the AF coupling upon irradiation are directly connected. Recently, a linear relationship between the GMR ratio and the AF coupling fraction has been deduced by Y. Takahashi and K. Inomata [96], in the form

$$MR = MR_0[1-(p+\alpha)] \tag{5.11}$$

where p is the volume fraction of the ferromagnetically coupled regions, $\alpha$ is a correction due to the local ferromagnetic coupling or magnetic anisotropy, and $MR_0$ is the MR of the multilayer should the AF coupling be perfect. Experimentally, this relationship has been confirmed in series of Co/Cu multilayers deposited under various conditions [96]. However, to our knowledge, no results have ever been reported regarding this relationship in a *single* Co/Cu multilayer with systematically modified interfaces, due to the difficulty of modifying the AF coupling fraction over a wide range in a single sample. Fig. 5.19, however, shows that using ion irradiation, the $(1-M_r/M_s)$ of a multilayer can be altered extensively between about 0.3 and 0.7, so such a comparison is possible with our samples. Fig. 5.20 combines the data in Fig. 5.13 and Fig. 5.19, with the GMR of the [Co(17 Å)/Cu(22 Å)]×30 multilayer irradiated at various doses. In addition, since a small degree of magnetic anisotropy is observed in this multilayer, the magnetization data measured along both the hard axis and the easy axis are presented. Clearly, at lower

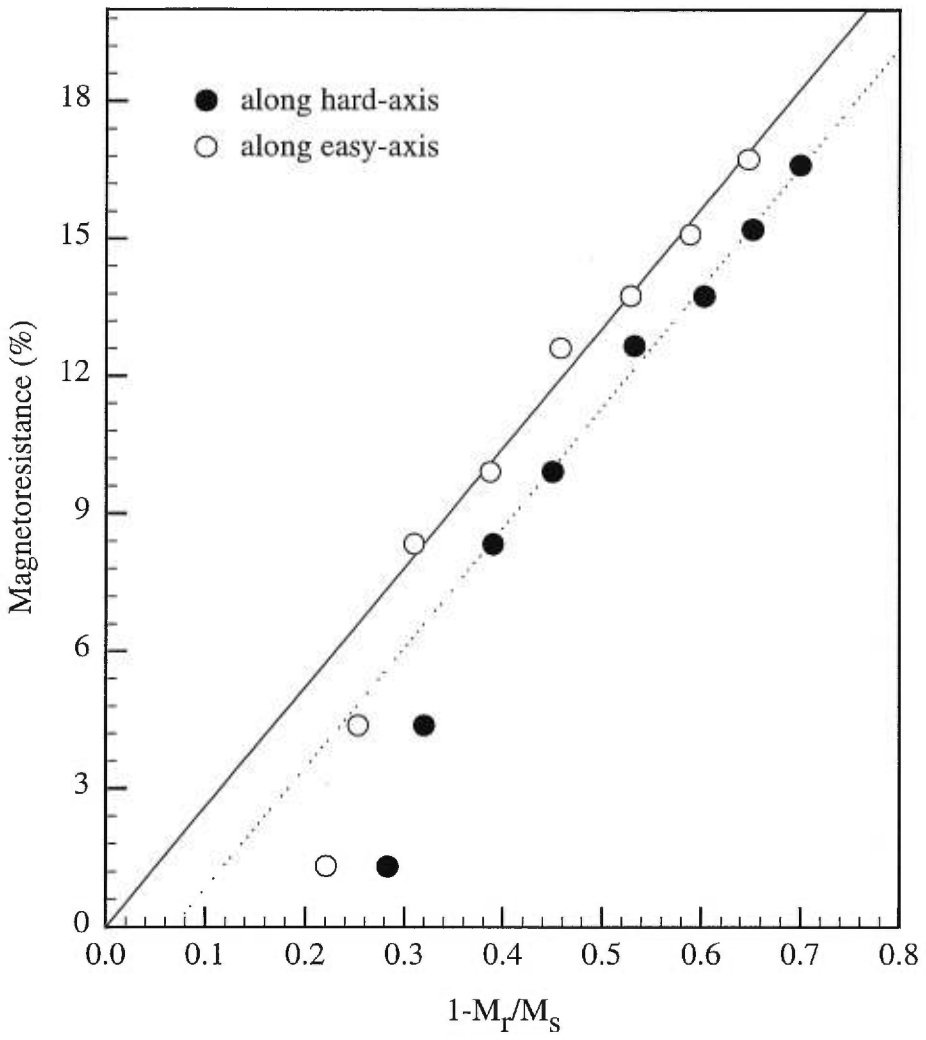


Figure 5.20. MR ratio vs $(1-M_r/M_s)$ for the [Co(17 Å)/Cu(22 Å)]×30 multilayer of Fig.5.13 and Fig.5.19. The lines are linear fits for the data with $(1-M_r/M_s)$ larger than 0.3. The easy axis and hard axis data are measured with the magnetic field in the longitudinal and transverse directions of the sample respectively.

doses, the GMR increases linearly with $(1-M_r/M_s)$. Fitting with Eq. 5.11 yields $\alpha \approx 0$ (as expected) and $MR_0 \approx 26\%$ for the easy axis, and $\alpha \approx 0.06$ and $MR_0 \approx 24\%$ for the hard axis. It can be concluded that the decrease of GMR upon irradiation at low doses ($\leq 2\times10^{14}$ ions/cm$^2$) is directly controlled by the suppression of the AF coupling. At higher doses, the GMR decreases more rapidly than the reduction in AF coupling fraction. One

possible explanation is that, as the interfaces are further mixed, strong electron scattering in the disordered intermixed regions may effectively confine the carriers of both spin-channels within individual layers, a scenario which is consistent with the rapid decrease in the electron transmission coefficient at interfaces as seen in Fig. 5.19.

Concluding section 5.4, ion beam irradiation of Co/Cu mulilayers at low doses provides a means of intermixing Co/Cu interfaces over a short range. It is found that the GMR is indeed strongly dependent on the interface sharpness and structure, and can be altered over a wide range by ion irradiation. It has also been suggested that the variation of GMR upon irradiation is directly controlled by the suppression of the AF interlayer coupling, and no evidence is observed that enhanced interface electron scattering may either increase GMR or even compensate the negative effects of reduced AF coupling on GMR. In the next chapter, we will address the annealing effects on these irradiated GMR multilayers. We will show that annealing such multilayers can provide further insight into the questions that we have discussed in this section.

## Chapter 6: Annealing Effects of Co/Cu multilayers

It is well known that the structural properties, including defects, grain sizes, texture and interfaces, of a multilayer are modified substantially by post-growth thermal annealing. Such a technique has proven very successful in clarifying the role of intermixing in GMR in certain systems. As mentioned in chapter 1, for Fe/Cr multilayers, annealing at moderate temperatures significantly increases the magnitude of the GMR, a fact which has been ascribed to increased interface roughness and related enhancement in *spin-dependent* interface electron scattering.

In contrast, for Co/Cu multilayers, early studies reported by Hall *et al.* [42] indicate that annealing always leads to decrease in GMR. They argued that in Co/Cu, annealing also leads to intermixing, but unlike the case of Fe/Cr, the interfacial scattering processes in Co/Cu are independent of the spin direction of the conduction electrons. However, given the fact that the Co and Cu are strongly immiscible in the equilibrium state, this is highly unlikely the case. Instead, more recent studies [55] [97] [98] using both specular and diffuse x-ray reflectivity analyses indicate that, at least at moderate temperatures, annealing causes no change in the Co/Cu interface structures. This observation has also been confirmed by the nuclear-magnetic-resonance measurements of Thomson, Riedi, and Hickey [99].

It is also interesting to note that the effects of thermal annealing on GMR has been found to be strongly dependent on the spacer (Cu) layer thickness $t_{Cu}$ . Zhang *et al.* [98] reported that for the multilayer at the first GMR peak ($t_{Cu}$ = 9.2 Å), GMR decreases monotonically with annealing temperature (which agrees with the results of Hall et al), while for the multilayers around the second or third GMR peak, GMR initially increases slightly and passes through a maximum before decreasing. Such spacer layer thickness dependence tends to point to the explanation that the annealing induces diffusion of Co (or Cu) atoms along the columnar grain boundaries in Cu (or Co) layers. As the diffusion length of Co becomes comparable to the thickness of Cu layer thickness, direct magnetic bridging between the two neighboring Co layers results, suppressing indirect interlayer AF exchange coupling. Such an explanation, however, is far from conclusive. Many other factors might also be involved. For example, the interlayer coupling energies are very different for the multilayers at the three peaks. Also, the interlayer coupling at the first

peak is extremely sensitive to interface disorder or effective spacer thickness. In addition, the structural characteristics of the spacer layer might be very different in these cases. Any of these possibilities might account for the spacer layer thickness dependence of annealing effects in Co/Cu multilayers.

NMR measurements [49] indicate that annealing at very high temperatures (>500 °C), disrupts the entire multilayer and destroys GMR. Nevertheless, GMR typically starts to drop substantially at intermediate annealing temperatures (300 °C - 450 °C), where the overall mutlilayer structure persists and the effects on the interfaces are too subtle to be deduced from x-ray analysis. Furthermore, NMR study [49] has suggested a progressive increase in the atomic short-range order parameter at interface regions upon annealing at these temperatures. This effect is related to the segregation of Co. It is still unclear what roles such a subtle effect plays in the suppression of GMR.

To clarify some of the above questions, in section 6.1, we present the annealing effects on the GMR of a series of [Co($t_{co}$)/Cu(22 Å)]×30 multilayers with $t_{co}$ ranging from 2.5 Å to 14 Å and $t_{cu}$ fixed at the second AF peak. Since the spacer layer thickness is constant, we expect any interface modification resulting from annealing to be similar for all the multilayers. It is thus interesting to see how the annealing effects depend on the Co layer thickness.

## 6.1. Co Layer Thickness Dependence of Annealing Effects on GMR

The GMR and magnetic properties of the series of [Co($t_{co}$)/Cu(22 Å)]×30 multilayers before annealing have been discussed in detail in chapter 3. Briefly, all the multilayers except the one with the smallest $t_{co}$ (2.5 Å) display large GMR (>10%) and significant interlayer coupling. These multilayers were annealed in vacuum ($10^{-6}$ Torr) with annealing temperatures ($T_A$) ranging from 140 °C to 400 °C. The annealing period is 4 hours for $T_A$ < 200 °C, 2 hours for 200 °C < $T_A$ < 300 °C, one hour for 300 °C < $T_A$ < 400 °C.

As shown in Fig. 6.1(a), the resistivites of all the multilayers decrease with increasing $T_A$. This behaviour, at least partially, can be explained by the grain growth effects during annealing. A systematic increase in the linewidth (and thus grain size) of

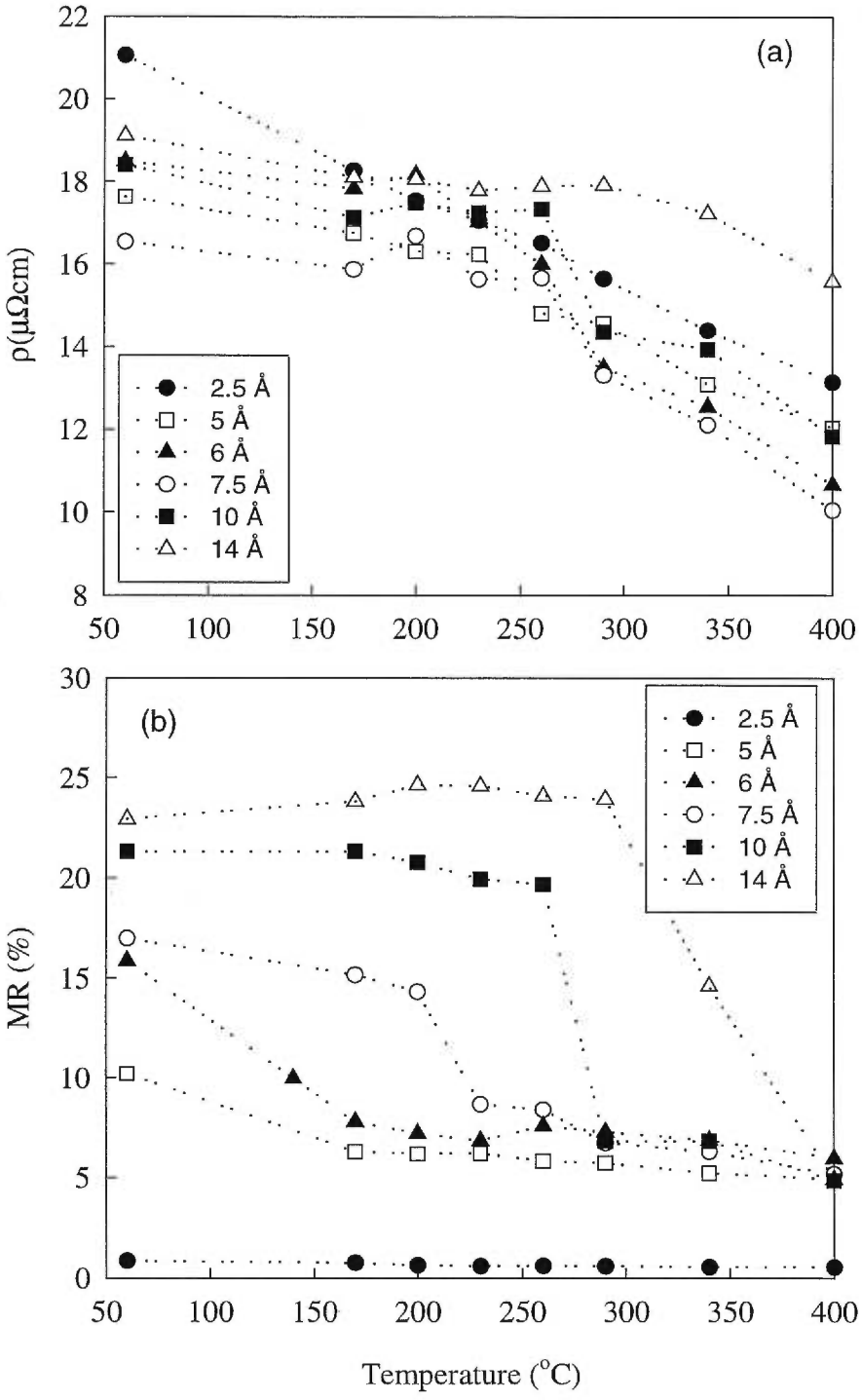


Figure 6.1. (a) MR ratios and (b) resistivity for a for a series of [Co($t_{Co}$ Å)/Cu(22 Å)]×30 multilayers (with $t_{Co}$ ranging from 2.5 to 14 Å) as functions of thermal annealing temperature.

high-angle (111) x-ray diffraction peak upon annealing have been reported by H. Zhang [98] for very similar Co/Cu multilayers, and will not be repeated here. Meanwhile, the magnitude of the decrease in resistivity varies from sample to sample, being fastest for the one with $t_{Co}$ = 2.5 Å , for which the Co atoms exist in the form of dispersed small particles, and annealing may lead to the segregation of these particles. Since the smallest decrease occurs for the largest $t_{Co}$ (14 Å), the change in resistivity might also be related to the variation of multilayer structure. Unfortunately, it is not possible to separate such effects.

Fig. 6.1(b) clearly shows that the effect of annealing on GMR strongly depends on the thickness of the Co layer. There is a threshold $T_A$ for each Co thickness above which GMR starts to drop considerably; this threshold increases with increasing $t_{Co}$. For $t_{Co}$ = 6 Å, GMR drops significantly at $T_A$ as low as 140 °C. In contrast, for the multilayer with $t_{Co}$ = 14 Å, GMR does not decrease until $T_A$ arrives at 300 °C. Below the threshold, the GMR increases slightly with $T_A$ for most of the multilayers. Finally, it is interesting to note that the residual GMR (~ 5 %) is similar for all the multilayers (except for $t_{Co}$ = 2.5 Å) when $T_A$ is raised to 400 °C, independent of the as-deposited GMR of a multilayer.

If the quenching of GMR upon irradiation is the result of the modification in the interface structure, the strong Co thickness dependence of the annealing effects is not expected. On the other hand, these results can be easily understood if we assume that the annealing promotes atomic diffusion through grain boundaries. Transmission electronic microscopy (TEM) analysis has confirmed that due to columnar growth, sputtered Co/Cu typically has vertical (111)-texture and more or less vertical columnar grain boundaries. As Cu penetrates the Co layers along such grain boundary channels, structural discontinuities are created which tend to partition each Co layer into tiles separated by nonmagnetic Cu gaps. If the resulting gaps in the Co layers are sufficiently large and the lateral dimensions of the Co islands are sufficiently small, the condition of quantum confinement of the electrons within individual spacer layers (upon which interlayer AF exchange coupling is based) is violated. In such cases, the interlayer exchange becomes so weak that thermal agitation disrupts the mutual alignment of the magnetic moments in neighboring Co layers, as in the granular-alloy case. In this picture, before Co layers are disrupted, annealing should have little effect on the GMR of a multilayer, and it is also

obvious that with thinner Co layers, Co layers should be broken up at earlier stages of thermal annealing and hence GMR should be quenched at relatively lower annealing temperatures. Both of these predictions are confirmed by our experimental results. Meanwhile, it is conceivable that Co atoms may also penetrate Cu layers along grain boundaries and leads to direct magnetic bridging that suppresses GMR. Such an effect, however, can only explain the Cu thickness dependence of annealing effects. Given the strong Co thickness dependence currently observed, it is very likely that for these multilayers, the breakup of the Co layers is the major reason responsible for the quenching of GMR upon annealing. This is not unexpected since for these multilayers, the Cu layers are much thicker than the Co layers, so that direct magnetic bridging may occur at higher annealing temperatures than the breakup of the Co layers. On the other hand, for Co/Cu multilayers around the first GMR peak, where the Cu spacer layer is much thinner, bridging effects are much more likely.

The above picture is also consistent with the evolution of the shape of the MR curve upon annealing. Fig. 6.2 presents the MR curves of two of the multilayers at various annealing stages. For the first sample, with a 6 Å Co layer thickness, the Co layers might be discontinuous even before annealing. However, as long as the gaps are small, inter-layer exchange or magnetostatic coupling remains strong enough to preserve the AF alignments of magnetic moments in the neighboring Co layers, giving rise to the sharp central peaks in the MR curve. Moreover, granular-like contributions to the MR from relatively smaller Co islands separated by larger Cu gaps may coexist with the multilayer contribution, as is evidenced by the tails in the MR curve which does not saturate at a field of 1 kOe. Upon annealing, the central peaks are progressively suppressed and the granular-like contribution becomes more and more important in the total MR. This suggests that smaller and smaller Co islands are formed and the separations between these islands are increased on average. When the annealing temperature is increased to 230 $^{o}$C, the central peaks completely disappears and the contribution from the AF interlayer coupling is no longer detectable. Further annealing has little effect on the magnitude of GMR while the hysteresis increases with annealing temperature. For the [Co(14 Å)/Cu(22 Å)]×30 multilayer, on the contrary, the much larger thickness improves the integrity of the Co layers, and leads to greater GMR

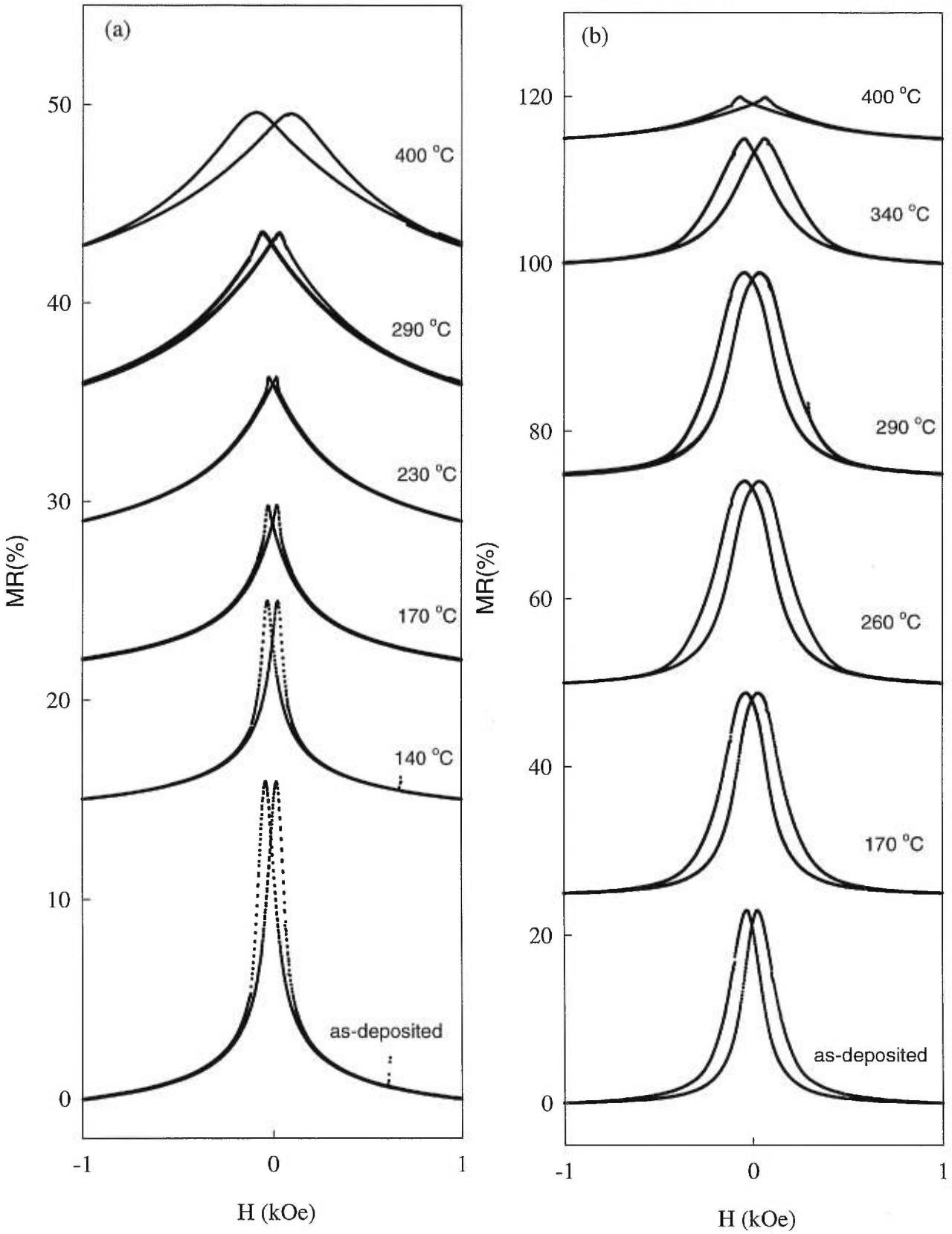


Figure 6.2. A comparison of the evolutions of the MR curves upon annealing for (a) a [Co(6 Å)/Cu(22 Å)]×30 multilayer and (b) a [Co(14 Å)/Cu(22 Å)]×30 multilayer.

associated with AF interlayer exchange. The MR curves are well saturated at a field of 1 kOe indicating that the granular-like contribution is negligible before annealing. The MR curves are nearly unchanged upon annealing below ~ 300 °C except that the hysteresis increases progressively. Annealing at 340 °C, however starts to decrease GMR substantially. Once the GMR originating from the AF interlayer exchange is destroyed, the MR curve becomes characteristic of granular-like material, with a large saturation field, upon heating to 400 °C. In fact, it has been found that such a granular-like contribution is very similar for all the multilayers with Co thickness between 5 Å and 14 Å after they have been annealed at high temperatures, and gives rise to a residual MR of 4-5 %.

In summary, considering the strong layer thickness dependence of the thermal annealing effects on GMR in Co/Cu multilayers, as well as the fact that Co and Cu are immiscible, we suggest that the suppression of GMR upon annealing is primarily associated with the atomic diffusion through columnar grain boundaries. Interestingly, it is noticed that both thermal annealing and ion irradiation lead to the reduction of GMR. The remaining question therefore is: does ion irradiation suppress GMR through similar mechanisms? This question will be discussed in the next section.

## 6.2. Annealing Irradiated Multilayers

To answer the question whether the decrease of GMR upon ion irradiation is also dominated by grain boundary diffusion, we annealed three identical [Co(17 Å)/Cu(22 Å)]×30 multilayers. Before annealing, two of the multilayers had been subjected to ion irradiation at doses of $1.3\times10^{14}$ ions/cm$^2$ and $2.6\times10^{14}$ ions/cm$^2$ respectively. The third multilayer had not been irradiated, and was included as a reference. The annealing temperature ranged from 200 °C to 325 °C, and the annealing periods were four hours at temperatures below 250 °C and two hours at 250 °C and over. The evolutions of the resistivity, the GMR, and the magnetic properties were measured for the three samples after each annealing step.

Fig. 6.3 shows the variation in resistivity for the multilayers; the error bars in the figure indicate the small differences in the initial resistivities of the three samples. As

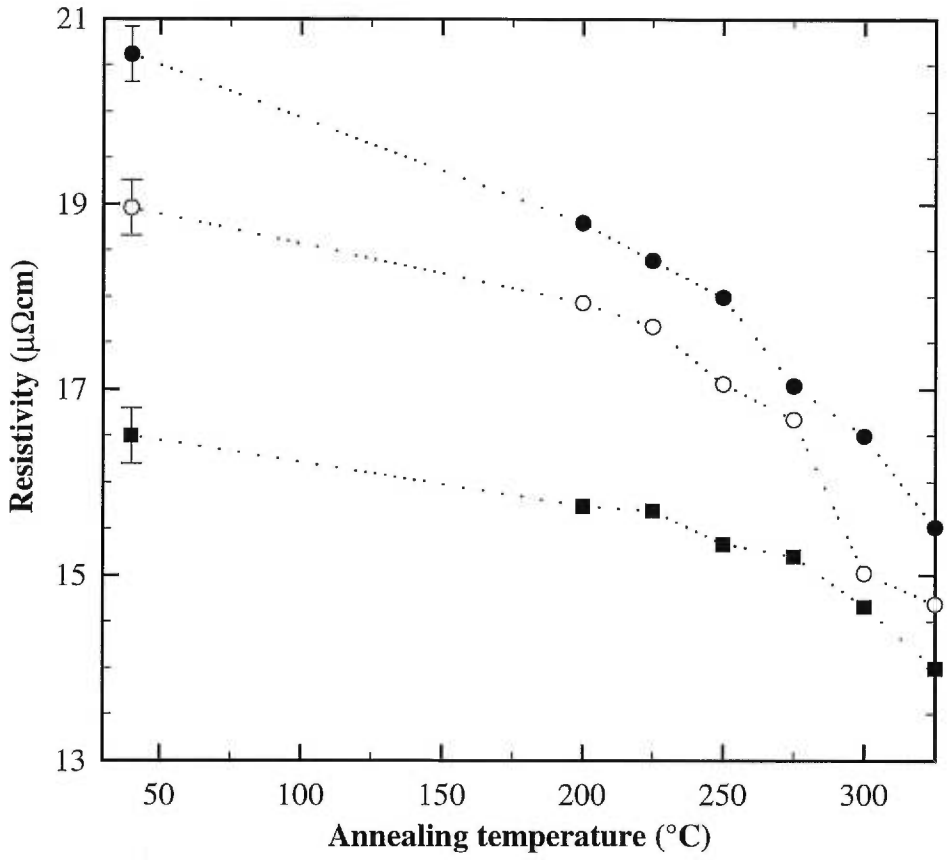


Figure 6.3. Resistivity versus annealing temperature for three [Co(17 Å)/Cu(22 Å)]×30 multilayers: as-deposited (solid squares), irradiated at $1.3\times10^{14}$ ions/cm$^2$ (open circles), and at $2.6\times10^{14}$ ions/cm$^2$ (solid circles). The Error bars indicate the small differences in resistivity among the samples before irradiation.

shown, the resistivity of the irradiated multilayers decrease dramatically upon subsequent annealing. The resistivity of the non-irradiated multilayer also drops but to a lesser extent; this decrease is probably related to minor grain growth during annealing, as mentioned in the last section. Nevertheless, Fig. 6.3 demonstrates that the resistivities of the multilayers irradiated at various doses are approaching that of the non-irradiated sample. Since Co and Cu are strongly immiscible in equilibrium, such behavior might be related to the back-diffusion provoked by annealing at moderate temperatures from the metastably mixed regions.

To explore this possibility, Fig. 6.4 presents the low-angle reflectivity spectra of a [Co(17 Å)/Cu(34 Å)]×30 multilayer, (a) as-deposited, (b) after irradiation with a dose of

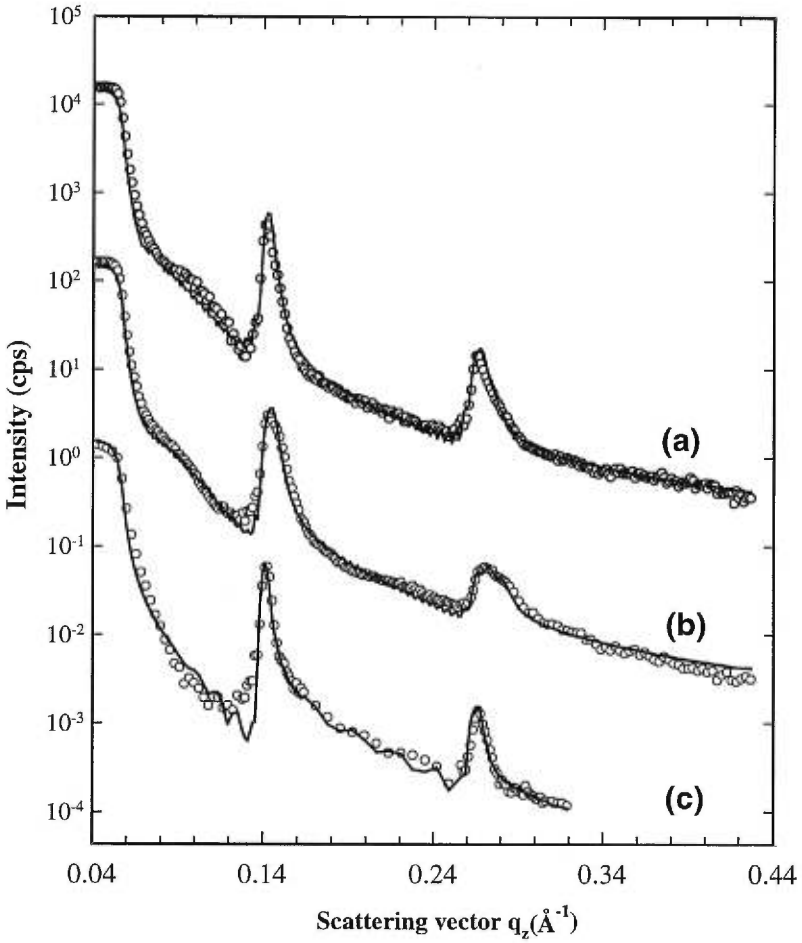


Figure 6.4. Low-angle x-ray reflectivity spectra for a [Co(17 Å)/Cu(34 Å)]×30 multilayer (a) as-deposited, (b) after irradiation at $2\times10^{14}$ ions/cm$^2$, and (c) after annealing at 250 °C for four hours. The solid lines are fitted curves as described in the text.

$2\times10^{14}$ ions/cm$^2$ and (c) after subsequent annealing for four hours at 250 °C. The fittings to the spectra (a) and (b) have been described in detail in Chapter 5. In brief, in order to simulate the ion-beam mixing effect, two extra layers have been introduced at each interface, corresponding to a Co-rich region ($Co_{1-x}Cu_x$, where $x<0.5$) and a Cu-rich region ($Cu_{1-x}Co_x$) respectively. Fitting to the spectrum (b) yields a value of $x$ in the range from 0.05 to 0.3, and an intermixing width between 6 Å and 12 Å. As indicated by the spectrum (c), after annealing, the intensities and the linewidths of the superlattice peaks have fully recovered. Quantitatively, this spectrum can be fitted without the interfacial layers introduced for spectrum (b), with a slight increase of the interfacial roughness from

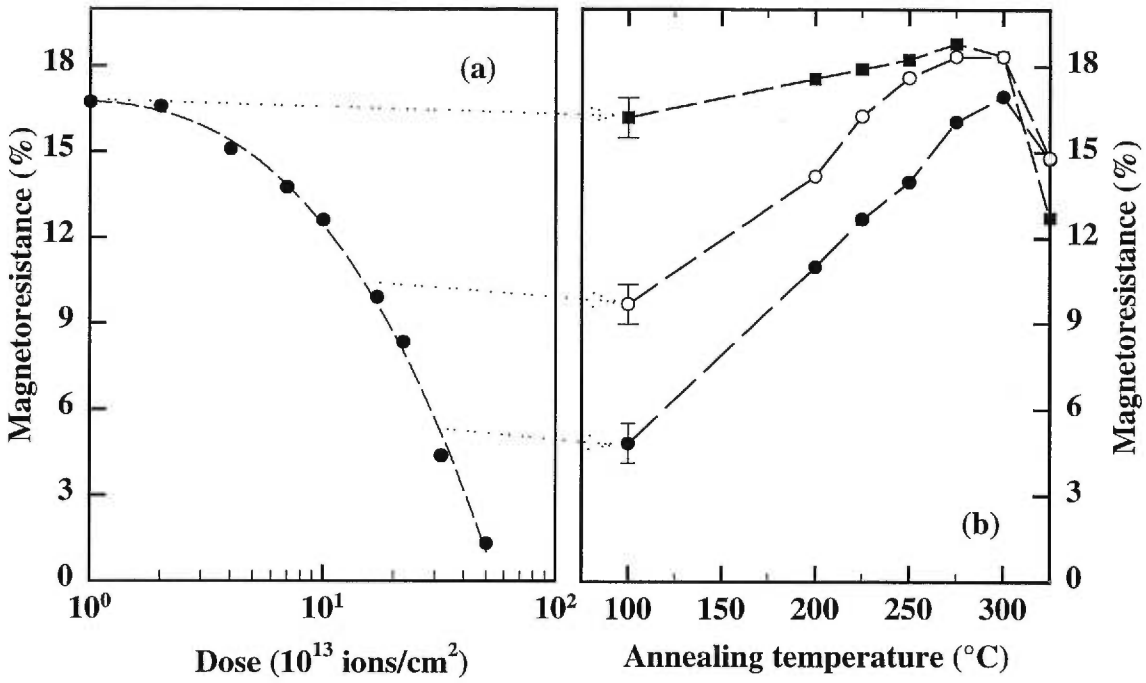


Figure 6.5: (a) Decrease in MR with ion dose for a [Co(17 Å)/Cu(22 Å)]×30 multilayer. (b) Variations in the GMR with annealing temperature for three [Co(17 Å)/Cu(22 Å)]×30 multilayers subjected to ion doses of 0 (solid squares), $1.3\times10^{14}$ (open circles) and $2.6\times10^{14}$ (solid circles) ions/cm$^2$, respectively.

5.7 ± 0.5 Å (for the as-deposited or irradiated multilayer) to 6.3 ± 0.2 Å. In contrast, x-ray reflectivity spectra of virgin Co/Cu multilayers are little affected by annealing at the same temperature [98]. The current result therefore confirms that for an irradiated Co/Cu multilayer, significant demixing occurs on heating, which results in the reformation of relatively abrupt Co/Cu interfaces.

In the process of interfacial demixing by annealing, the GMR increases sharply, as shown in the right panel of Fig. 6.5 for the two irradiated [Co(17 Å)/Cu(22 Å)]×30 multilayers; also shown is the minor increase in MR for the as-deposited mulitlayer. As a reference, the left panel of Fig. 6.5 plots the decrease of GMR with ion dose. The slight increase in MR ratio for the as-deposited multilayer is the result of the decrease in the resistivity related to grain growth, as mentioned in section 6.1. The much more significant rise in the GMR of the irradiated multilayer is, on the other hand, due mostly to the increase in $\Delta\rho$ and is more likely to be associated with the demixing process. As shown, the GMR of the multilayer irradiated at higher dose increases nearly a factor of

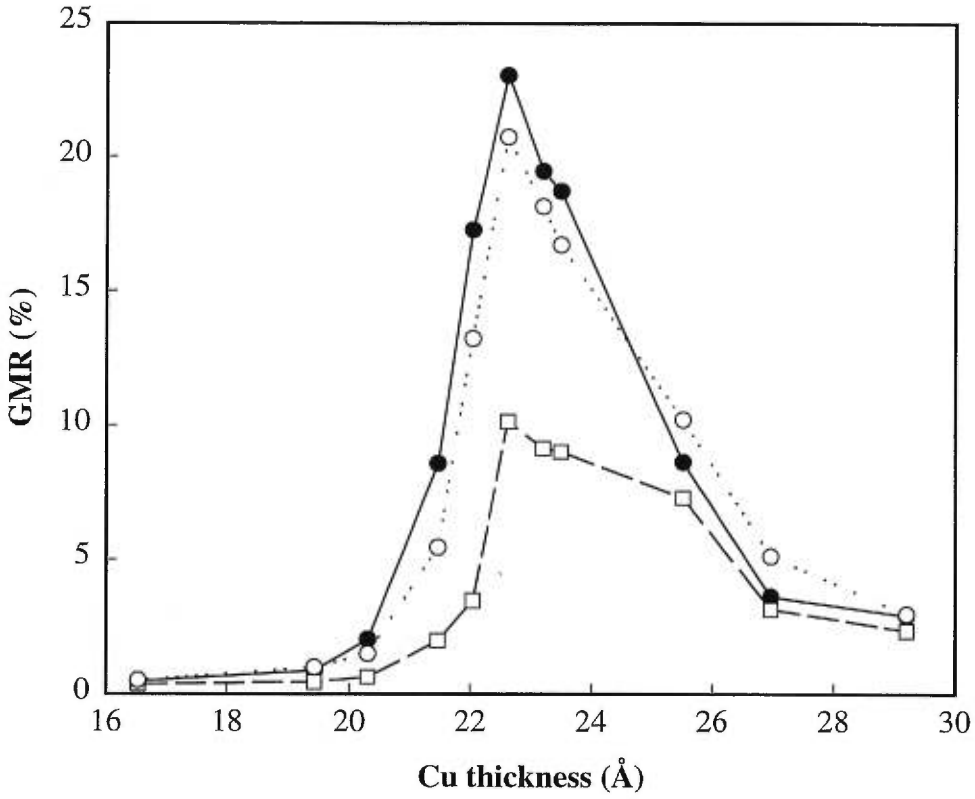


Figure 6.6. The GMR ratios of a series of [Co(17 Å)/Cu(t Å)]×30 multilayers with 16 Å < t < 30 Å before irradiation (solid circles), after irradiation with a dose of $2\times10^{14}$ ions/cm$^2$ (open squares), and after annealing at 240°C for four hours and at 260 °C for two hours following the irradiation (open circles).

three, from about 4% to about 12% upon annealing at 200 °C. Also, the MR of the multilayer irradiated at the lower dose has fully recovered to the as-deposited value after annealing at 250 °C. For annealing temperature over 300 °C, the GMR starts to fall off for all the multilayers, as the multilayer structure begins to break down. However, at each annealing step below this temperature, the GMR increases systematically. This effect has been found for all the mulitlayers near the second peak of the GMR oscillation, with ion doses below $3\times10^{14}$ions/cm$^2$. However, for the multilayers near the first peak, or those irradiated at heavy doses ($\geq 10^{15}$ ions/cm$^2$), no clear effect is observed.

Since in Co/Cu, GMR may also originate from a granular-like contribution, it is necessary to clarify the mechanism of GMR restored by annealing. Fig. 6.6 shows the GMR of a series of multilayers near the second peak before irradiation, after irradiation

with a dose of $2\times10^{14}$ ions/cm$^2$, and after subsequent annealing (first for 4 hours at 240 °C, and then for 2 hours at 260 °C). While irradiation suppresses the GMR and distorts the GMR peak, upon annealing, the GMR of all the irradiated multilayers recover well and, in particular, the oscillation peak is essentially restored. The reformation of the GMR oscillation peak confirms that the mechanism of GMR remains the same, which originates from the AF interlayer exchange coupling, and the possibility of granular-like contribution can be excluded.

As expected, the increase in GMR upon annealing is accompanied by a systematic improvement in the AF coupling between Co layers. Fig. 6.7 shows the magnetization curves of the [Co(17 Å)/Cu(22 Å)]×30 multilayer (a) as-deposited, (b) after irradiation at $2\times10^{14}$ ions/cm$^2$, and (c) after subsequent annealing at 250 °C for four hours. As shown in the figure, the features of AF interlayer coupling suppressed by ion irradiation are clearly recovered by the annealing. The magnetization curve after annealing exhibits low remanence ratio and high saturation field similar to those of the magnetization before irradiation. Fig. 6.8 presents details of the increase in $(1-M_r/M_s)$, which characterize the volume fraction of AF-coupled regions, with annealing temperature for the same three nearly-identical [Co(17 Å)/Cu(22 Å)]×30 multilayers described earlier. As shown in the figure, $(1-M_r/M_s)$ increases systematically with annealing temperature for all three multilayers until about 300 °C. However, it is obvious that the increase in $(1-M_r/M_s)$ is far more dramatic for the two irradiated multilayers than for the non-irradiated multilayer. For the multilayer irradiated at the lower dose, the remanence ratio becomes very similar to the as-deposited value when the annealing temperature reaches 250 °C. For the multilayer irradiated at the higher dose, though not fully recovered, $(1-M_r/M_s)$ is sharply increased as well upon annealing. These variations can also be explained by the back-diffusion upon annealing which improves the AF exchange coupling between layers by producing sharper and more atomically ordered interface regions. Finally, annealing at temperatures above 300 °C reduces $(1-M_r/M_s)$, which can be ascribed to the breakdown of the multilayer structure, for the reason similar to the decrease of GMR at these annealing temperatures.

Fig. 6.9 further correlates the increase of GMR and $(1-M_r/M_s)$ upon annealing by plotting the GMR data in Fig. 6.5 *vs.* $(1-M_r/M_s)$ data in Fig. 6.8. For comparison, the data

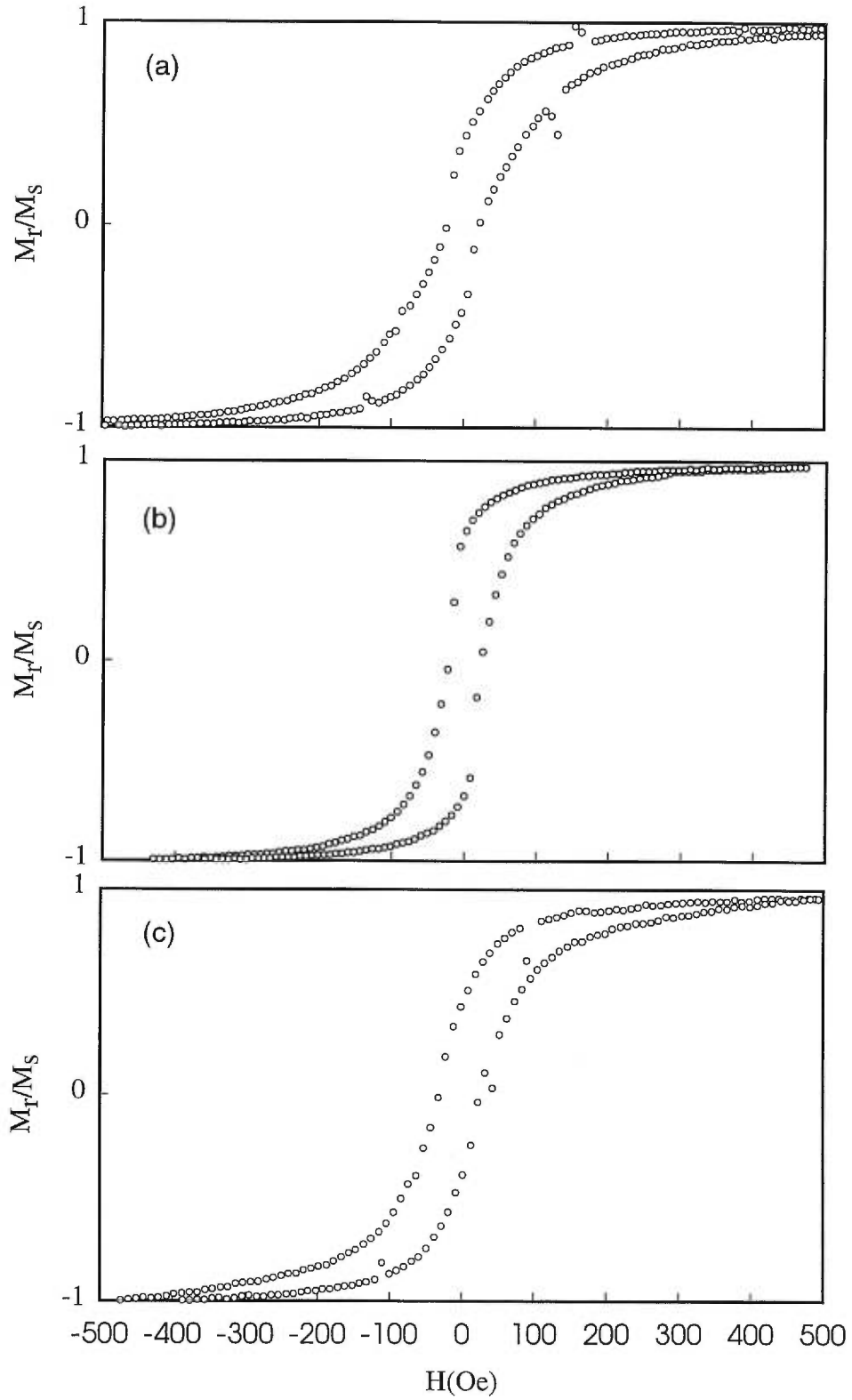


Figure 6.7. Magnetization curves of a [Co(17 Å)/Cu(22 Å)]×30 multilayer (a) as-deposited, (b) after irradiation at $2\times10^{14}$ ions/cm$^2$, and (c) after subsequent annealing at 250 °C for four hours.

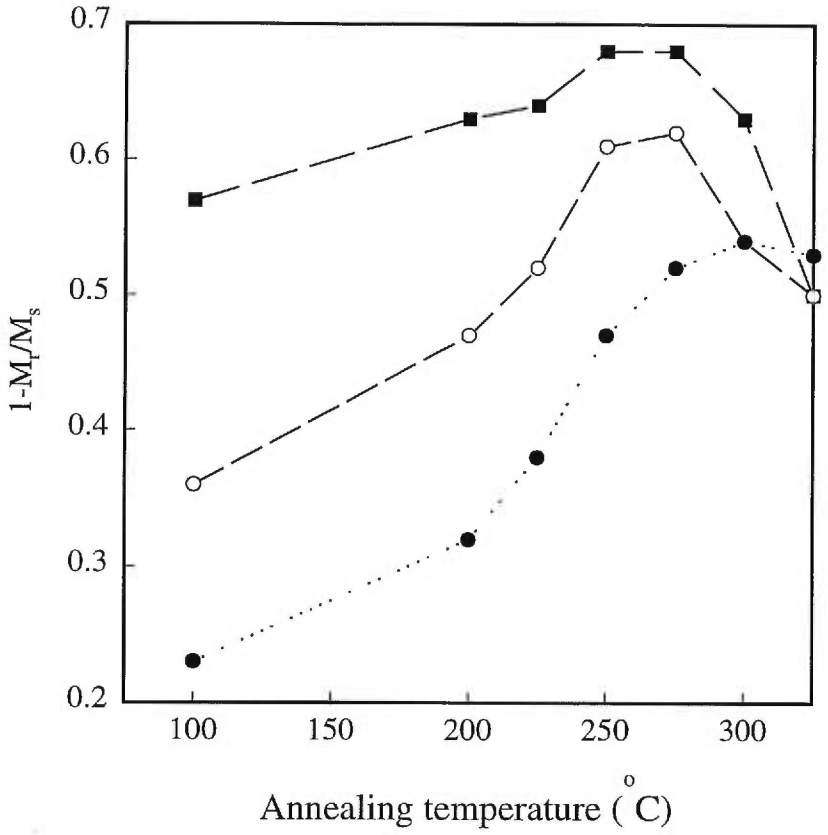


Figure 6.8. Variations in $(1- M_r/M_s)$ with annealing temperature for three [Co(17 Å)/Cu(22 Å)]×30 multilayers subjected to ion doses of 0 (solid squares), $1.3\times10^{14}$ (open circles) and $2.6\times10^{14}$ (solid circles) ions/cm$^2$, respectively.

in Fig. 5.20 are also re-plotted and represented by solid circles. For the purpose of clarity, only the data measured along the magnetic easy axis are shown, but measurements along the hard axis yield similar results. For the non-irradiated multilayer, annealing below 300°C alters the remanence only slightly, thus the corresponding data are only varied over a small range. For the irradiated multilayers, in contrast, the effects of annealing on GMR and AF coupling fraction are *amplified*, and both GMR and AF coupling are tuned over much wider ranges. As can be seen, nearly all experimental points fall approximately on a straight line, suggesting that the recovery of GMR upon annealing in the irradiated multilayers is the direct consequence of the improvement of AF coupling. For any fixed value of $(1-M_r/M_s)$, the GMR of the annealed multilayer is systematically larger, reflecting the effects of grain growth upon annealing.

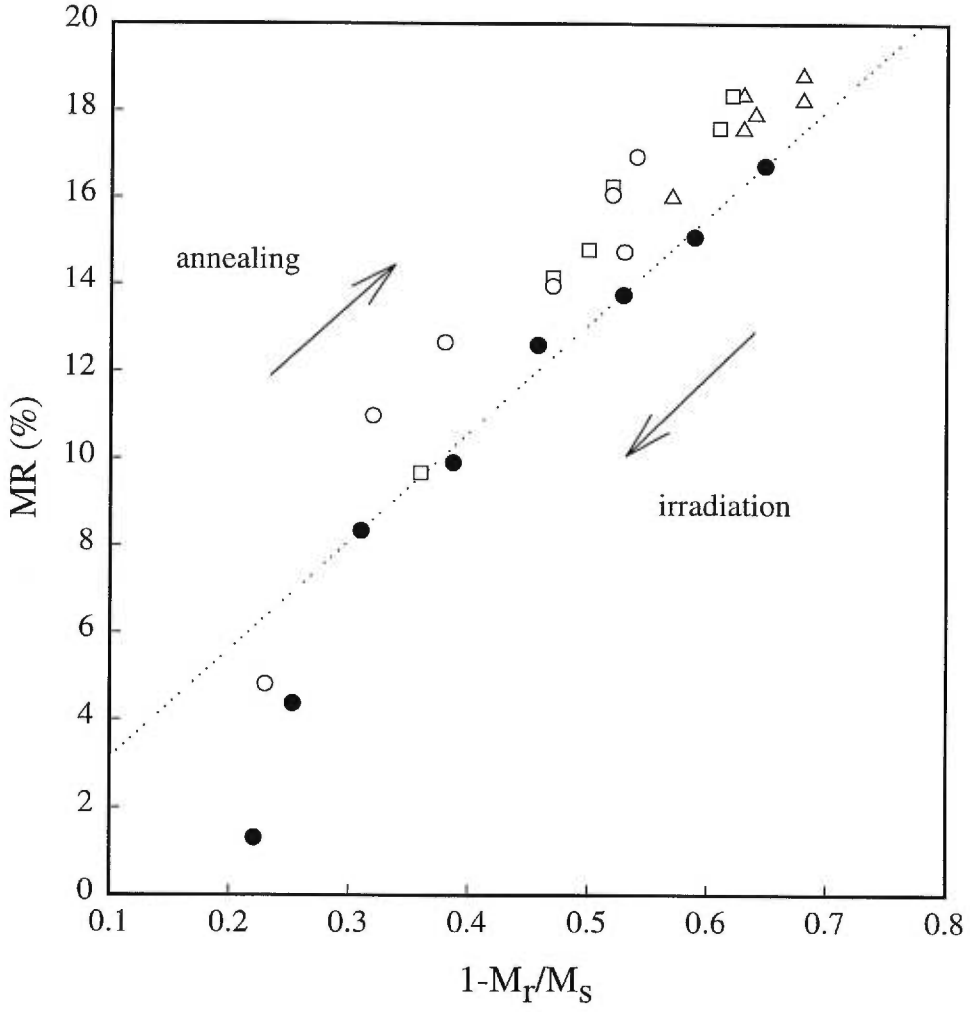


Figure 6.9. GMR vs (1- $M_r/M_s$) for the [Co(17 Å)/Cu(22 Å)]×30 multilayer (solid circles) of Fig. 5.20, and for the three multilayers of Figs. 6.5 and Fig. 6.8 which were subjected to ion doses of 0 (open triangles), $1.3\times10^{14}$ (open squares) and $2.6\times10^{14}$ (open circles) ions/cm$^2$, respectively.

Combining low-dose ion bombardment and subsequent thermal annealing provides an effective *ex-situ* technique to modify Co/Cu interface structure *controllably* and tune the GMR and the AF interlayer coupling *reversibly* of a *single* Co/Cu multilayer over a wide range. Structural analysis, resistivity, magnetoresistance, and magnetization measurements all point to the conclusion that low-dose ion irradition is capable of generating non-equilibrium intermixing at the Co/Cu interfaces while subsequent annealing on irradiated multilayers provokes back-diffusion and restores abrupt interfaces. It is also concluded that GMR and AF interlayer coupling are directly connected and are strongly dependent on the interface sharpness and structure. Sharp and atomically ordered interface improves AF coupling and thus leads to large GMR, while interfacial mixing suppresses AF coupling and reduces GMR. In no case does enhanced interfacial electron scattering introduced by intermixing increase the GMR and it seems that such electron scattering process does not play any decisive role in the variation of GMR as the interface structure of a Co/Cu multilayer is modified by low-dose irradiation or subsequent annealing.

From the fact that thermal annealing can restore the GMR and sharp interface structure of a lightly irradiated multilayer, the possibility that ion irradiation generates atomic diffusion along grain boundary (similar to thermal annealing) can be precluded. Furthermore, if intermixing had occurred over distances greater than about half a layer thickness, it is inconceivable that reformation of a sharp multilayer structure could occur. As a result, it is believed that the intermixing generated by low-dose ion irradiation under our experimental conditions is of very short range.

Finally, even at ion fluences where interface mixing was barely detectable by x-ray reflectivity, large changes in the magnetoresistivity could be observed. Hence, magnetoresistance measurements can be used as a very sensitive probe to detect subtle interfacial mixing induced by ion beam, or interfacial demixing provoked by thermal annealing. Such a probe is particularly valuable for the Co/Cu system, since there is very small atomic contrast between Co and Cu, and thus it is very difficult to detect the initial stages of ion-beam mixing by alternative techniques.

# Chapter 7: Conclusions

High quality Co/Cu multilayers have been prepared by RF sputtering. Structural characterization of these multilyers using low-angle x-ray reflectivity measurements has revealed well-defined compositional modulation along the film growth direction. The analysis of the reflectivity data with a matrix method based on an optical model shows that the interface roughness is confined to 4 – 6 Å and does not depend sensitively on the thickness of the individual layers or number of bilayer periods in a multilayer structure (with 30 periods or less). High-angle x-ray diffraction measurements indicate that the films have a polycrystalline structure with a preferred fcc (111) orientation and grow coherently across interfaces with a vertical structural coherence length of 100 - 200 Å. The giant magnetoresistance (GMR) ratio is typically over 20 % at room temperature and oscillates as a function of Cu-layer thickness ($t_{Cu}$) with a period of about 10 - 12 Å. Strong oscillatory interlayer magnetic coupling has also been observed in these multilayers. Large GMR ratios (> 10 %) are found for multilayers with Co-layer thickness ($t_{Co}$) above 5 Å, although the GMR effect is optimized for $t_{Co}$ between 10 Å and 20 Å. The multilayers with very thin Co layers (5-7 Å), however, exhibit reduced magnetoresistive hysteresis, which might be interesting for sensor applications.

In order to correlate the structural properties (in particular, interface structures) and GMR, various techniques have been applied to modify the structures of Co/Cu multilayers. These include varying the deposition temperature, post-growth thermal annealing, ion beam irradiation and the combination of the irradiation and annealing. The modifications in interface roughness and its lateral correlation, interfacial mixing, film texture and grain size imposed by these techniques have been investigated by a variety of methods based on x-ray scattering technique, including low-angle reflectivity, low-angle diffuse scattering, and high-angle diffraction measurements. The effects of these structural modifications on the GMR and interlayer antiferromagnetic (AF) coupling have been discussed in an effort to clarify the mechanism of GMR in Co/Cu multilayers.

Substrate temperature during deposition can be used to optimize the multilayer structure of Co/Cu and influence its electrical and magnetic properties. The highest structural quality is obtained at the deposition temperature of 15 $^{\circ}$ C, as characterized by

small interface roughness, good layer thickness uniformity, and large vertical structural coherence length. Increasing deposition temperature rapidly increases the interface roughness due to enhanced interaction at the interface between the film and the substrate. On the other hand, decreasing deposition temperature reduces the thickness uniformity of the film. The crystallographic texture of a Co/Cu multilayer also changes dramatically with the deposition temperature. Deposition at low temperatures results in Co/Cu multilayers with perfect fcc (111) texture, while multilayers deposited at high temperatures are dominated by both (111) and (200)-orientated grains. It is also shown that, in order to obtain Co/Cu multilayers with reasonably large GMR, the deposition temperature should be maintained between 0 $^{o}$C and 60 $^{o}$C. The highest GMR is observed in the multilayer with the optimized interface quality, and various kinds of structural imperfections reduce the GMR through either suppressing AF interlayer coupling or introducing spin-independent electron scattering. However, the variation of deposition temperature affects many aspects (interface roughness, structural uniformity, grain size, texture, defects, etc.) of the structure of a multilayer simultaneously. The layer thicknesses might also vary slightly from sample to sample and influence the GMR as well. Therefore, it is difficult to separate a particular factor and evaluate its effects.

Thermal annealing allows one to modify the structure in a *single* multilayer. It has been shown that the effects of annealing on the GMR of Co/Cu multilayers depend not only on the Cu-layer thickness but also on the Co-layer thickness. For each Co-layer thickness, there is a threshold annealing temperature beyond which the GMR drops drastically. The progressive increase of this threshold temperature with increasing Co-layer thickness strongly suggests that in the immiscible system of Co/Cu, thermal annealing mainly promotes atomic diffusion through columnar grain boundaries. Annealing at high temperatures breaks down the multilayer structures and gives rise to a residual GMR attributed to granular-effects, which is almost independent of the Co-layer thickness or the original GMR values.

Low temperature ion-beam irradiation has been proven to be a very useful non-equilibrium technique to tune the interface structures of a *single* Co/Cu multilayer. At high ion doses, irradiating Co/Cu multilayers generate metastable Co-Cu alloys, whose electrical and magnetic properties have been found to be very similar to the Co-Cu alloys

fabricated by other non-equilibrium methods. The ion-beam mixing efficiency has been determined by assuming an error function interface profile and combining the x-ray scattering analysis and magnetic measurements. The ion-mixing width has been found to increase linearly with ion dose with a mixing efficiency close to that predicted by the ballistic mixing model. It is concluded that ballistic mixing is the principal mechanism in the ion mixing of Co/Cu multilayers at low temperatures. At low ion doses, ion-beam irradiation of Co/Cu multilayers generate interfacial mixing of short range with no significant effects on other structural properties such as grain size or film texture. As a result, it is possible to isolate the effects of interface structure on the magnetic and magntotransport properties. It is found that the GMR is indeed strongly depend on the interface sharpness and structure, and can be altered over a wide range by ion irradiation. In addition, it is shown that the interface electron transmission coefficient is reduced by a factor of two for an ion dose up to $5 \times 10^{14}$ ions/cm$^2$. Despite the considerable increase in interface electron scattering, GMR decreases with ion doses monotonically, a fact which rules out the possibility that the GMR in Co/Cu multilayers is dominated by the spin-dependent impurity scattering due to intermixing. On the other hand, the decrease of GMR with ion dose has been ascribed to the suppression of AF interlayer coupling resulting from the interfacial disorder induced by ion-beam irradiation.

Ion irradiation suppresses both GMR and interlayer AF coupling; upon subsequent annealing, both parameters recover sharply. This behaviour has been found to be associated with the back-diffusion from the metastably mixed regions and the reformation of relatively abrupt interfaces. As a result, combining ion irradiation and subsequent thermal annealing provides an effective *ex-situ* technique to modify Co/Cu interface structure *controllably* and tune the GMR and the AF interlayer coupling *reversibly* over a wide range in a *single* multilayer. Using this method, a linear relationship has been observed between the GMR and the volume fraction of AF coupled regions in Co/Cu multilayers. Moreover, since GMR is very sensitive to the Co/Cu interface structure, GMR measurement provides a promising probe to detect subtle ion beam mixing or thermal demixing processes in these materials.

As for future studies, it would be interesting to apply the ion-beam irradiation method to other GMR systems, especially those with large positive heat of mixing. It

would be equally interesting to study how the ion-beam mixing and the related thermal demixing could affect other magnetic properties (for example, perpendicular magnetic anisotropy in similar systems.). Advanced structural analysis techniques, for example, transmission electron microscopy (TEM), or diffuse x-ray study using a synchrotron radiation source, would be particularly helpful in further clarifying the structural modifications induced by various techniques and, therefore, in elucidating the origin of GMR in Co/Cu multilayers.

## References


[1] B. Dieny, J. Magn. Magn. Mat. 136, 335 (1994).

[2] M. N. Baibich, J.M. Broto, A. Fert, F. Nguyen van Dau, F. Petroff, P. Etienne, G. Creuzet, A. Friederich, and J. Chazelas, Phys. Rev. Lett. 61, 2472 (1988).

[3] A. B. Pippard, *Magnetoresistance in Metals* (Cambridge University Press, Cambridge, 1989).

[4] T. R. McGuire and R. I. Potter, IEEE. Trans. Magn. MAG-11, 1018 (1975).

[5] D. H. Mosca, F. Petroff, A. Fert, P. A. Schroeder, W.P. Pratt, Jr., R. LaLoee, and S. Lequien, J. Magn. Magn. Mat. 94, 1 (1991).

[6] S. S. P. Parkin, in Ultrathin Magnetic Structures II, edited by B. Heinrich and J.A.C. Bland (Springer-Verlag, Berlin, 1994).

[7] P. Bruno and C. Chappert, Phys. Rev. B46, 261 (1992).

[8] Mark van Schilfgaarde and Walter A. Harrison, Phys. Rev. Lett. 71, 3870 (1993).

[9] R.E. Camley and J. Barnas, Phys. Rev. Lett. 63, 664 (1989).

[10] S. Zhang, P.M. Levy and A. Fert, Phys. Rev. B45, 8689 (1992).

[11] N.F. Mott, Adv. Phys., 13, 325 (1964).

[12] J. Friedel, Theory of Magnetism in transition metals, (Academic Press, New York, 1967).

[13] A. Fert and I.A. Campbell, J. Phys. F6, 849 (1976).

[14] J. Inoue, A. Oguri, and S. Maekawa, J. Phys. Soc. Jpn. 60, 376 (1991).

[15] R.Q. Hood, L.M. Falicov, and D.R. Penn, Phys. Rev. B49, 368 (1994).

[16] M.D. Stiles, J. Appl. Phys. 79, 5805 (1996).

[17] A.E. Berkowitz, J.R. Mitchell, M.J. Carey, S. Zhang, F.T. Parker, A. Hutten and G. Thomas, Phys. Rev. Lett. 68, 3745 (1992).

[18] J.Q. Xiao, J.S. Jiang, and C.L. Chien, IEEE. Trans. Magn. 29, 2688 (1993).

[19] B. Dieny, V.S. Speriosu, S.S.P. Parkin, B.A. Gurney, D.R. Wilhoit, and D. Mauri, Phys. Rev. B43, 1297 (1991).

[20] T.L. Hylton, K.R. Coffey, M.A. Parker, and J.K. Howard, Science 261, 1021 (1993).

[21] R. Loloee, P.A. Schroeder, W.P. Pratt Jr., J. Bass, and A. Fert, Physica B 204, 274 (1995).

[22] K. Honda, H. Sato, Y. Aoki, and S. Araki, J. Phys. Soc. Jpn. 64, 2191 (1995).

[23] J.C. Slonczewski, J. Magn. Magn. Mat. 129, L123 (1994).

[24] S.S.P. Parkin, Z.G. Li, and D.J. Smith, Appl. Phys. Lett. 58, 2710 (1991).

[25] P. Bruno and C. Chappert, Phys. Rev. Lett. 67, 1602 (1991).

[26] W.F. Egelhoff and M.T. Kief, Phys. Rev. B 45, 7795 (1992).

[27] S.S.P. Parkin, R.F. Marks, R.F.C. Farrow, G.R. Harp, Q.H. Lam, and R.J. Savoy, Phys. Rev. B 46, 9262 (1992).

[28] E.E. Fullerton, D.M. Kelly, J. Guimpel, I.K. Schuller, and Y. Bruynseraede, Phys. Rev. Lett. 68, 395 (1992).

[29] F. Petroff, A. Barthelemy, A. Hamzic, A. Fert, P. Etienne, S. Lequien, and G. Creuzet, J. Magn. Magn. Mat. 93, 95 (1991).

[30] Belien, R. Schad, C.D. Potter, G. Verbanck, V.V. Moshchalkov, and Y. Bruynseraede, Phys. Rev. B 50, 9957 (1994).

[31] D.M. Kelly, I.K. Schuller, V. Korenivski, K.V. Rao, K.K. Larsen, J. Bottinger, E.M. Gyorgy, and R.B. van Dover, Phys. Rev. B50, 3481 (1994).

[32] J.F.W. Dorleijin and A.R. Miedema, J. Phys. F7, L23 (1977).

[33] B.A. Gurney, Phys. Rev. Lett. 71, 4023 (1993).

[34] M. A. M. Gijs and M. Okada, Phys. Rev. B 46, 2908 (1992).

[35] P. Baumgart, B. A. Gurney, D. R. Wilhoit, T. Nguyen, B. Dieny, and V. S. Speriosu, J. Appl. Phys. 69, 4792 (1991).

[36] L. H. Chen, T.H. Tiefel, S. Jin, R. B. Van Dover, E. M. Gyorgy, and R. M. Fleming, Appl. Phys. Lett. 63, 1279 (1993).

[37] B. J. Daniels and B. M. Clemens, Appl. Phys. Lett. 66, 520 (1995).

[38] N. Kataoka, K. Saito, and H. Fujimori, Materials Transactions, JIM, 2, 151 (1992).

[39] S. S. P. Parkin, Appl. Phys. Lett. 60, 512 (1992).

[40] T.C. Huang, J.-P. Nozieres, V. P. Speriosu, B. A. Gurney, and H. Lefakis, Appl. Phys. Lett. B 62, 1478 (1993).

[41] R. F. C. Farrow, S.S.P. Parkin, and R. F. Marks, Appl. Phys. Lett. 69, 1963 (1996).

[42] M. J. Hall, B. J. Hickey, M. A. Howson, M. J. Walker, J. Xu, D. Greig, and N. Wiser, Phys. Rev. B 47, 12,785 (1993); J. Phys. : Condens. Matter. 4, L495 (1992).

[43] T. Thomson, P. C. Riedi, and D. Greig, Phys. Rev. B 50, 10,319 (1994).

[44] K. LeDang, P. Veillet, E. Velu, S.S.P. Parkin, and C. Chappert, Appl. Phys. Lett. 63, 108 (1993).

[45] R. J. Highmore, W.C. Shih, R. E. Somekh, and J. E. Evetts, J. Magn. Magn. Mat. 116, 249 (1992).

[46] H. Ueda, O. Kitakami, Y. Shimada, Y. Goto, and M. Yamamoto, Jpn. J. Appl. Phys. 33, 6173 (1994).

[47] M. Suzuki and Y. Taga, Phys. Rev. B 52, 361 (1995); J. Appl. Phys. 74, 4661 (1993).

[48] Nathan Wiser, Physica A 200, 770 (1993).

[49] Y. Saito, K. Inomata, K. Yusu, A. Goto, and H. Yasuoka, Phys. Rev. B 52, 6500 (1995).

[50] J. M. George, Mat. Res. Symp. Proc. 313, 737 (1993).

[51] S. S. P. Parkin, Appl. Phys. Lett. 61, 1358 (1992).

[52] S. S. P. Parkin, Phys. Rev.Lett. 71, 1641 (1993).

[53] S. K. J. Lenczowski, M. A. M. Gijs, J. B. Giesbers, R. J. M. van de Veerdonk, and W. J. M. de Jonge, Phys. Rev. Rev. B 50, 9982 (1994).

[54] W. P. Pratt, J. Appl. Phys. 73, 5326 (1993).

[55] H. Laider and B. J. Hickey, J. Appl. Phys. 75, 6250 (1996).

[56] S. Roorda, F. Schiettekatte, M. Cai, T. Veres, and A. Tchebotareva, Proc. SPIE, 3413, 165 (1998).

[57] J. F. Ziegler and J. P. Biersack, *The stopping and Range of Ions in Solids*, Pergamon Press, New York, 1985.

[58] D. E. Savage, J. Kleiner, Y. H. Phang, T. Jankowski, J. Jacobs, R. Kariotis, and M. G. Lagally, J. Appl. Phys. 69, 1411 (1991).

[59] J. B. Kortright, J. Appl. Phys. 70, 3620 (1991).

[60] X. Bian, Ph.D. Thesis, McGill University, 1994.

[61] R. W. Cochrane, B. J. Kastner, and W. B. Muir, J. Phys. E 9, 163 (1976).

[62] For a review, see e.g., E. Chason and T. M. Mayer, Critical Reviews in Solid State and Materials Sciences, 22, 1 (1997).

[63] M. Born and E. Wolf, *Principles of Optics*, Pergamon, Oxford, 1964.

[64] Y. Huai, R.W. Cochrane, and M. Sutton, Phys. Rev. B 48, 2568 (1993).

[65] A. de Bernabe, M. J. Captian, H. E. Fisher, and C. Prieto, J. Appl. Phys. 84, 1881 (1998).

[66] T. Gu, A. I. Goldman, and M. Mao, Phys. Rev. B 56, 6474 (1997).

[67] A. Guinier, Théorie et Technique de la Radiacristallographie (Dunod, Paris, 1964).

[68] Z. Q. Qiu, J. Pearson, and S. D. Bader, Phys. Rev. B 46, 8659 (1992).

[69] C. Christides, S. Stavroyiannis, N. Boukos, A. Tavlos, and D. Niarchos, J. Appl. Phys. 83, 3724 (1998).

[70] R. J. Highmore, R. E. Somekh, W. C. Shih, I. M. Mcloughlin, and J. E. Evetts, Appl. Surf. Sci. 65/66, 124 (1993).

[71] H. Holloway and D. J. Kubinski, J. Appl. Phys. 83, 2705 (1998).

[72] H. Holloway and D. J. Kubinski, J. Appl. Phys. 79, 7090 (1996).

[73] Y. Saito, J. Phys. Soc. Jpn. 62, 1450 (1993).

[74] J. R. Childress and C. L. Chien, Phys. Rev. B 43, 8089 (1991).

[75] M. Natasi and J. W. Mayer, Mater. Sci. and Eng. R12, 1 (1994).

[76] D. H. Lee, R. R. Hart, D. A. Kiewit and O. J. Marsh, Phys. Stat. Sol. A 15, 645 (1973).

[77] Y. T. Cheng, Mater. Sci. Rep. 5, 47 (1990).

[78] P. Sigmund and A. Gras-Marti, Nucl. Instr. Methods 182/183, 25 (1981).

[79] P. Sigmund, Radiat. Eff., 1, 15 (1969).

[80] F. Rossi, M. Nastasi, M. Cohen, C. Olsen, J. R. Tesmer and C. Egen, J. Mater. Res. 6, 1175 (1991).

[81] T. Veres, M. Cai, S. Germain, M. Rouabhi, F. Schiettekatte, S. Roorda, and R. W. Cochrane, submitted to J. Appl. Phys. (1999).

[82] A. R. Miedema, Philips Tech. Rev. 36, 217 (1976).

[83] M. Hansen, *Constitution of Binary Alloys* (McGraw-Hill, New York, 1958), p.469.

[84] E. Kneller, J. Appl. Phys. 33S, 1355 (1962).

[85] R. H. Yu, X. X. Zhang, J. Tejada, and J. Zhu, Phys. Rev. B 52, R6987 (1995).

[86] L. F. Schelp, M. Carara, A.D.C. Viegas, M. A. Z. Vasconcellos, and J. E. Schmidt, J. Appl. Phys. 75, 5262 (1994).

[87] A. E. Berkowitz, J. R. Mitchell, M. J. Carey, A. P. Young, S. Zhang, F. E. Spada, F. T. Parker, A. Hutten, and G. Thomas, Phys. Rev. Lett. 68, 3745 (1992).

[88] G. Gladyszewski, Thin Solid Films 204, 473 (1991).

[89] F. Tamsier, V. Jaouen, Ph. Guerin, and G. Gladyszewski, Thin Solid Films 275, 247 (1996).

[90] L. C. Wei and R. S. Averback, J. Appl. Phys. 81, 613 (1997).

[91] H. H. Anderson, Appl. Phys. 18, 131 (1979).

[92] S. K. Sinha, E. B. Sirota, S. Garoff, and H. B. Stanley, Phys. Rev. B 38, 2297 (1988).

[93] S. N. Okuno and K. Inomata, Phys. Rev. Lett. 70, 1711 (1993); J. Kudrnovsky, V. Drchal, P. Bruno, I. Turek, and P. Weinberger, Phys. Rev. B 54, R3738 (1996).

[94] G. Gladyszewski and A. Smal, Nucl. Instr. Methods B52, 6500 (1992).

[95] J. Kudrnovsky, V. Drchal, I. Turek, M. Sob, and P. Weinberger, Phys. Rev. B 54, R3738 (1996).

[96] Y. Takahashi and K. Inomata, J. Appl. Phys. 79, 8598 (1996).

[97] H. Laidler, I. Pape, C. I. Gregory, B. J. Hickey, and B. K. Tanner, and R. Schad, J. Magn. Magn. Mater (in press).

[98] H. Zhang, R. W. Cochrane, Y. Huai, M. Mao, X. Bian, and W. B. Muir, J. Appl. Phys. 75, 6535 (1994).

[99] T. Thomson, P. Reidi and B. J. Hickey (unpublished).